UILU-ENG-70-105

CIVIL ENGINEERING STUDIES

STRUCTURAL RESEARCH SERIES NO. 369

FLEXURAL STRENGTH OF REINFORCED CONCRETE SLABS WITH EXTERNALLY APPLIED IN-PLANE FORCES

by

A. G. Girolami , M. A. Sozen,
W. L. Gamble

AND

STRENGTH OF SLABS SUBJECTED TO MULTIAXIAL BENDING AND COMPRESSION

by

W. L. Gamble, H. Flug
M. A. Sozen

A REPORT TO THE
DEPARTMENT OF DEFENSE
OFFICE OF THE SECRETARY OF THE ARMY
OFFICE OF CIVIL DEFENSE
Contract DAHC 20-67-C-0136
Subcontract 12472 (6300 A-030) US
OCD Work Unit 1127D

UNIVERSITY OF ILLINOIS
URBANA ILLINOIS
OCTOBER, 1970

SUMMARY

FLEXURAL STRENGTH OF REINFORCED CONCRETE SLABS WITH EXTERNALLY APPLIED IN-PLANE FORCES

by

A. G. Girolami
M. A. Sozen
W. L. Gamble

Technical Report
prepared for

OFFICE OF CIVIL DEFENSE
OFFICE OF THE SECRETARY OF THE ARMY
DEPARTMENT OF DEFENSE
Contract DAHC 20-67-C-0136
Subcontract 12472 (6300 A-30)US
OCD Work Unit 1127D

University of Illinois
Urbana, Illinois
October 1970

FLEXURAL STRENGTH OF REINFORCED CONCRETE SLABS WITH EXTERNALLY APPLIED IN-PLANE FORCES

by

A. E. Girolami, M. A. Sozen, and W. L. Gamble

Reinforced concrete slabs, bounded by elements which can develop horizontal reactions, have flexural capacities considerably in excess of the load calculated by an orthodox application of the yield-line analysis. The additional capacity results primarily from changes in geometry of the slab which generate in-plane forces reacting against the bounding elements. Calculation of the effect of the in-plane forces on slab flexural strength is essential for a realistic evaluation of the slab capacity because the increase in load caused by the in-plane forces is not negligible, especially for short-time loading.

The investigation described in this report was concerned with the development of a simple method of calculation for the flexural strength of reinforced concrete slabs with in-plane forces and to check the applicability of the method by experiments.

Six reinforced concrete slabs with spandrel beams were built, instrumented, and tested. The test slabs, which were six-ft square and 1.75 in. deep, were reinforced with intermediate grade steel (yield stress was approximately 48,000 psi) and the concrete strength was approximately 4500 psi. The slab and the spandrel beams had both negative and positive moment reinforcement to simulate an interior panel in a two-way slab designed to carry 150 psf. Three of the test slabs were supported only at the corners while three were supported at several points along the spandrel beams to investigate the effect of nonyielding beams.

Three types of loads were applied on each test slab. At first, a set of horizontal loads were applied at five equally spaced points on each side of the slab. Each loading jack reacted against a yoke which transmitted the reaction to the point on the opposite side of the slab. In effect, the horizontal loading equipment was supported by the slab and did not impede deflection in the vertical plane. The vertical slab load was applied at sixteen points on the slab to simulate a uniform loading. In addition, a set of eight loads were applied at cantilever extensions of the beams in order to maintain a certain amount of restraint at the corners. All vertical loads and reactions were applied through systems of long hangers in order to minimize the possibility of extraneous boundary conditions.

Each test was carried out over a period of 8 to 12 hours. After the application of the horizontal loads, the slab and beam loads were increased proportionally until failure was obtained. Load magnitudes, deflections of the slab, crack patterns, and strains in the steel and the concrete were recorded.

The three slabs with flexible beams initially developed a typical positive-moment yield pattern in the form of a diagonal cross but ultimately failed with the yield lines running parallel to the edge of the slab. The beams participated in the failure mechanism. Failure was limited to the slab in the three test specimens with nondeflecting beams. Collapse of the slab was abrupt and caused by reaching the rotation capacity of the negative-moment yield line. Evidently the rotation capacity of the slab was reduced by the in-plane force.

An iterative procedure was developed for calculating the flexural strength of reinforced concrete slabs with in-plane forces. This procedure uses the basic concepts of the yield-line analysis but recognizes the increase in flexural capacity of the sections along the yield lines and the effects of the deflected shape of the slab. The slab load capacities calculated by a routine application of the yield-line analysis and by the proposed iterative procedure compared as follows with the measured loads for the six test slabs:

	Total Load Capacity in kips		
Mark	Yield-line	Iterative Procedure	Measured
FS1	18.5	28.5	31.8
FS2	18.5	28.5	32.9
FS3	18.5	28.5	31.4
FS4	18.5	33.0	38.6
FS5	18.5	33.0	33.7
FS6	18.5	33.0	34.7

The proposed procedure provides a simple and satisfactory method for calculating the flexural load capacities of reinforced concrete slabs.

SUMMARY

STRENGTH OF SLABS SUBJECTED TO MULTIAXIAL BENDING AND COMPRESSION

by

W. L. Gamble
H. Flug
M. A. Sozen

Technical Report to the
DEPARTMENT OF DEFENSE
OFFICE OF THE SECRETARY OF THE ARMY
OFFICE OF CIVIL DEFENSE
Contract DAHC 20-67-C-0136
Subcontract 12472 (6300 A-030)US
OCD Work Unit 1127D

DEPARTMENT OF CIVIL ENGINEERING
UNIVERSITY OF ILLINOIS
URBANA, ILLINOIS
October 1970

STRENGTH OF SLABS SUBJECTED TO MULTIAXIAL BENDING AND COMPRESSION

by

W. L. Gamble, H. Flug, and M. A. Sozen

Reinforced concrete slab panels which are supported so that horizontal displacements of the edges of the panels are prevented are often capable of supporting considerably more load than would be indicated by simple yield-line analysis methods because of in-plane compression forces developed during deflection. The purpose of the series of tests and analysis described in this report was to demonstrate that the basic principals used in predicting the strength of reinforced concrete elements subjected to bending moments and thrusts in one direction, as in the case of columns, can also be used satisfactorily to predict the strength and behavior of slabs subjected to bending and in-plane forces acting in several directions at once.

The importance of the in-plane forces can perhaps be best illustrated by reference to a set of tests conducted by Ockleston on a large reinforced concrete building. A single interior beam-supported panel carried a uniformly distributed load of 753 psf, while the computed capacity, using the yield-line analysis technique, was 295 psf. The very high load capacity is attributable to the presence of in-plane compression forces generated when the surrounding panels restrained the lateral movements of the edges of the loaded panel.

Six hexagonal reinforced concrete slabs were constructed and tested in order to investigate the effects of the reinforcement ratio and magnitude of in-plane forces on the strength and behavior of slabs. The slabs were reinforced with steel having a yield stress of about 50 kips/in.^{2} and the average concrete strength was about 6,300 lb/in.^{2} The slabs were four in.

thick, and the basic hexagon measured about 6 ft 2 in. across flats. The edges of the hexagon were slotted to form loading wings, and the load was applied so as to produce constant bending moments in all directions within a three ft diam. central portion of the slab.

In three slabs the reinforcement ratio was 0.005 and it was 0.01 in the remaining three. One slab with each reinforcement ratio was tested with no applied in-plane compression forces. In-plane compression forces were applied to the other four slabs by means of prestressing strands which passed through ducts formed in the slab. Three strands were used, each extending across the hexagonal slab tip to tip, and they crossed at center of the slab. The applied forces were either 0.55 kip/in. or 1.10 kip/in. of width of slab section. The slab was supported and loaded through long hanger rods so that these systems would not be able to introduce appreciable in-plane restraints.

The three prestressing strands used to introduce the in-plane compression forces were at slightly different levels so each introduced small moments due to the different eccentricities which had to be taken into account in the analysis of the test results. The bias introduced was such that the most critical sections and locations of the failures were predetermined in the slabs with in-plane forces.

The applied forces, deflections, reinforcement strains, and concrete strains were measured during the tests. The progress of cracking was also observed and recorded. The applied forces were used to determine the applied unit bending moments and thrusts, and the deflection data were analyzed to give measured average curvature values within the central test area of the specimens.

The strengths of the specimens with 0.01 reinforcement ratios agreed very closely with the theoretical values. The measured failure moments for

the slabs with reinforcement ratios of 0.005 were 11 to 13 percent higher than the theoretical values, with the discrepancies being explained primarily by strain-hardening of the reinforcement. The reinforcement strain measurements do not allow direct confirmation of this, as most of the gages failed before strain-hardening strains were reached, but the measured concrete strain-moment relationships are consistent with strain-hardening.

In the slabs with 0.005 reinforcement ratios, application of an in-plane compression force of 0.55 kip/in., or 138 psi, caused an increase in moment capacity of 32 percent, while 1.10 kip/in., or 275 psi, caused an increase of 57 percent. For the slabs with 0.01 reinforcement ratios, the same in-plane compression forces produced increases in moment capacity of 16 and 37 percent, respectively. In both cases the increases followed the increases predicted by the use of moment-thrust interaction diagrams for concrete sections very closely.

While the failures always occurred at the edges of the central test area, the behavior of the slab within the test area was predictable on the basis of the simple theory of flexure for bending in one direction taking into account the in-plane compressions. The only modifications needed would be those required to take into account large deflections, and this becomes a factor only long after yield when the central test area has been deformed into the shape of a spherical segment.

UILU-ENG-70-105

FLEXURAL STRENGTH OF REINFORCED CONCRETE SLABS WITH EXTERNALLY APPLIED IN-PLANE FORCES

by

A. G. Girolami
M. A. Sozen
W. L. Gamble

A Technical Report to the
DEPARTMENT OF DEFENSE
OFFICE OF THE SECRETARY OF THE ARMY
Contract DAHC 20-67-C-0136
Subcontract 12472 (6300 A-030)US
OCD Work Unit 1127D

University of Illinois
Urbana, Illinois
October 1970

TABLE OF CONTENTS

		Page
1.	INTRODUCTION	1
	1.1 Object and Scope	1
	1.2 Acknowledgments	2
2.	DESCRIPTION OF TEST SPECIMENS	3
3.	MATERIALS AND CONSTRUCTION	4
	3.1 Reinforcement	4
	3.2 Steel Assembly and Placement	6
	3.3 Concrete	6
4.	LOADING SYSTEM	8
	4.1 Reaction Frame	8
	4.2 Vertical Loading System	8
	4.3 Horizontal Loading System	9
	4.4 End Beam Loading System	9
	4.5 Hydraulic System	10
5.	INSTRUMENTATION	12
	5.1 Strain Measurements	12
	5.2 Load Measurements	12
	5.3 Deflection Measurements	13
6.	TESTING PROCEDURE	14
7.	BEHAVIOR	15
	7.1 Slabs with Deflecting Beams	15
	7.2 Slabs with Nondeflecting Beams	20
8.	AN ITERATIVE METHOD FOR THE CALCULATION OF THE FLEXURAL STRENGTH OF SLABS WITH IN-PLANE FORCES	24
	8.1 Introductory Remarks	24
	8.2 Comparison of Calculated and Measured Capacities	25
	8.3 Calculation of Deflections	28
9.	SUMMARY	30
10.	LIST OF REFERENCES	32
	TABLES	
	FIGURES	

1.1 Object and Scope

It has been established through experience in actual structures as well as through various experimental investigations that reinforced concrete slabs failing in flexure possess load capacitites well above what may be attributed to the flexural moment capacity of the yielding sections. The explicit causes for the reserve strength, in addition to strain hardening of the reinforcement and possible arching of the load, are changes in the geometry of the slab and forces generated in the plane of the slab by the changes in geometry. At small deflections, the in-plane forces are compressive, and directly enhance the moment capacities of the under-reinforced slab cross sections.

In order to obtain a realistic estimate of the flexural strength of a slab, it is necessary to calculate the effects of the in-plane forces. Especially for short-time loading of panels bounded by elements capable of providing lateral reactions, ignoring the effects of the in-plane forces results usually in a gross underestimate of the slab capacity.

A rigorous numerical analysis of the strength of slabs with in-plane forces requires no more than a statement of the conditions of equilibrium, functions describing the response of the bounding elements, information on the moment-rotation properties of the reinforced concrete slab, and time on a large-capacity digital computer. For general application in practice, the success of such an approach is trivial. The desirable goal is a simple and reasonably accurate method of analysis which can be modified on the basis of intelligible principles to apply to various cases encountered in actual structures.

The primary object of this report is to describe an iterative method developed for calculating the transverse-load strength of reinforced concrete

slabs subjected to in-plane forces. The method is based on the yield-line analysis and rules developed for estimating the deflections of reinforced concrete slabs.

The behavior of six test slabs with flexible and nondeflecting edge beams is described. The test slabs were subjected to known in-plane forces as they were loaded transversely to failure. The transverse load was applied equally at 16 points to simulate a uniform loading. In order to minimize the influence of unknown boundary conditions, all loads and reactions were applied through long rods hinged at both ends.

The observed strengths of the test slabs are compared with the results of the proposed iterative method.

1.2 Acknowledgments

The work reported here was part of the investigation of structural interaction in building members carried out in the Structural Research Laboratory of the University of Illinois Civil Engineering Department with the sponsorship of the Department of Defense, Office of the Secretary of the Army, Office of Civil Defense, under contract DAHC 20-67-C-0136, Subcontract 12472 (6300 A-030)US. The subcontract is under the management of Stanford Research Institute.

Acknowledgment is due Juan Salinas-Pacheco, H. Flug, and A. E. Fiorato, Research Assistants in Civil Engineering, for their invaluable help in the conduct of the tests and study of the data.

2. DESCRIPTION OF THE TEST SPECIMENS

The test slabs were designed to represent interior panels supported by beams, cast monolithically with the slab, on all four edges. The thrusts and bending moments simulating the restraint caused by the adjacent panels were provided by the loading system. The overall plan dimensions of the test slab (Fig. 1), 6 by 6 ft on support center lines, were arbitrarily chosen. The slab thickness was nominally 1.75 in. The beams were 6-in. deep and 3-in. wide as shown in Fig. 1.

The slab was reinforced in accordance with the requirements of Method 1 for two-way systems of the ACI Building Code (4)* for a total unit load of 150 psf. The slab reinforcement and the web reinforcement in the beams was cut from No. 7 gage steel wire. Number 2 deformed bars were used to reinforce the beams. The effective depths and reinforcement ratios for the slab and beam sections are listed in Table 1.

The beams were extended for a distance of 1 ft 11.5 in. beyond the center of the corner supports in order to provide anchorage for the beam reinforcement and also to provide a lever for the application of a vertical load to restrain the beam rotation at the support.

In order to prevent torsional distress, stirrups were used in the beams as shown in Fig. 2 and 3. The No. 7 gage wire stirrups formed close loops with a 2-in. lap. Stirrups satisfying ACI Code minimum requirements were sufficient to resist the design shear forces.

One of the governing concerns in the design of the test setup was that uncertain boundary conditions be minimized. Accordingly, both loads

*Numbers in parentheses refer to entries in the List of References.

and reactions were applied through hangers. To accommodate the hangers for the application of a simulated uniform load, one-in. round holes were formed through the slab at locations shown in Fig. 1.

3. MATERIALS AND CONSTRUCTION

3.1 Reinforcement

(a) Slab Reinforcement

To provide a reasonable spacing of the slab reinforcement without exceeding the design requirements for the total amount of steel, it was necessary to use small-scale bars. These were cut from No. 7 gage wire which was subjected to two special treatments.

To improve its stress-strain characteristics, the wire was annealed for two hours at 800°F. After annealing, the wire was washed with a 50-percent solution of muriatic acid to remove the mill scale. To improve its bond characteristics, the surface of the wire was knurled.

A representative stress-strain curve for the No. 7 gage wire is shown in Fig. 6. The average yield stresses for the reinforcement in the test slabs are listed in Table 2.

(b) Beam Reinforcement

The deformed No. 2 reinforcing bars used in the beams were purchased from the Triangle Steel and Supply Company, Los Angeles. Because these bars had been cold worked, they had an unstable stress-strain curve which was very sensitive to the loading rate even at ordinary loading speeds. To stabilize the stress-strain response, the bars were annealed for two hours at 1200°F. A representative stress-strain curve is shown in Fig. 7.

(c) Stirrup Steel

The stirrups were bent from the No. 7 gage steel wire that was used for the slab reinforcement.

3.2 Steel Assembly and Placement

The beam top and bottom reinforcement and the stirrups were tied into cages before being placed in the form. The bottom slab reinforcement was supported on 3/16 in. diameter steel wire, cut into lengths of about one in. The reinforcement was then wired securely to the bottom of the form. The top bars in the slab were supported by the beam reinforcement at one end and by a chair at the other end.

Cork blocks were wired to the reinforcement at each location a steel strain gage was to be located. The reinforcement was smoothed with a file and emergy cloth at each of these locations prior to wiring the cork block on it.

3.3 Concrete

(a) Mix Proportions

The mix proportions by weight were 1:1:4 (cement:fine sand:sand) with a water/cement ratio of 0.7. The aggregate was a mixture of fine lake sand and Wabash River sand. Sieve analysis results for the fine lake sand are shown in Fig. 8 and the gradation of the combined aggregate in Fig. 9. The cement used was type III. A representative stress-strain curve for the concrete is shown in Fig. 10.

Eight 4 by 8 in. cylinders were cast for each slab. Four were used for compression tests and four for split-cylinder tests. Four 2x2x8-in. beams were cast for modulus-of-rupture tests. The control specimens were tested at the time the slabs were tested. The averages of these results for each specimen are tabulated in Table 2.

(b) Casting and Curing

Three batches of concrete were used for casting each of specimens FS1, 2 and 3. The concrete for the second series of specimens FS4, 5, and 6 was mixed in one batch.

The slabs and beams were vibrated internally with an electric vibrator. The beams were also vibrated externally to insure consolidation. The concrete in the slab was finished using a wooden screed and a metal trowel.

About two hours after casting, the metal tubes used for making the holes in the slab were removed. After eight hours, the slabs were covered with wet burlap which was kept wet for five days. At the end of five days, the burlap was removed and the forms were stripped. The control specimens were cured under the same conditions as the slab.

4. LOADING SYSTEM

4.1 Reaction Frame

The loading system was designed to minimize uncertainties in the boundary conditions. As illustrated in Fig. 11 and 12, the vertical loads on the slab and on the beam ends as well as the corner reactions were applied through long steel hangers which would cause negligible lateral restraint. The horizontal loads (Fig. 13) were applied using frames resting on the beams: deflection of the beams did not generate vertical reactions in the horizontal-load system.

The corner reactions were supported by two structural-steel frames (Fig. 11 and 12) spanning 12 ft in the east-west direction and spaced 6 ft center-to-center from each other. The corner reactions were transmitted from the slab to the frame with 0.75-in. round "Fatigue Proof"* steel rods ten ft in length.

For specimens FS4 through 6, the reaction system included two additional hanging supports (Fig. 11 and 12) for the beams on each side of the specimen.

4.2 Vertical Loading System

The vertical load on the test panel was applied by four jacks and distributed to 16 load distribution plates by means of four loading trees. Each distribution plate was centered over the holes in the slab of the test specimens shown in Fig. 1.

Each quarter of the slab was loaded by an identical loading tree. The base of the loading tree was a 6 ft long main tension rod which extended through a hole in the test floor. A 30-ton center-hole, double-acting

*Trademark of La Salle Steel Company

hydraulic ram and an electric dynamometer was attached to the end. The other end of the rod was connected to the center of a main distribution beam. Two steel rods, 15 in. long and spaced 9 in. on either side of the main tension rod, extended upward from the main tension beam. Each of these secondary tension rods was connected to the center of a secondary distribution beam. Two tension rods 4 ft in length were connected to each secondary distribution beam 9 in. to either side of the secondary tension road. These rods reacted on the distribution plates.

All the rods were pin-connected at both ends except the main tension rod which was pinned at the top end. The pinned connection was achieved by using convex spherical washers and concave spherical seats at each of the bolted connections. All the rods were made from 3/4 in. diameter "Fatigue Proof" steel rods except for the main tension rod, which was 1 in. in diameter.

The load distribution plates were 8 in. square steel plates 1 in. thick. Each plate had a concave spherical seat for convex spherical washers.

The main distribution beams were made using two ft lengths of 7 in. channels weighing 14.75 lb per ft. The channels were connected by the pinned connections which held the tension rods. Lighter channels weighing 9.8 lb. per ft of the same dimensions were used for the secondary beams.

4.3 Horizontal Loading System

The horizontal loads were applied by independent loading units along five axes in each direction as shown in Fig. 13b. The loading units rested

on the test specimen so that vertical deflections of the slab would not develop vertical reactions in the horizontal loading system.

Each loading unit consisted of two ten-ft long one-in. round "Fatigue Proof" steel rods threaded at each end and two steel "yokes" cut from standard structural tubing. The rods in the north-south direction were in planes nine in. from the centroidal plane of the slab while the rods in the east-west direction were at 6 in. from the centroidal plane. A 30-ton center-hole ram applied the force on each rod which was equipped with an electric load cell.

4.4 End Beam Loading System

Vertical loads were applied on the extended ends of the edge beams of the slab in order to restrain the beam rotation over the corner support. These loads were also applied through hangers. A yoke, connected to a 0.75-in. round "Fatigue Proof" steel pull rod, fitted around the end of the beam at a distance of 1 ft 6 in. from the corner reaction. The pull rod was acted on by a hydraulic ram bearing against the test floor. The applied force was measured by an electric load cell.

4.5 Hydraulic System

The basic parts of the hydraulic systems were thirty-two 30 ton center-hole, double-acting, hydraulic rams, three electric hydraulic pumps and one handpump. The hydraulic system was divided into three parts.

(a) Vertical Load Hydraulic System

The four rams of the vertical loading system were connected to an electrically operated hydraulic pump through input and output manifolds.

All four jacks were loaded simultaneously by opening all the control valves on the input lines.

(b) Horizontal Load Hydraulic System

The hydraulic system for the jacks in the north-south and east-west directions were independent of one another. In each system, each of the ten jacks was connected to input and output manifolds, which in turn were connected to an electric hydraulic pump. Control valves on the input lines made it possible to adjust each pair of jacks independently of the others.

(c) End Beam Load Hydraulic System

Each of the jacks used for the end beams was connected to one input and one output manifold, which were in turn connected to a hydraulic handpump. The input hydraulic fluid lines had control valves so each jack could be loaded independently if necessary.

5. INSTRUMENTATION

5.1 Strain Measurements

Concrete and steel strains were measured electrically in the north-south direction on both the top (Fig. 14) and bottom (Fig. 15) surfaces of the test specimens. Strains were measured across lines of negative and positive maximum moment. The locations of the gages in the concrete matched those of the gages on the reinforcement.

(b) Steel Strain Gages

Budd "Metal-Foil" C-6 121B foil gages (0.25-in. gage length) were used for measuring reinforcement strains.

The gages were mounted with Eastman 910 adhesive after removing the cork blocks described in Section 3.2 and cleaning the exposed bar surface with acetone.

(b) Concrete Strain Gages

Concrete strains were measured using SR4 A-156 wire gages with a gage length of 13/16 in.

The surface of the concrete was prepared for the application of the strain gage by smoothing the surface with a small electric grinder and cleaning the smoothed area with acetone. Eastman 910 cement was used to apply the gages.

5.2 Load Measurements

A total of 32 load cells were used to measure the loads applied. Four of these measured the vertical slab load and eight measured the vertical loads on the beams. The horizontal loading system required twenty dynamometers.

The load cells were machined from 6061-T6 aluminum rods, (f_y = 30 kis). Each dynamometer was 6 in. long with a milled outside diameter of 2 in. and an inside diameter of 1 1/8 in. The strain gages (Budd Metal-Foil C6-141B) on the load cell were wired to form a four arm bridge.

The load capacity of the load cell was computed as 57 kips. During the calibration a maximum load of 50 kips was reached with no sign of yielding. Of the 37 dynamometers 26 had a sensitivity of between 80 and 85 lb. per dial division, 4 had a sensitivity of 25 lb. per dial division and two had sensitivities of about 110 lb. per dial division. The strain indicator used was considered accurate to one half of a dial division (a dial division equals 10 microinches per in.).

5.3 Deflection Measurements

Vertical deflections were measured using 0.001-in. dial gages. Different deflection systems were used for the slabs supported at the corners (FS1, 2 and 3) and the slabs which had additional supports under the beams (FS4, 5 and 6).

(a) For test slabs FS1, 2 and 3 deflections were measured at the midpoints of the beams and at the quarter and center points of the panel centerline in the east-west direction, (Fig. 16).

A slotted angle framework supported the dial gages. The legs of the framework were steel pipe sections which encased the corner hanger rods and rested on the slab, (Fig. 16).

(b) For test slabs FS4, 5, and 6 deflections were measured at the midpoints of the beams and at the quarter and center points of both panel center-lines.

The steel pipe legs of the deflection framework encased the hangers at the third points of the beam as shown in Fig. 17.

6. TESTING PROCEDURE

The loading process was complicated by the fact that three different load systems had to be applied on the test specimen. Furthermore, the individual rams in each system had to be maintained at the same load as the other rams in that particular system.

The horizontal loads were applied first. The forces on the rams were adjusted individually after one half the target load of 12,000 lb. per ram was applied. Subsequently, the remainder of the load was applied and the individual ram loads adjusted again to conform to the desired level. Care was taken to insure that the forces in the top and bottom rams of each loading unit were equal. No further adjustments in the horizontal loads were made during the test.

The end beam loads were applied in one increment for tests FS1, 4, 5, and 6, in four increments for FS2, and in two increments for FS3, (see Sections 7.1a and 7.2a).

The vertical load was applied in increments of four to six kips until yield, then deflection at the panel center was used to control loading.

After each load increment the beams and slab of the test specimen were examined for cracks.

7. BEHAVIOR

7.1 Slabs with Deflecting Beams

(a) Development of Cracking and Deflections

The deflection and crack development up to maximum load was quite similar in the three slab specimens tested without supports under the beams. In Fig. 18 the total vertical loads are plotted as functions of the deflections at the panel centers (deflections measured with respect to the corner supports) for each one of the specimens FS1, FS2, and FS3. Two features of the plots should be discussed generally.

The deflections refer to the position of the slab at initiation of vertical loading on the slab. The deflections corresponding to the application of the horizontal loads are not shown. These were zero for FS1, 0.07 in. for FS2, and 0.15 in. for FS3. The calculated downward deflection for horizontal loads applied at the slab centroid is approximately 0.05 in. The deviations indicated for the test specimens are attributable to accidental eccentricities of the horizontal loads.

The abrupt reductions in deflection which can be seen in all three curves in Fig. 18 are due to the application of vertical loads at the cantilever ends of the beams. For FS2, the deflection reductions are less obtrusive because the beam loads were applied in several increments as compared with one increment for FS1 and two for FS3.

The response of only one of these three specimens, specimen FS2, will be discussed in the following paragraphs in order to provide a detailed account of the observed phenomena.

The response of specimen FS2 can be divided into two stages with the boundary provided by development of cracking in the bottom of the slab at a load of 24 kips.

Cracking in the positive and negative maximum moment sections of the beams was observed at a vertical load of approximately 6 kips. Initiation of cracking in the beams did not affect the overall load-deflection response of the specimen.

Except in portions monolithic with the negative moment sections of the beams, no cracking was observed in the slab until a vertical load of 19.7 kips had been applied. At that load, cracking was observed along the beam-slab boundary on all four sides. Maximum strains measured in the slab top reinforcement were on the order of 0.0004.

Beam top reinforcement yielded at a load of slightly less than 20 kips, after the application of the last increment of beam loads.

Positve-moment cracking in the slab was observed at a load of 24 kips. The overall stiffness of the slab was critically affected by the development of these cracks. After this load, deflections increased at a rapid rate as did the network of positive-moment cracking.

The general yielding sequence is indicated below.

(1) Yielding occurred at the negative-moment sections of the beams at a load of 20 kips.

(2) Slab negative-moment yield lines formed completely at a load of approximately 30 kips.

(3) Positive-moment yield lines in the slab formed along the panel diagonals simultaneously with the negative-moment yield lines.

(4) Positive-moment yield hinges in the beams developed at a load of 32 kips. These hinges generated yield lines in the slab along panel centerlines leading to the formation of a "beam mechanism."

As deflections increased, failure occurred by crushing of the concrete across a panel centerline. Photographs of the top and bottom of specimen FS2 after the test are shown in Fig. 19.

(b) Strain Distributions

Figures 20 and 21 contain strain distributions measured in specimen FS2 at the negative and positive moment sections for three loading stages: (1) immediately after application of horizontal loads, (2) at a total vertical load of 24 kips which corresponds to the general development of positive-moment cracking in the slab, and (3) at a total vertical load of 32 kips which corresponds to the initiation of the final yield mechanism. The locations of the strain measurements are indicated on a section of the specimen given in each figure. The exact positions of the electric strain gages are shown in Fig. 14 and 15.

A finite-element solution, based on linear elastic elements, for stresses in the slab and beams at the critical sections under horizontal loading is given in Fig. 22. The positive-moment section has a flat strain distribution along the top and bottom of the slab. The bottom of the beams are in tension. It should be noted that a stress analysis based on a linear strain distribution ($P/A \pm Mc/I$) with the load applied at the mid-height of the slab would indicate compression in the bottom fiber of the beams. Evidently, in the finite-element solution the in-plane force is not transferred into the beams at the rate implicitly assumed in the simpler

analysis. The negative-moment section has a uniform compressive strain top and bottom. The strains in the slab approach zero near the beams and are very small in the beams.

Stage 1: At the negative moment section the beam strains were negligible. This is due to the arrangement of the horizontal jacks and the geometry of the specimen (Fig. 13). The horizontal load was not transferred into the beams at this section.

At the positive-moment section, the beams are in tension at the bottom as the finite-element analysis suggests. Furthermore, part of the tensile strain may have been contributed by the accidental eccentricities of the in-plane forces.

The strain distribution in the slab was relatively uniform at the positive and negative moment sections. Both sections had compressive strains that were of the same magnitude top and bottom.

Stage 2: The steel strains indicate positive-moment cracking over the middle half of the slab and negative-moment cracking over the entire section.

The concrete strains were greater than the steel strains at both positive and negative-moment sections. The measured steel strains in the slab were larger at the positive moment sections with the strains increasing almost linearly up to maximum strain in the middle of the slab.

The beams at the negative-moment section were yielded. At the positive-moment section the beams were near yielding.

Stage 3: The steel strains in the slab at the positive moment section indicate yielding across most of the section and the distribution

is more uniform, not peaked. The steel strains in the slab were larger than the concrete strains. The yield hinges had formed in the beams.

At the negative-moment section the strains indicate yielding across most of the section. The steel strains in the slab were larger than the concrete strains.

(c) Horizontal Load

In Fig. 23 the horizontal load in the NS and EW directions are plotted versus the deflection of panel center for specimen FS2. Figure 24 contains the horizontal load in the NS and EW directions versus the total vertical load for specimens FS1, FS2, and FS3.

For test specimen FS2 the response of the horizontal load to the vertical load, (Fig. 24-b), could be divided into 2 stages: (1) the horizontal load decreased linearly up to a total vertical load of 24 kips, and (2) remained essentially constant beyond 24 kips.

Figure 23 indicates the same behavior. The horizontal load decreased until a center of panel deflection at about .38 inches or a total vertical load of 24 kips, and then remained relatively constant. The deviations from a linear reduction in horizontal load up to a deflection of .38 inches was due to the vertical loads applied to the cantilevered end beams.

The reduction in horizontal load during the first stage of behavior is due to the fact that up to a vertical load of 24 kips, the length of the mid-height of the slab was being reduced. Above 24 kips, the increase in the length of the mid-height of the slab due to general cracking and shifting of the slab neutral axis compensated for the effective reduction in horizontal length due to curvature.

7.2 Slabs with Nondeflecting Beams

(a) Development of Cracking and Deflections

The deflection and crack development up to maximum load was quite similar in the three slab specimens tested with supports under the third points of the beams.

In Fig. 25 the total vertical loads are plotted as functions of the deflections at the panel centers (deflections measured with respect to the beams) for each one of the specimens FS4, FS5, and FS6.

The deflections refer to the position of the slab at initiation of vertical loading on the slab. The deflections corresponding to the application of the horizontal loads were 0.093 in. for FS4, 0.061 in. for FS5, and 0.025 in. for FS6.

The reductions in deflection due to the application of vertical loads at the cantilever ends of the beams are barely discernible in the load-deflection plots because the deflections of the supported beams change very little as a result of the applied loads.

The response of only one of these three specimens, FS6, will be discussed in the following paragraphs in order to provide a detailed account of the observed phenomena.

The response of specimen FS6 can be divided into three stages with the two boundaries between the three stages provided by the development of cracking in the bottom of the slab at a load of 20 kips, and the formation of the yield line mechanism at 32 kips.

Negative moment cracking initiated at a total vertical load of 13 kips along the beam slab boundary. At this load, measured strains in the

slab top reinforcement were on the order of .0005. The effect of negative moment cracking on the behavior of the test specimen was small.

Positive-moment cracking in the slab initiated at a total vertical load of approximately 20 kips. The stiffness of the test specimen was critically affected by the development of these cracks. After this load, deflections increased rapidly as did the network of positive-moment cracking.

The general yielding sequence is indicated below.

(1) Slab negative-moment yield lines formed completely at a load of approximately 28 kips.

(2) Positive-moment yield lines in the slab formed along the panel diagonals at a load of approximately 32 kips.

After the development of the diagonal yield lines at the bottom of the slab, the slab started developing large deflections with very little increase in load. The slab capacity decayed beyond a deflection of approximately one in. Failure was abrupt and was due to the tearing of the slab away from the beams. Superficially, the failure resembled a shear failure in a slab. However, considering that the average nominal shear stress in the slab at maximum load was 75 psi, it is plausible that the primary course of failure was compression in the concrete: the slab-beam interface which was subjected to high compressive forces had reached its rotation capacity, so that shear failure followed failure of the concrete in compression. Photographs of the top and bottom of specimen FS6 after the tests are shown in Fig. 26.

(b) Strain Distributions

Figures 27 and 28 contain the measured strain distributions at the negative and positive moment sections for specimen FS6 for three loading

stages: (1) immediately upon application of the horizontal load, (2) at a total vertical load of 20 kips, which corresponds to the general development of positive-moment cracking in the bottom of the slab, and (3) at a total vertical load of 32 kips corresponding to development of the yield line mechanism. In each figure the location of the electric strain gages is indicated on the cross section. Figures 14 and 15 show the exact location of the strain gages.

Stage 1: At the positive-moment section strains in the slab were uniform top and bottom. Concrete strains were higher as expected because of the in-plane forces. The beams were in compression top and bottom with practically no strain gradient over the depth of the beam because of the support conditions. At the negative-moment section the beam strains were small because of the points of application of the in-plane forces and the additional supports for the beams. In the slab, the concrete strain were larger than the steel strains and the distribution was irregular.

Stage 2: At the positive-moment section, the steel strains indicated cracking in the middle half of the slab and in the beams. The concrete strains were larger than the steel strains and had the same distribution shapes with higher strains in the middle of the slab.

The negative-moment region of the slab was cracked across the entire section. Tensile strains in the beams were below cracking. The concrete strains were larger than the steel strains. The distribution of the steel and concrete strains was not uniform.

The steel and concrete strains were larger at the negative-moment section than those at the positive-moment section.

Stage 3: The strains across the centerline of the panel at the positive moment section reached a maximum in the middle of the panel. The steel strains in the middle indicated yielding whereas closer to the edges of the slab, the steel strains are less than the concrete strains. The strains in the supported beams are still below the yield stress. These observations are consistent with the observed yield lines along the diagonals.

The negative moment section had yielded completely across the center of the section. The strains nearer the edges were below yield because of the tendency of the negative-moment yield lines to form a circle within the square outlined by the beams.

(c) Horizontal Load

In Fig. 29 the horizontal load applied to specimen FS6 is plotted versus the center of panel deflection. Figure 30 is the horizontal load versus the total vertical load for specimens FS4, FS5, and FS6.

The horizontal load decreased as the total vertical load increased until a vertical load of 20 kips was reached, (Fig. 30c). The same response is seen in Fig. 29, (a center of panel deflection at about .2 in. corresponded to a total vertical load of 20 kips). As the center of panel deflection increased the horizontal load increased about 5 percent. The changes in the horizontal load were consistent with the changes in the length of the slab at mid-height indicated by the strain measurements.

8. AN ITERATIVE METHOD FOR THE CALCULATION OF THE FLEXURAL STRENGTH OF SLABS WITH IN-PLANE FORCES

8.1 Introductory Remarks

It is well known that an orthodox application of the yield-line theory fails to predict the strength of slabs with in-plane forces. This is not a failure of the theory but results from the inadequacy of specifying resisting moments along the yield lines without considering the influence of the in-plane forces. The effects of the in-plane forces may be interpreted as being made up of two compensating effects: the capacity is increased because the resisting moments are increased (provided the slab is not over-reinforced) while the capacity is decreased because the static moments acting on the yield lines are also increased depending on the deflected shape of the slab.

The objective of the iterative procedure described in this chapter is to provide a reasonably accurate and simple method of analysis to determine the load-carrying capacity of a panel acted upon by known or assumed in-plane forces. The proposed iterative method is based in general on the yield-line analysis (1) and the method developed by M. D. Vanderbilt (3) for calculating deflections of reinforced concrete slabs. In addition to the axioms involved in those two methods, the iterative method is based on the following assumptions.

(1) The resisting moments are calculated including the effects of the in-plane forces. (See Reference 2).

(2) The deflection along a yield line is assumed to vary parabolically from a support point to the point of maximum deflection. This is based on the assumption that at the time the yield lines first develop the deflection of the slab and beams are predominantly elastic.

(3) The axial load, (a) remains entirely within the slab and (b) is uniformly distributed in the slab.

The procedure for the trial-and-error analysis involves the following steps in the case of a symmetrical panel loaded uniformly:

(1) Calculate the relationship between load and deflection (based on cracked section) using the method developed in Reference 3.

(2) Calculate the load capacity using yield-line analysis with the unit resisting moments determined from an interaction diagram reflecting the increase in flexural capacity resulting from the applied load.

(3) Determine the deflection at mid-span corresponding to the load calculated from the relationship determined in Step 1. (In a slab bounded by flexible beams, the deflection would also have to be determined for the mid-points of the column center-lines).

(4) Recalculate the load capacity by considering the equilibrium of the slab segments bounded by the yield lines, recognizing the fact that the segment is deflected as calculated in Step 3. Assume that deflections vary parabolically along yield lines from points of support to points of maximum deflection.

Steps 3 and 4 are repeated until acceptable convergence is reached.

8.2 Comparison of Calculated and Measured Capacities

Before discussing the comparison of the calculated and measured capacities, it is necessary to record the essential details of the calculations.

In calculating the interaction diagrams for axial load and bending moment in the slab and in the beams the concrete strength was assumed to be 5000 psi. The limiting compressive strain in the concrete was taken as

0.003. The stress distribution was assumed to conform to the "rectangular stress block" with the maximum stress equal to $0.85f'_c$ acting over 85 percent of the compressed area.

The yield stress of the reinforcement was 50,000 psi for the beams in all test specimens. The steel yield stress for the slab reinforcement was taken as 48,000 psi for FS1-3 and 49,000 psi for FS4-6.

The resulting interaction diagrams for the slab sections are shown in Fig. 31.

Deflections required for Step 3 of the iterative procedure were obtained directly from the tables provided in reference 3. The relative beam stiffness, H, was assumed to be 1.75 for FS1-3 and 5.0 for FS4-6. The deflection coefficients used referred to point supports or c = 0. The cracked section moment of inertia was based on the "straight line formula" with the modular ratio (E_s/E_c) assumed to be seven.

The equilibrium conditions for Step 4 of the iterative procedure were different for the two sets of test specimens.

For specimens FS1-3,

$$W = \frac{8}{L}[M_1 + M_2 - P\Delta_{eff}] \qquad (1)$$

where $\Delta_{eff} = 4/3\ \Delta_{cs/mb} - 1/3\ \Delta_{mb}$,

M_1 = the total negative moment resistance of the slab plus the two rectangular beams

M_2 = the total positive moment resistance of the slab plus the two rectangular beams.

W = total vertical load capacity

P = the total horizontal force acting at the time the yield lines form

$\Delta_{cs/mb}$ = the relative deflection of the center of the slab with respect to the midpoint of the beams for fully cracked beams and slab

Δ_{mb} = the deflection at midspan of the beam for fully cracked beams

L = the clear span of the slab.

For specimens FS4-6,

$$W = \frac{24}{L}\left[m_1 L + m_2 L - \frac{2}{3} P\Delta_{cs}\right] \qquad (2)$$

where W = total vertical load capacity

m_1 = the negative yield moment per unit width of the slab

m_2 = the positive yield moment per unit width of the slab

L = the clear span of the slab

Δ_{cs} = the deflection at the center of the slab for fully cracked slab and nondeflecting beams.

P = the total applied horizontal force.

The results of the iterative solution were as follows.

SLAB CAPACITY

Mark	Yield Line Analysis kips	Iterative Proc. kips	Meas. kips	Meas. / It. Proc.
FS1	18.5	28.5	31.8	1.12
FS2	18.5	28.5	32.9	1.15
FS3	18.5	28.5	31.4	1.10
FS4	18.5	33.0	38.6	1.17
FS5	18.5	33.0	33.7	1.02
FS6	18.5	33.0	34.7	1.05

The last column of the table above indicates that the iterative procedure gave conservative results for all six test specimens. Because the stiffness of the slab is based on a completely cracked section in the analysis, the calculated results would be expected to be on the safe side in all instances. Accordingly, the results for specimens FS1 through FS4 are of the expected order. The test results for FS5 and FS6 appear to be

lower than what they would be expected to be. The maximum load is reached at a deflection approximately one half that assumed in the analysis. This condition implies that the resisting moments in the specimens were smaller than those assumed in the analysis, since the in-plane loads were measured. There is no readily apparent reason for the implied lower moment resistances in specimens FS5 and FS6.

The slab capacities calculated ignoring the effect of the in-plane forces are listed in the second column of the above table. As would be expected, these values amount only to a fraction of the measured loads. It should be mentioned that the calculated values refer to yield mechanisms confined to the slab. This was the correct pattern for specimens FS4 through FS6 which had supported beams but incorrect for specimens FS1 through FS3.

8.3 Calculation of Deflections

A reasonable approximation to the load deflection curve can be made using the following procedure.

(1) The uncracked slope is calculated directly from the tables provided in reference 3. This represents the uncracked portion of the load deflection curve.

(2) The moment at which cracking initiates at the negative moment section of the slab is calculated using the following relationship

$$M_{cr} = \sigma \frac{I}{c}$$

where $\sigma = \frac{P}{A} + f_r$

P = the initially applied horizontal force

A = the cross sectional area of the slab

f_r = the modulus of rupture

I = the uncracked slab moment of inertia per unit width

c = the distance from the neutral axis to the tension face of the slab.

(3) The load corresponding to this moment was computed using the moment coefficients given in reference (5). This load could also be calculated using standard plate theory. This cracking load is plotted on the line calculated in Step 1 above.

(4) The point calculated in Step 3 is connected by a straight line to the point of maximum load previously calculated by the trial and error procedure.

The resulting approximation to the load-deflection curves of the tested specimens is shown in Fig. 32. From this figure it can be seen that the above procedure gives a reasonable estimate of the energy absorbing capacity of the specimen.

9. SUMMARY

The overall objective of the work described in this report was to investigate experimentally the influence of in-plane forces on the flexural load capacity of reinforced concrete slabs and to develop a simple method in order to determine the strength of slabs with known or assumed in-plane forces.

The experimental program involved the testing to failure of six test slabs, each measuring 6 by 6 ft in plan (Fig. 1). The slab, designed to carry a nominal uniform load of 150 psf, was 1.75 in. thick. The spandrel beams measured 3 by 6 in. deep in cross section (Fig. 2). The concrete strength ranged from 4300 to 5500 psi. The reinforcement yield stress varied from 47,000 to 50,000 psi (Table 2).

In order to minimize experimental uncertainties caused by poorly defined reaction conditions, all loads and reactions were applied through hangers (Fig. 11 and 12). Horizontal in-plane loads were applied at five points on each side of the slab (Fig. 13).

Three test slabs were supported at the intersection points of the spandrel beams (corners.) Additional supports were provided along the spandrel beams in order to investigate the effect of strong nondeflecting beams in three other specimens.

In the test slabs with flexible beams, the yield mechanism formed initially in the slab, with the typical diagonal cross pattern, but was modified eventually to include the beams in the yield mechanism (Fig. 19). In the test slabs with nondeflecting beams, failure was limited to the

slab (Fig. 26). Collapse was abrupt and due to the reaching of the rotational capacity of the "hinge" at the negative-moment yield line along the faces of the spandrel beams.

As a result of the studies of the experimental data, an iterative analysis was developed for calculating the flexural load capacity of reinforced concrete slabs subjected to compressive in-plane forces.

10. LIST OF REFERENCES

1. K. W. Johansen, "beregening at Krydsarmerde Jaernbetonpladers Brudmoment," Bygningsstatiske Meddelelsen (Copenhagen), Vol. 3, 1931. (See also: Eivind Hognestad, "Yield-Line Theory for the Ultimate Flexural Strength of Reinforced Concrete Slabs," Proc. ACI, Vol. 49, 1953, pp. 637; Phil M. Ferguson, "Reinforced Concrete Fundamentals", John Wiley and Sons, New York, 1958, pp. 251.)

2. E. O. Pfrang, C. P. Siess, and M. A. Sozen, "Load-Moment Curvature Characteristics of Reinforced Concrete Cross Sections," ACI Journal, Proc. Vol. 61, July 1964, p. 763.

3. M. D. Vanderbilt, M. A. Sozen, and C. P. Siess, "Deflections of Multiple-Panel Reinforced Concrete Floor Slabs," Proc. ASCE Vol. 91, No. ST4, August 1965.

4. American Concrete Institute, Building Code Requirements for Reinforced Concrete (ACI 318-63).

5. W. L. Gamble, M. A. Sozen, and C. P. Siess, "Measured and Theoretical Bending Moments in Reinforced Concrete Floor Slabs," Civil Engineering Studies, Structural Research Series No. 246, University of Illinois, Urbana, Illinois, June 1962.

TABLE 1 SECTION PROPERTIES

Mark	Slab Reinf. Pos. Sect. p %	Slab Reinf. Pos. Sect. d in.	Slab Reinf. Neg. Sect. p %	Slab Reinf. Neg. Sect. d in.	Beam Reinf. Pos. Sect. p %	Beam Reinf. Pos. Sect. d in.	Beam Reinf. Neg. Sect. p %	Beam Reinf. Neg. Sect. d in.	Stirrup Spacing in.
FS1	.297	1.51	.354	1.47	.94	5.32	1.25	5.32	2
FS2	.297	1.51	.354	1.47	.94	5.32	1.25	5.32	2
FS3	.297	1.51	.354	1.47	.94	5.32	1.25	5.32	2
FS4	.297	1.51	.354	1.47	.60	5.32	1.25	5.32	1
FS5	.297	1.51	.354	1.47	.60	5.32	1.25	5.32	1
FS6	.297	1.51	.354	1.47	.60	5.32	1.25	5.32	1

p = reinforcement ratio

d = effective depth

TABLE 2 MATERIAL PROPERTIES

						Slab Reinf.	Beam Reinf.
	Age	f'_c	f_{sp}	f_r	E	f_y	f_y
Mark	days	psi	psi	psi	10^6 psi	ksi	ksi
FS1	150	5500	515	1070	-	48	50
FS2	180	4600	450	-	2.9	47	50
FS3	240	4890	490	1015	3.0	47	50
FS4	30	4450	480	775	2.4	49	50
FS5	30	4300	355	870	2.7	49	50
FS6	77	5405	-	1000	-	49	50

f'_c - compressive strength of concrete

f_{sp} - tensile strength of concrete (split cylinder)

f_r - modulus of rupture of concrete

E - secant modulus of deformation of concrete (@ $0.40f'_c$)

f_y - yield stress of steel

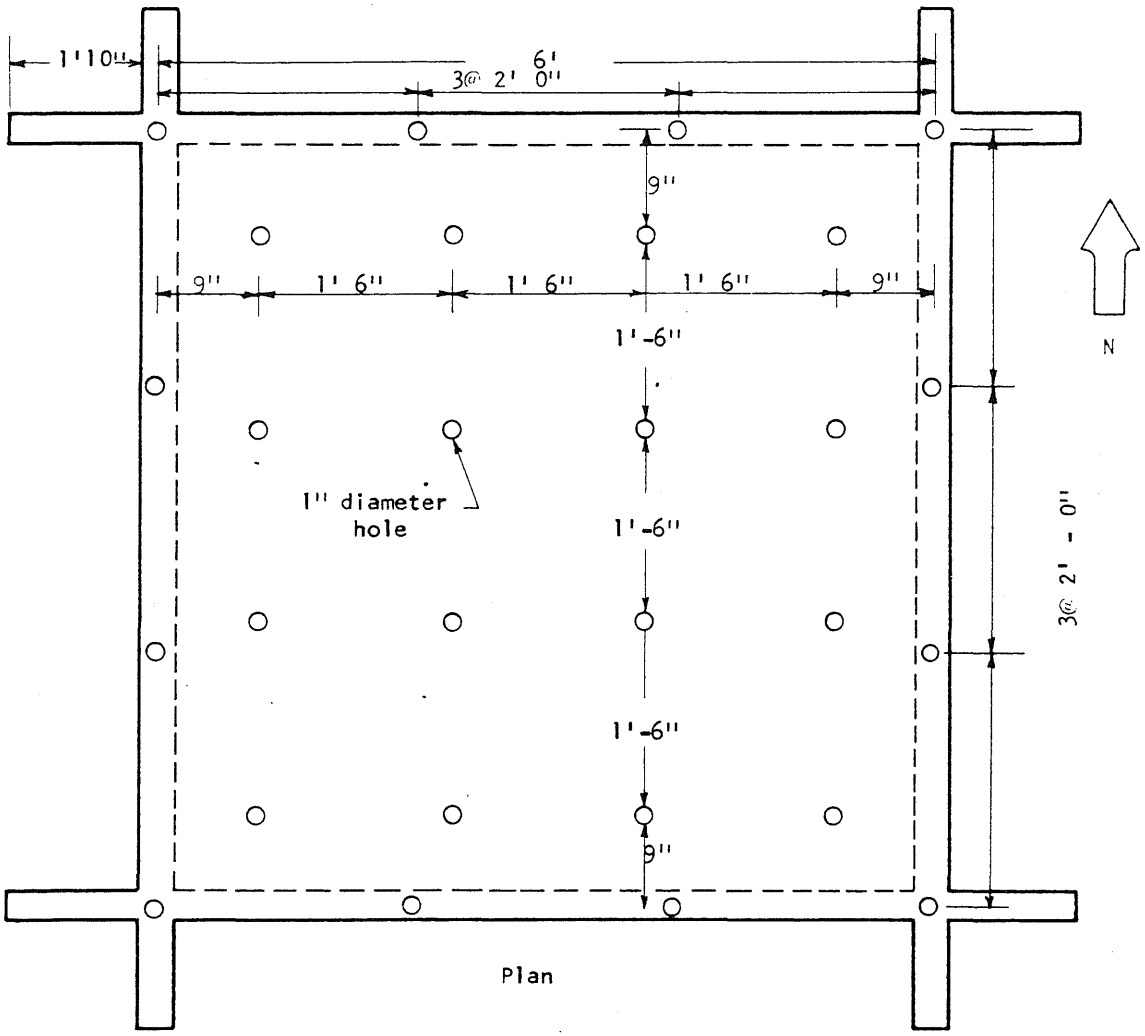

FIG. 1 TEST SPECIMEN

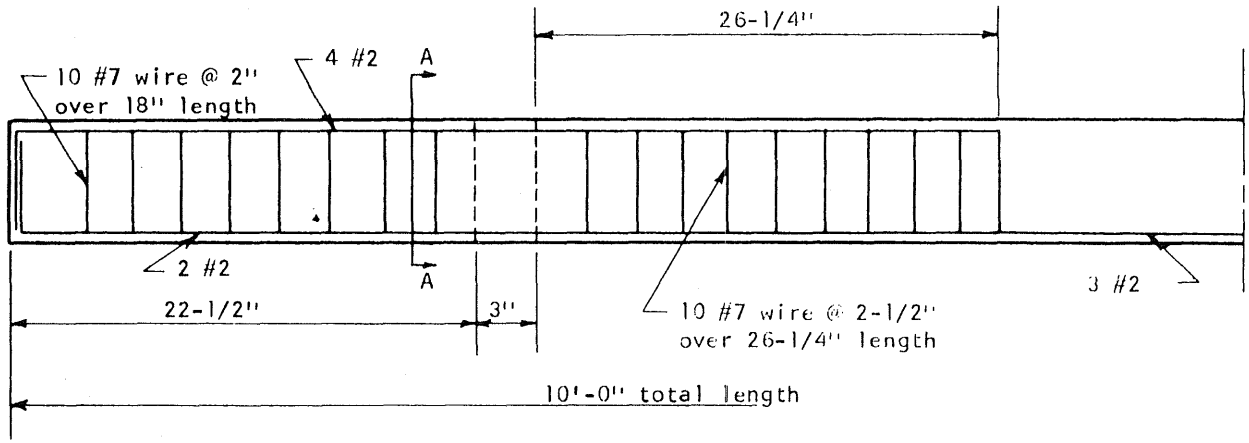

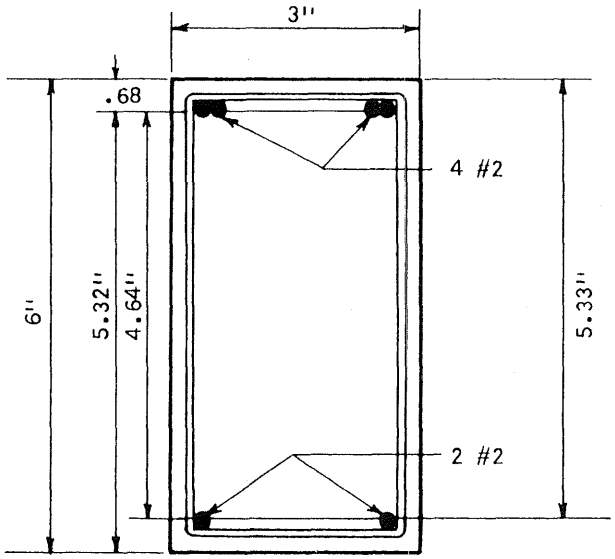

Section A-A

FIG. 2 BEAM REINFORCEMENT, SPECIMENS FS 1, 2, 3

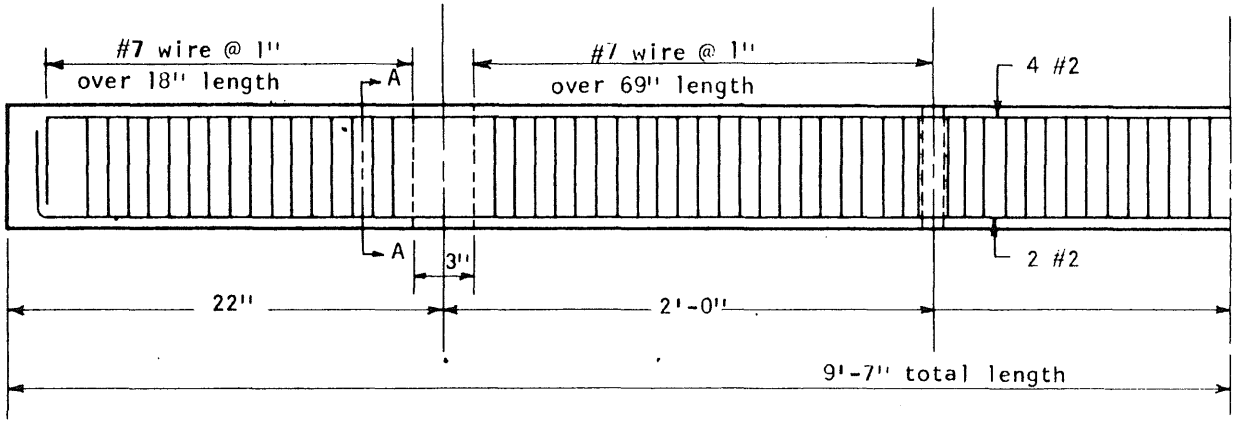

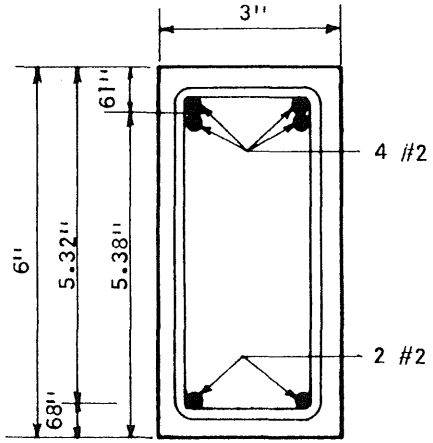

Section A-A

FIG. 3 BEAM REINFORCEMENT, SPECIMENS FS 4, 5, 6

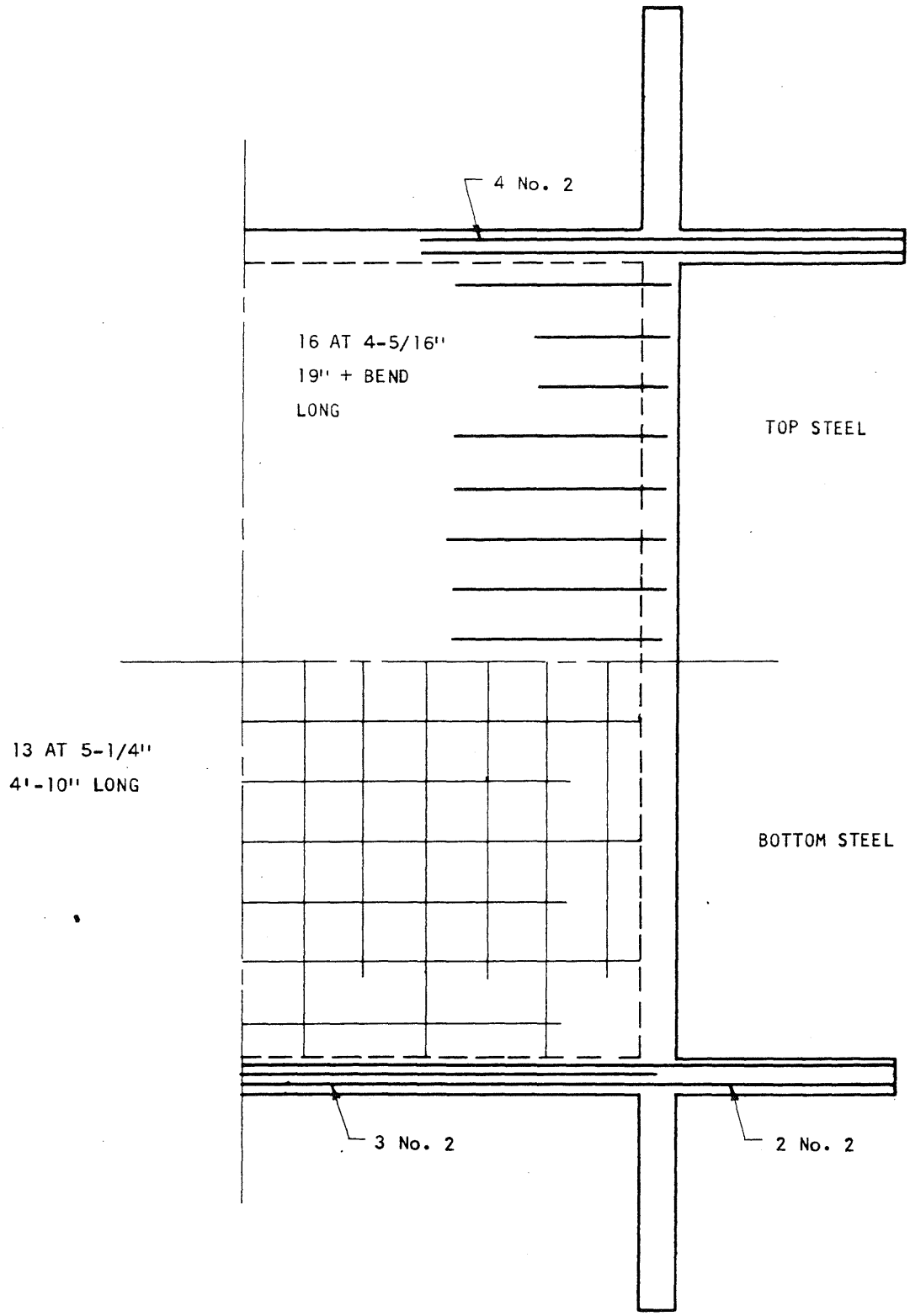

FIG. 4 SLAB REINFORCEMENT, FS 1, 2, 3

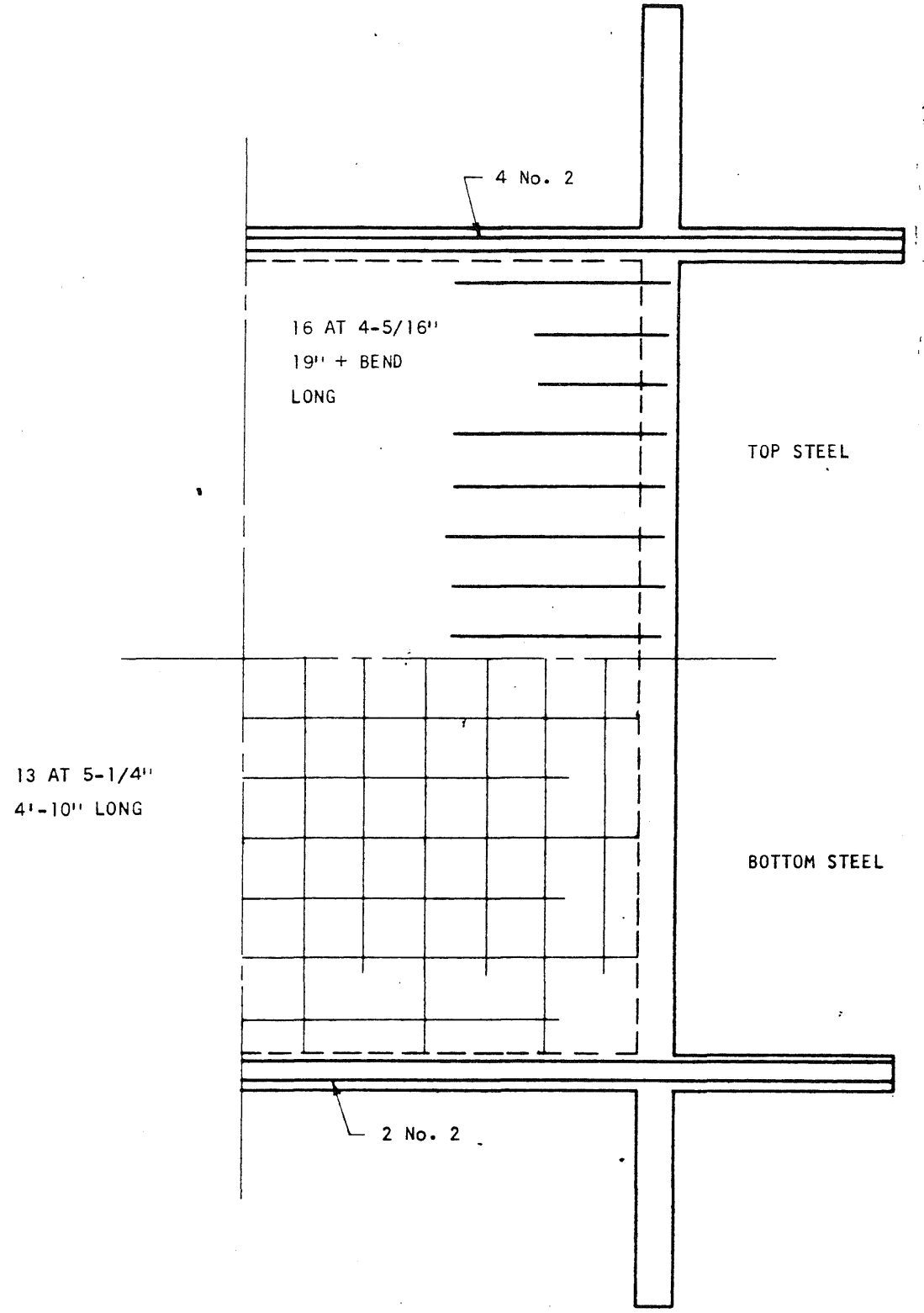

FIG. 5 SLAB REINFORCEMENT, FS 4, 5, 6

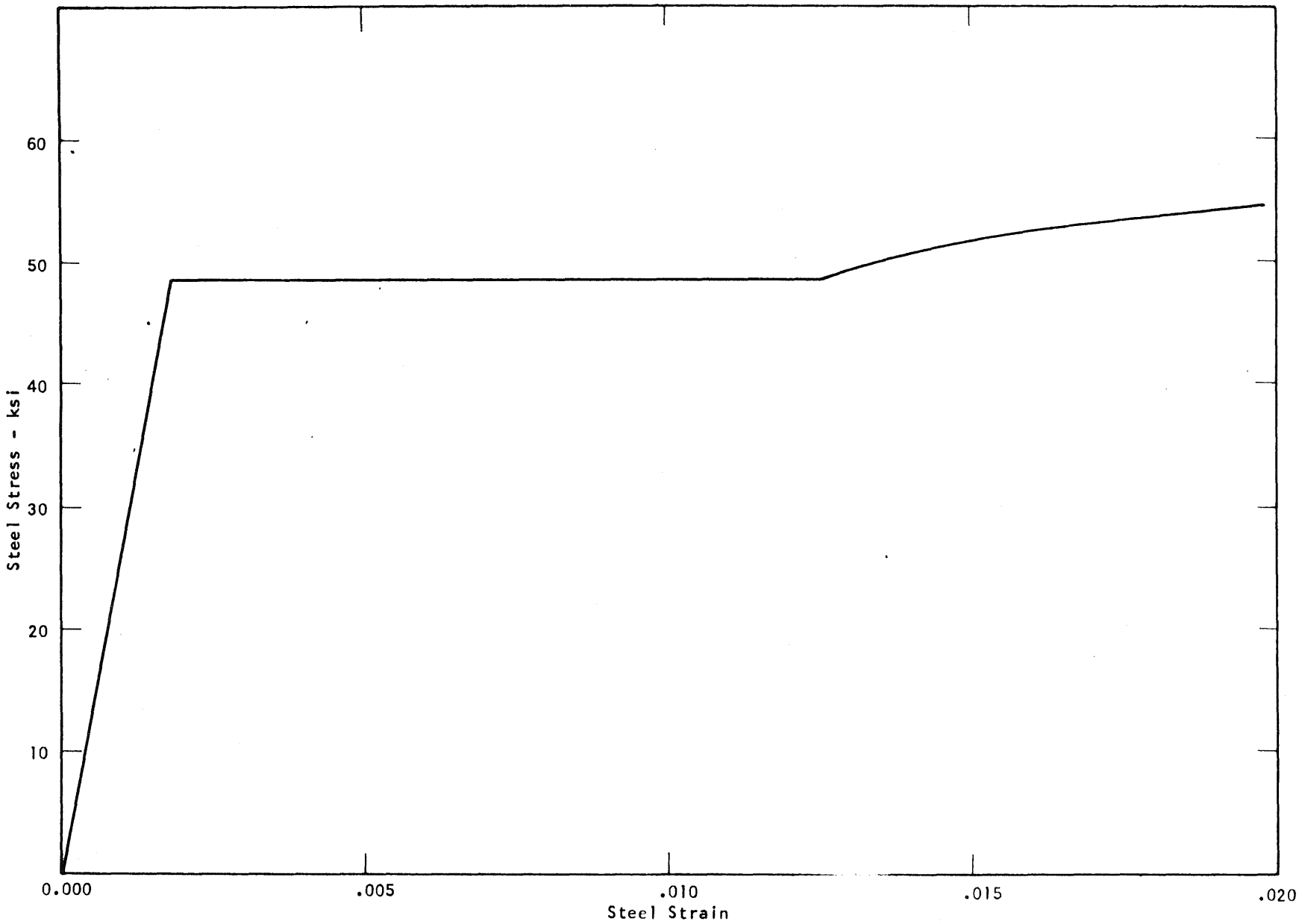

FIG. 6 REPRESENTATIVE STRESS-STRAIN CURVE FOR #7 GAGE STEEL WIRE

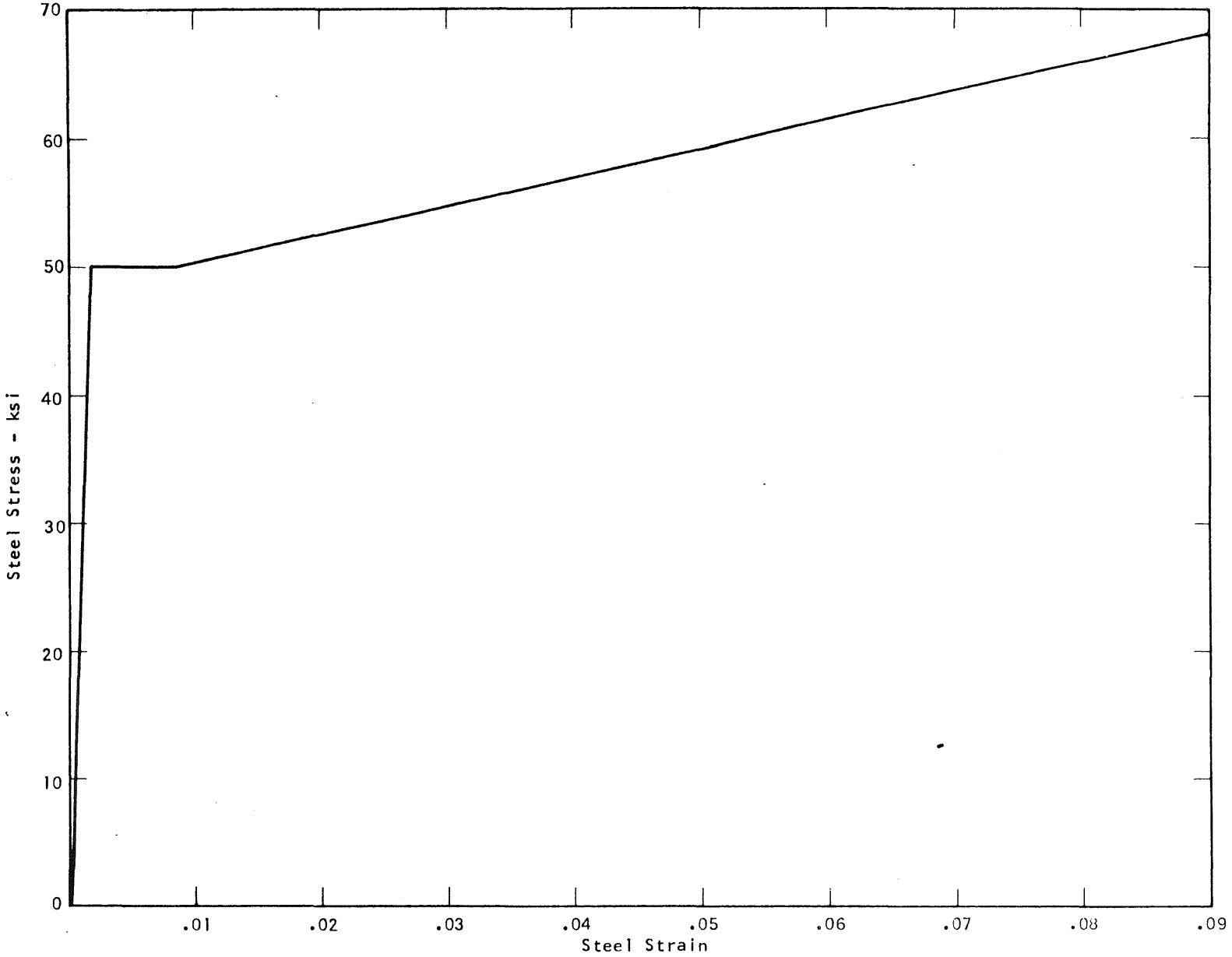

FIG. 7 REPRESENTATIVE STRESS-STRAIN CURVE FOR #2 REINFORCING BARS

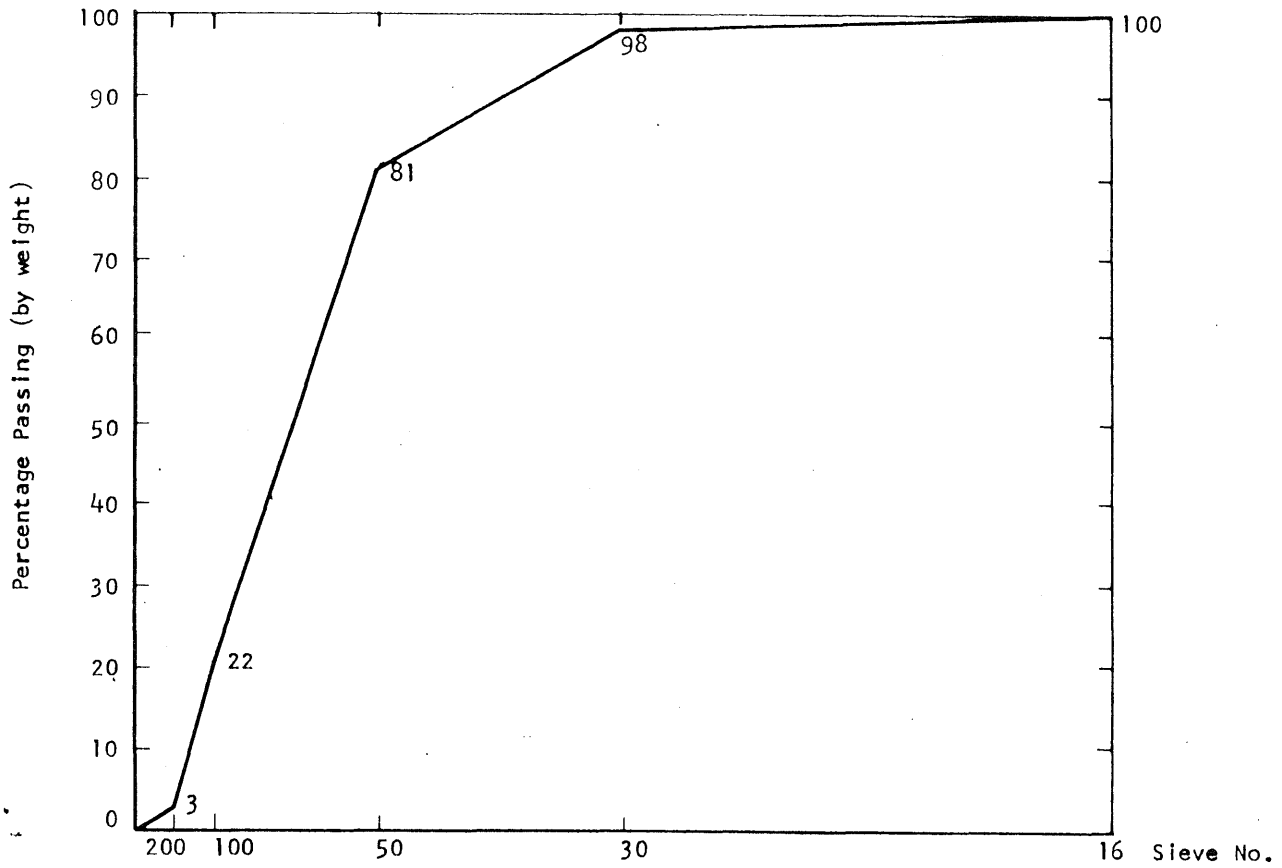

FIG. 8 GRADATION OF THE FINE LAKE SAND

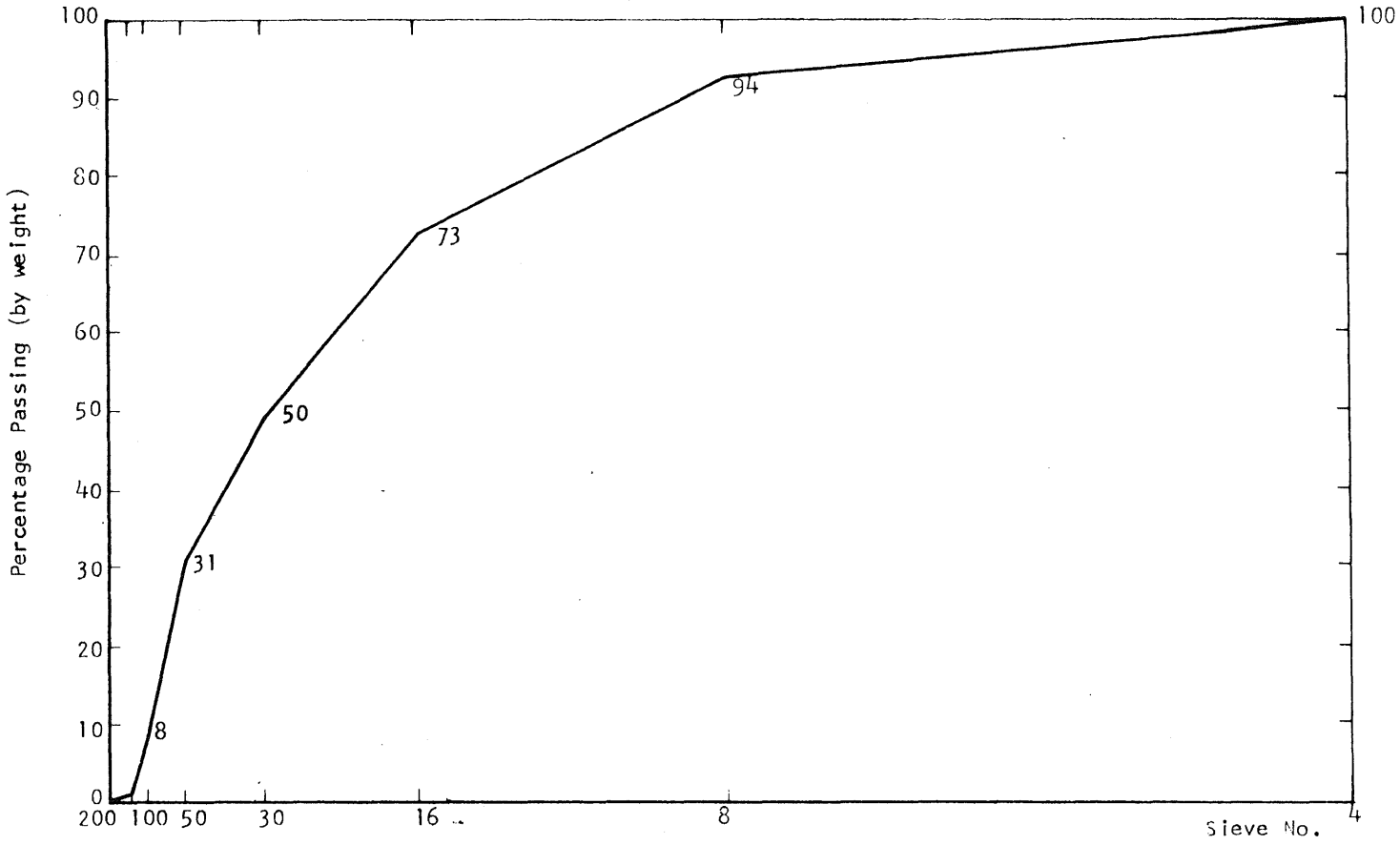

FIG. 9 GRADATION OF THE COMBINED AGGREGATE

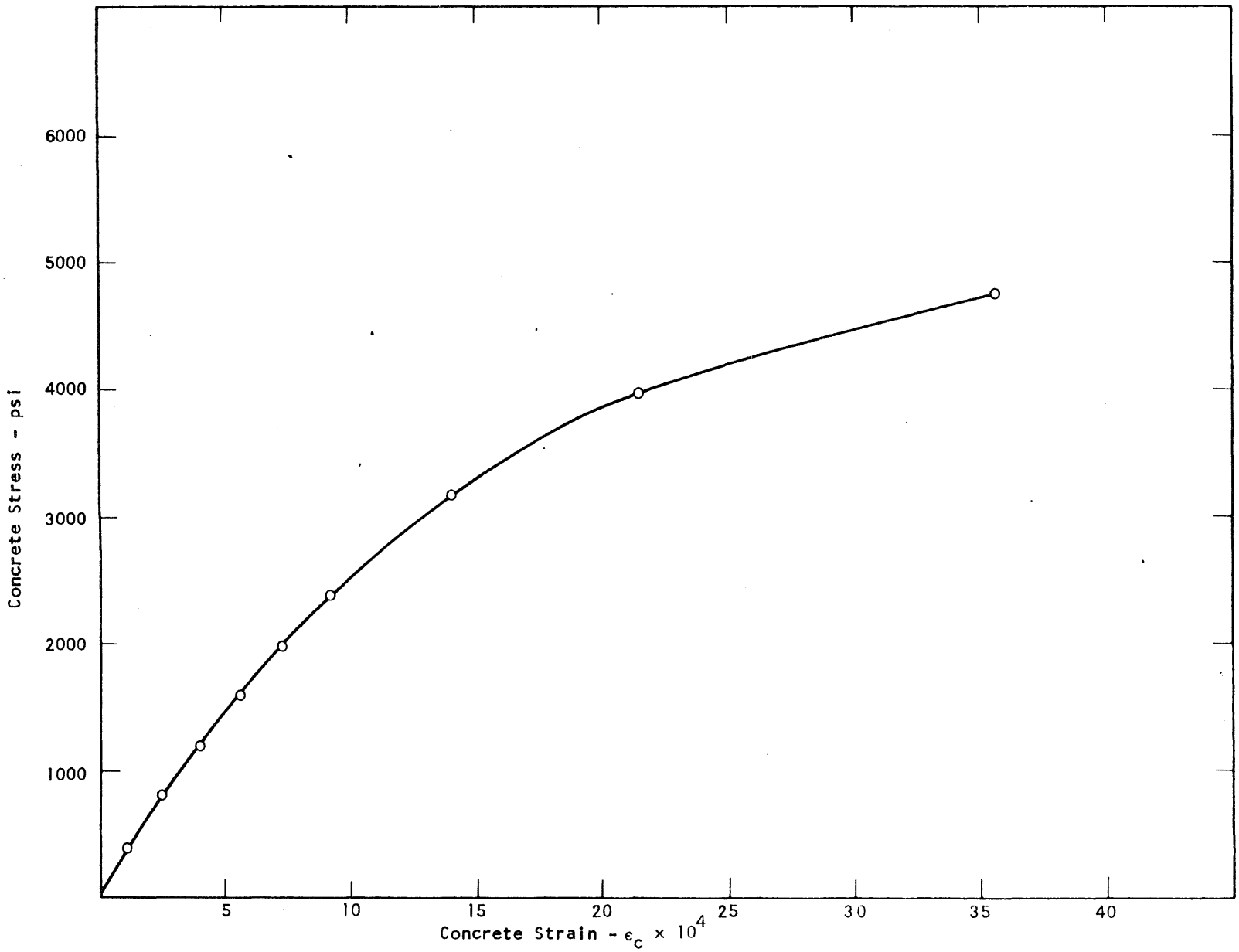

FIG. 10 REPRESENTATIVE STRESS-STRAIN CURVE FOR CONCRETE

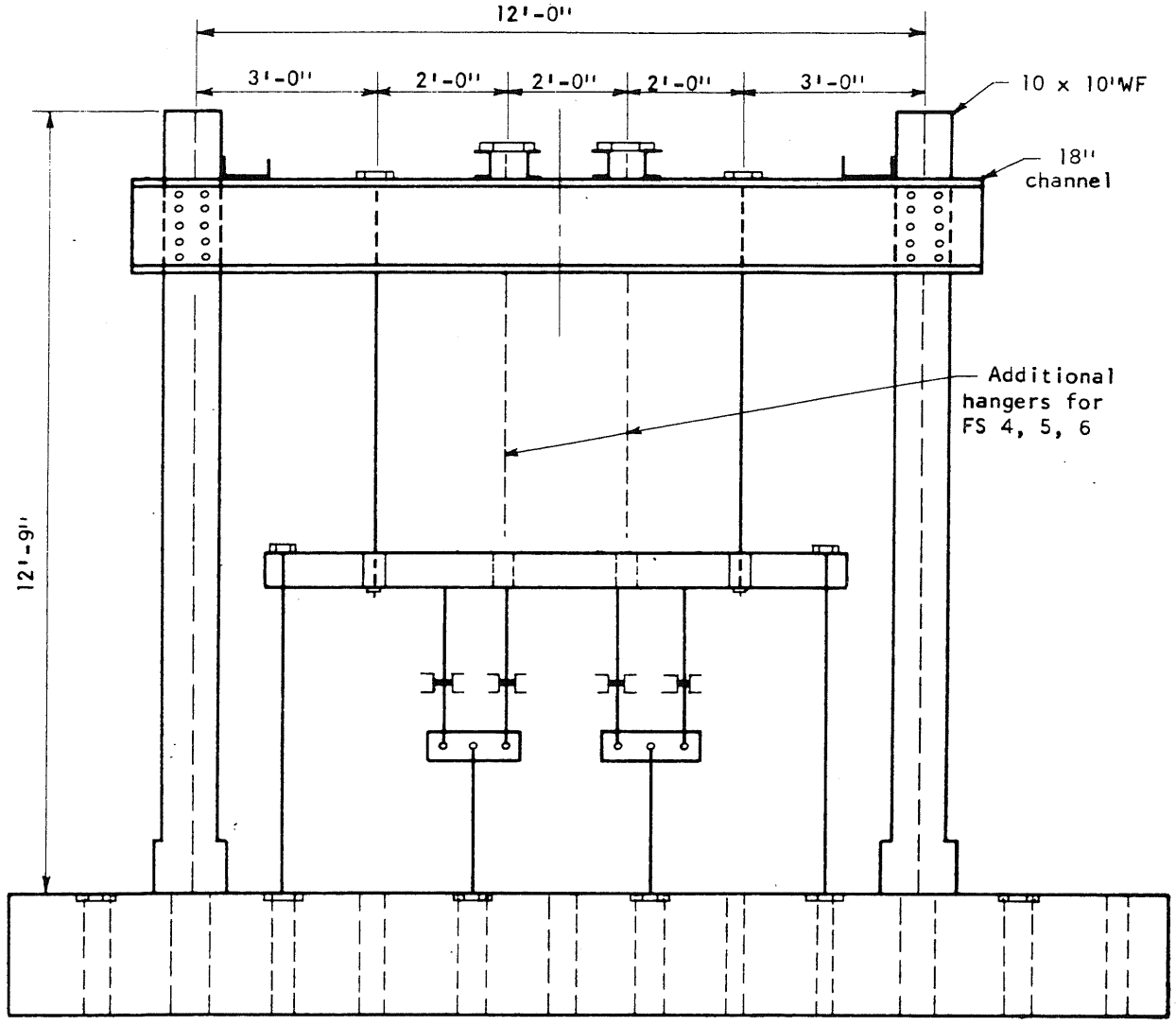

Front Elevation

FIG. 11 REACTION FRAME, VERTICAL AND END BEAM LOADING SYSTEMS

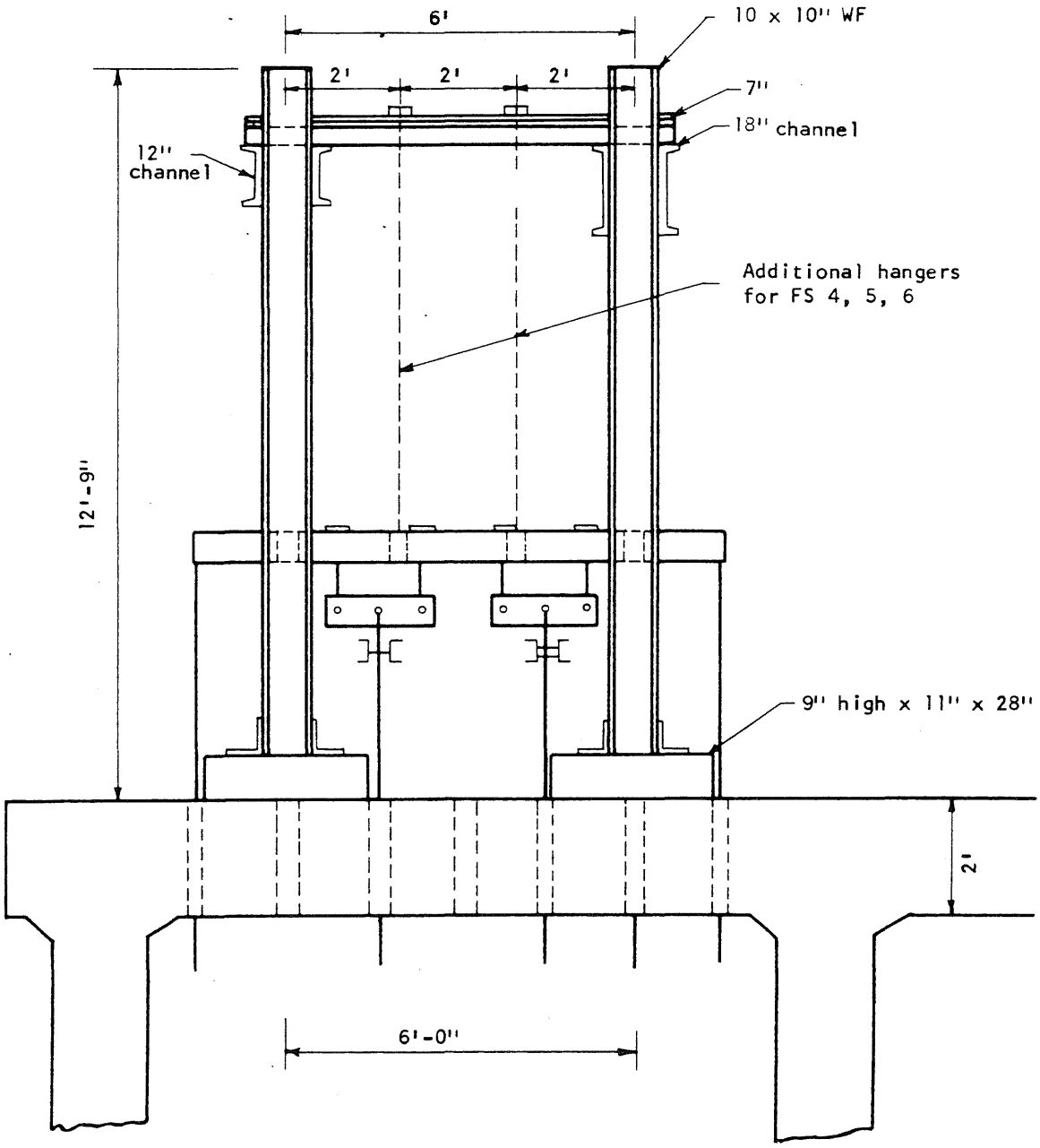

Side Elevation

FIG. 12 REACTION FRAME, VERTICAL AND END BEAM LOADING SYSTEMS

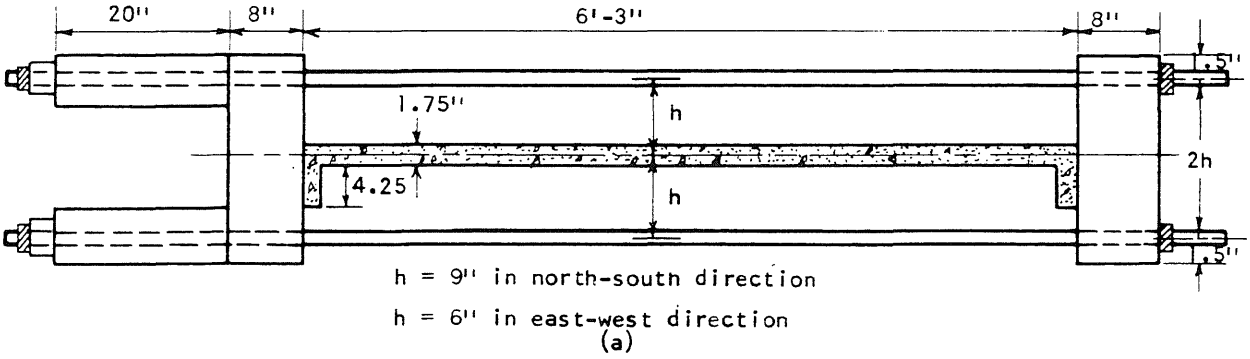

(a)

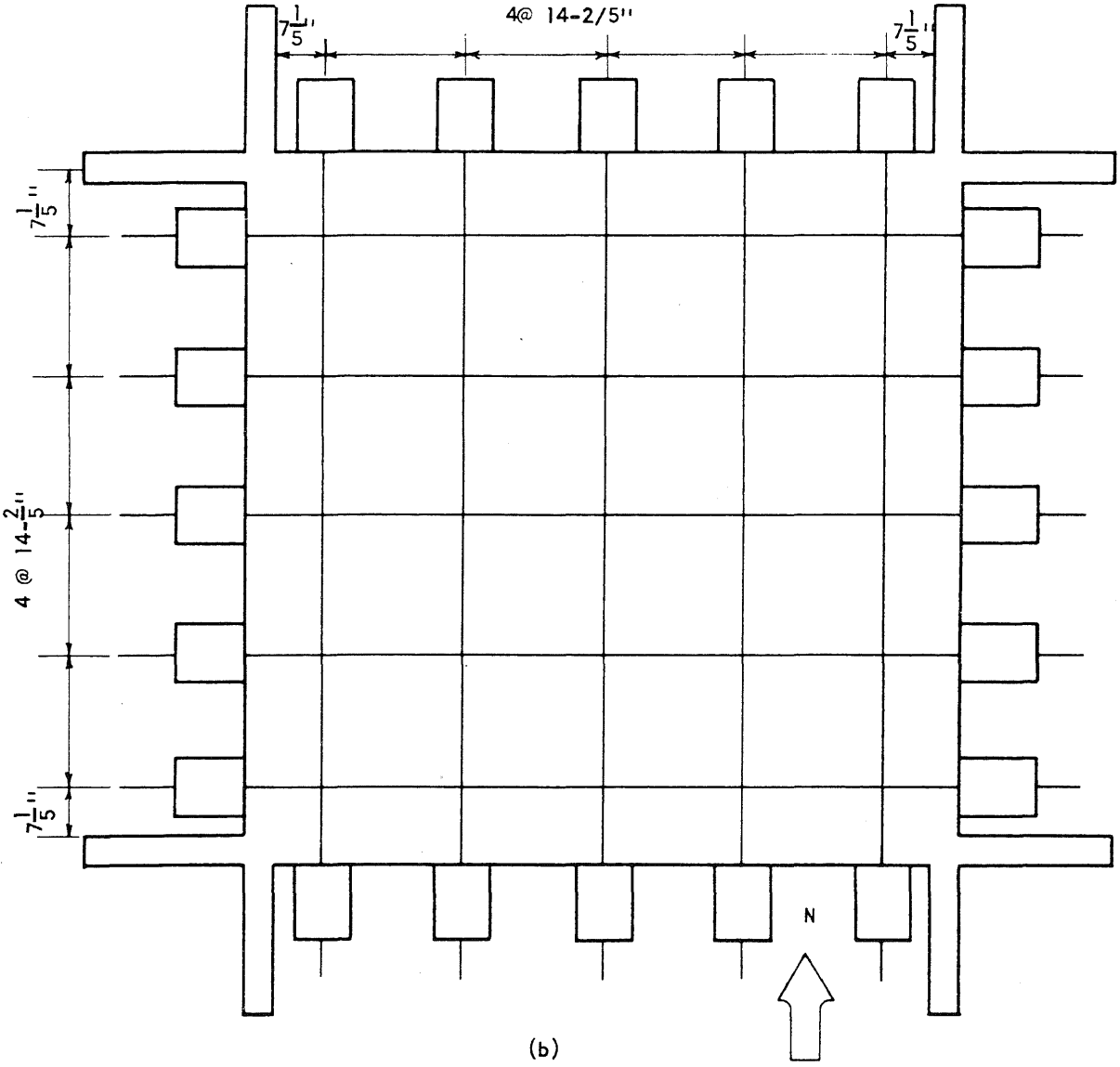

(b)

FIG. 13 HORIZONTAL LOADING SYSTEM

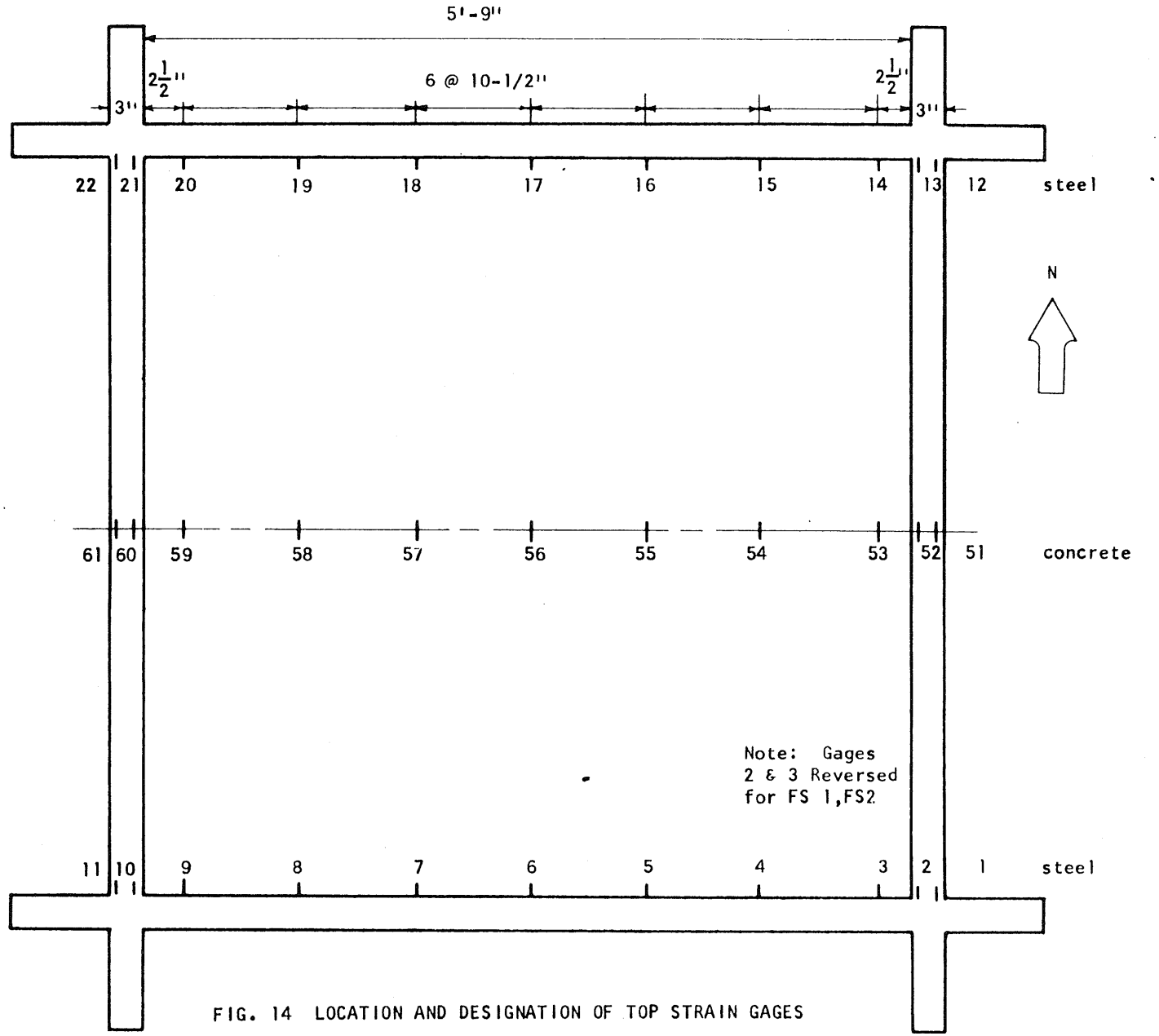

FIG. 14 LOCATION AND DESIGNATION OF TOP STRAIN GAGES

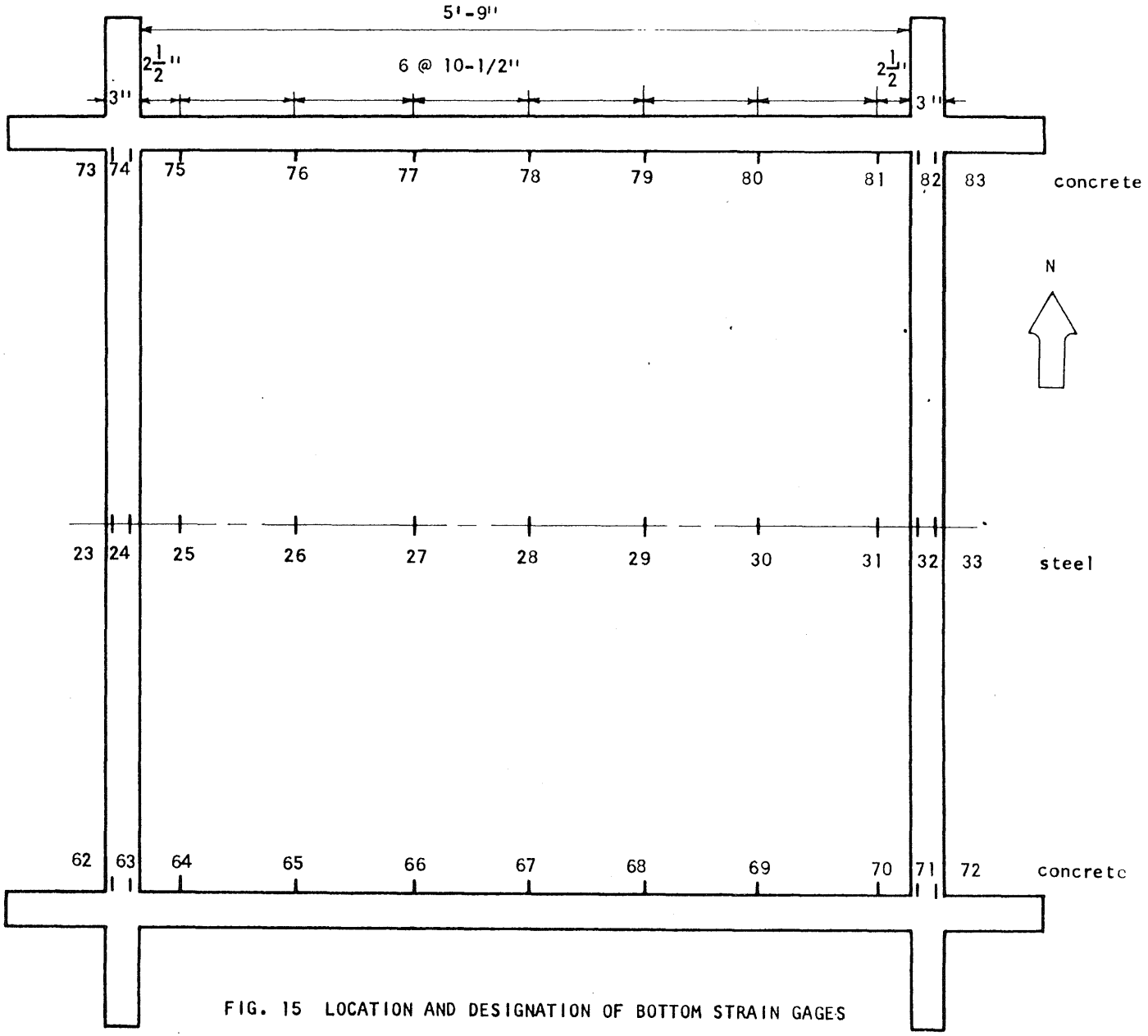

FIG. 15 LOCATION AND DESIGNATION OF BOTTOM STRAIN GAGES

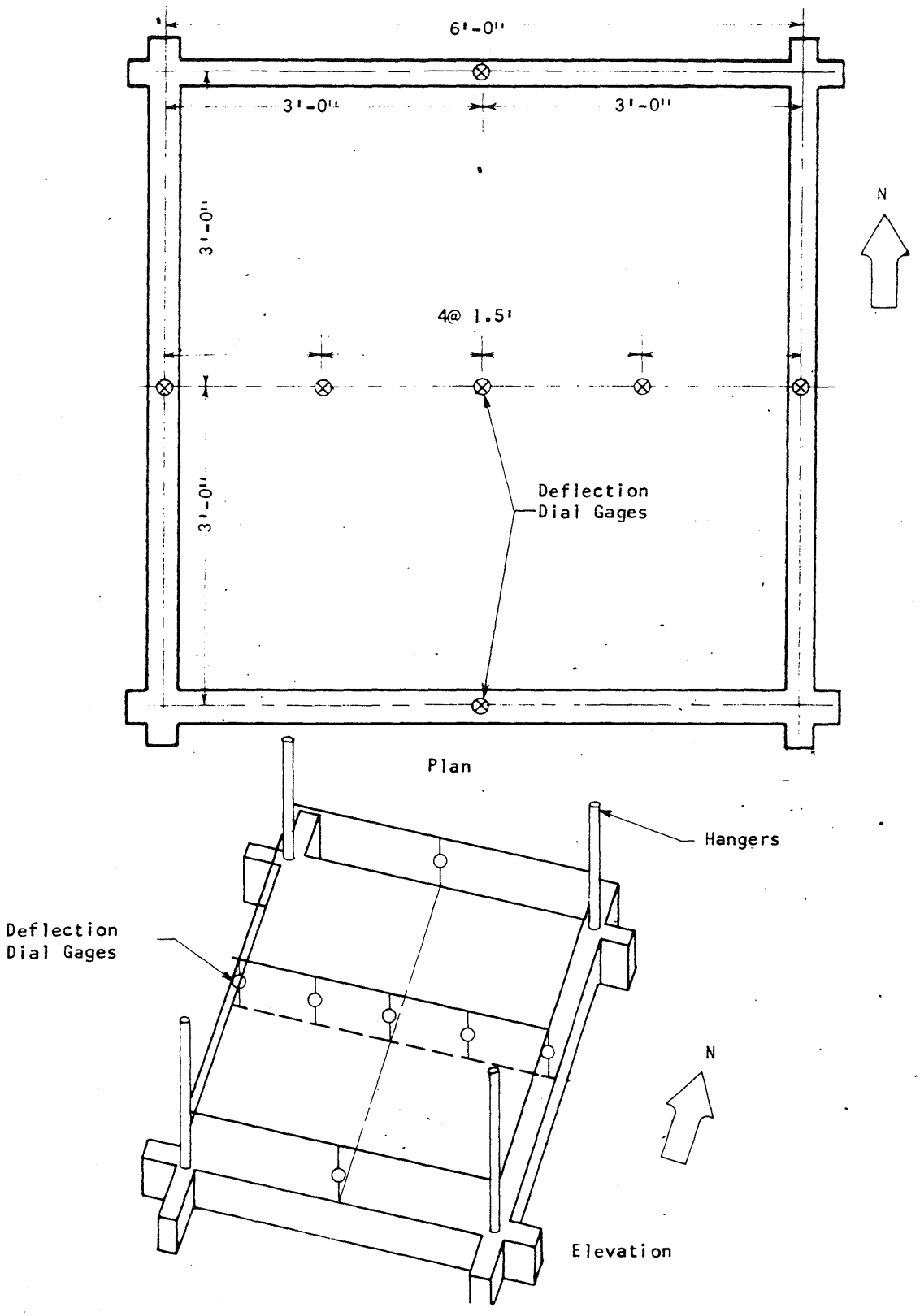

FIG. 16 LOCATION OF DIAL GAGES FOR SPECIMENS FS1, 2, 3

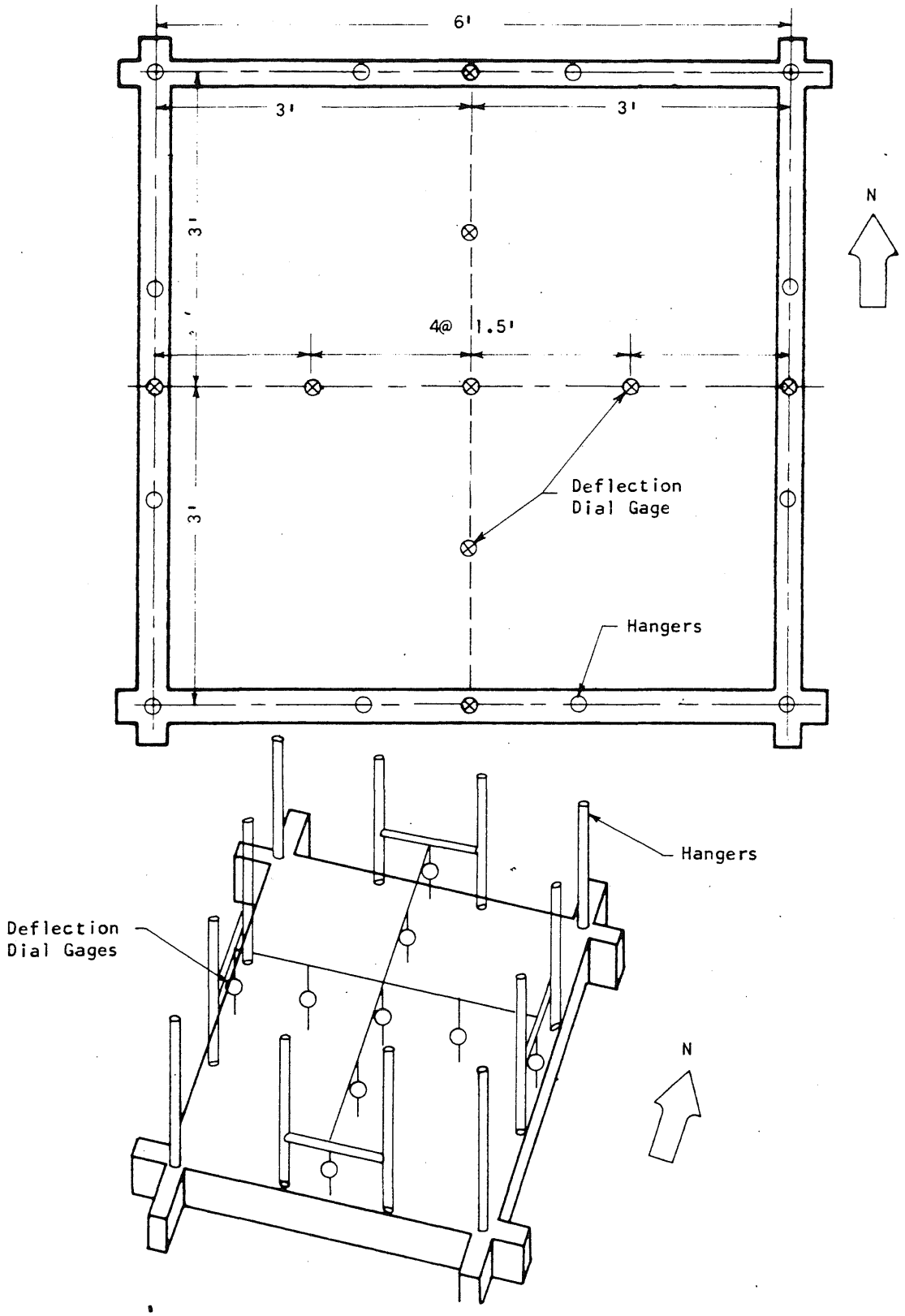

FIG. 17 LOCATION OF DIAL GAGES FOR SPECIMENS FS4, 5, 6

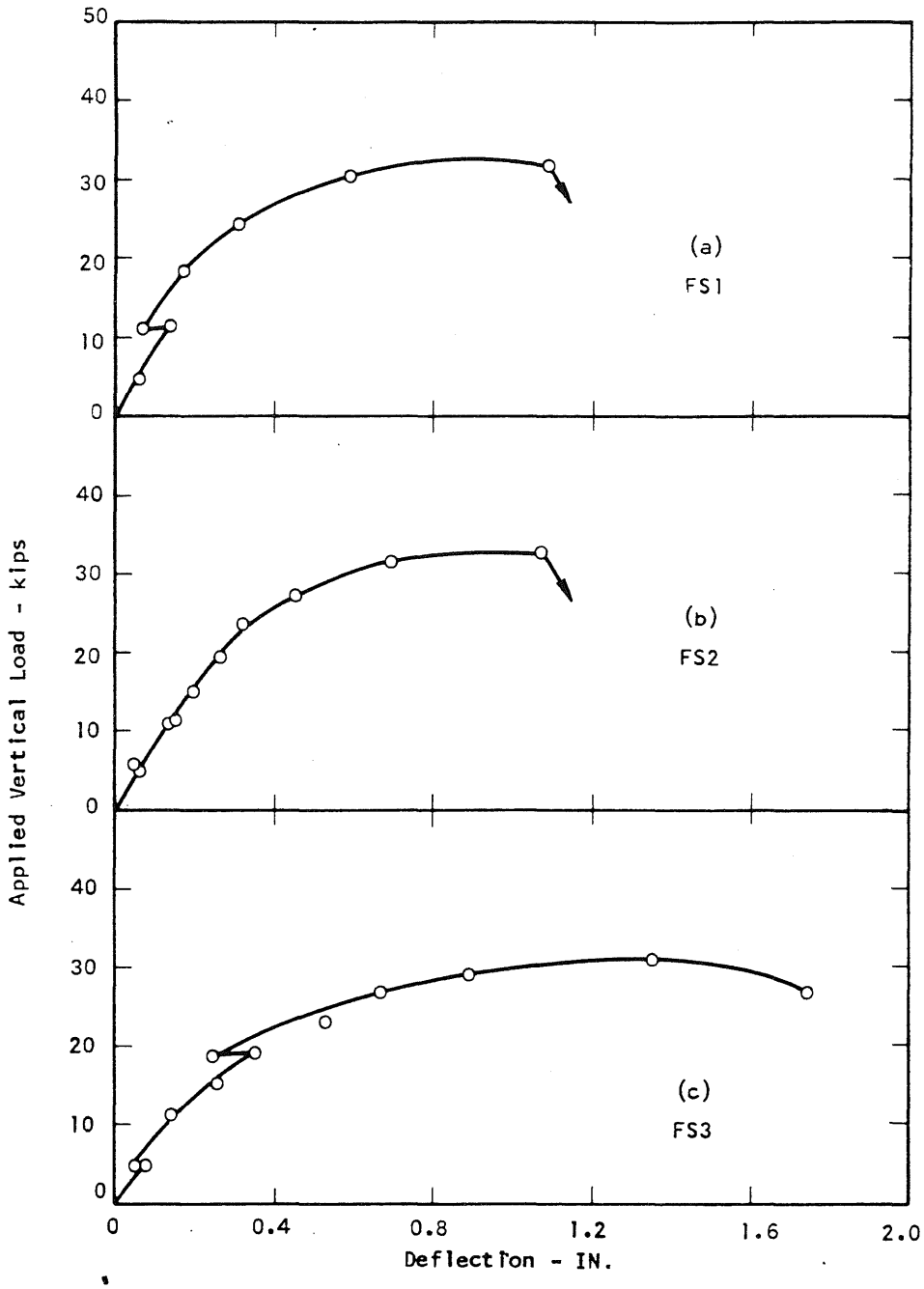

FIG. 18 VERTICAL LOAD vs. CENTER DEFLECTION

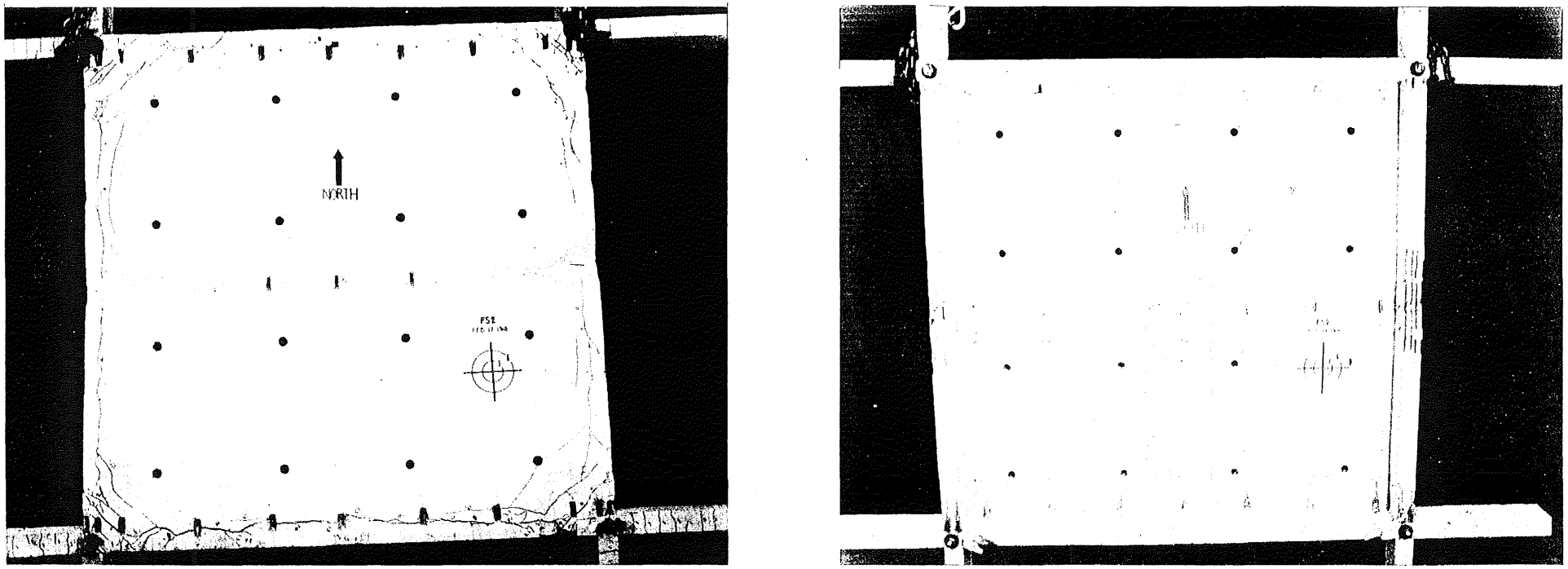

FIG. 19 TOP AND BOTTOM VIEWS OF FS2

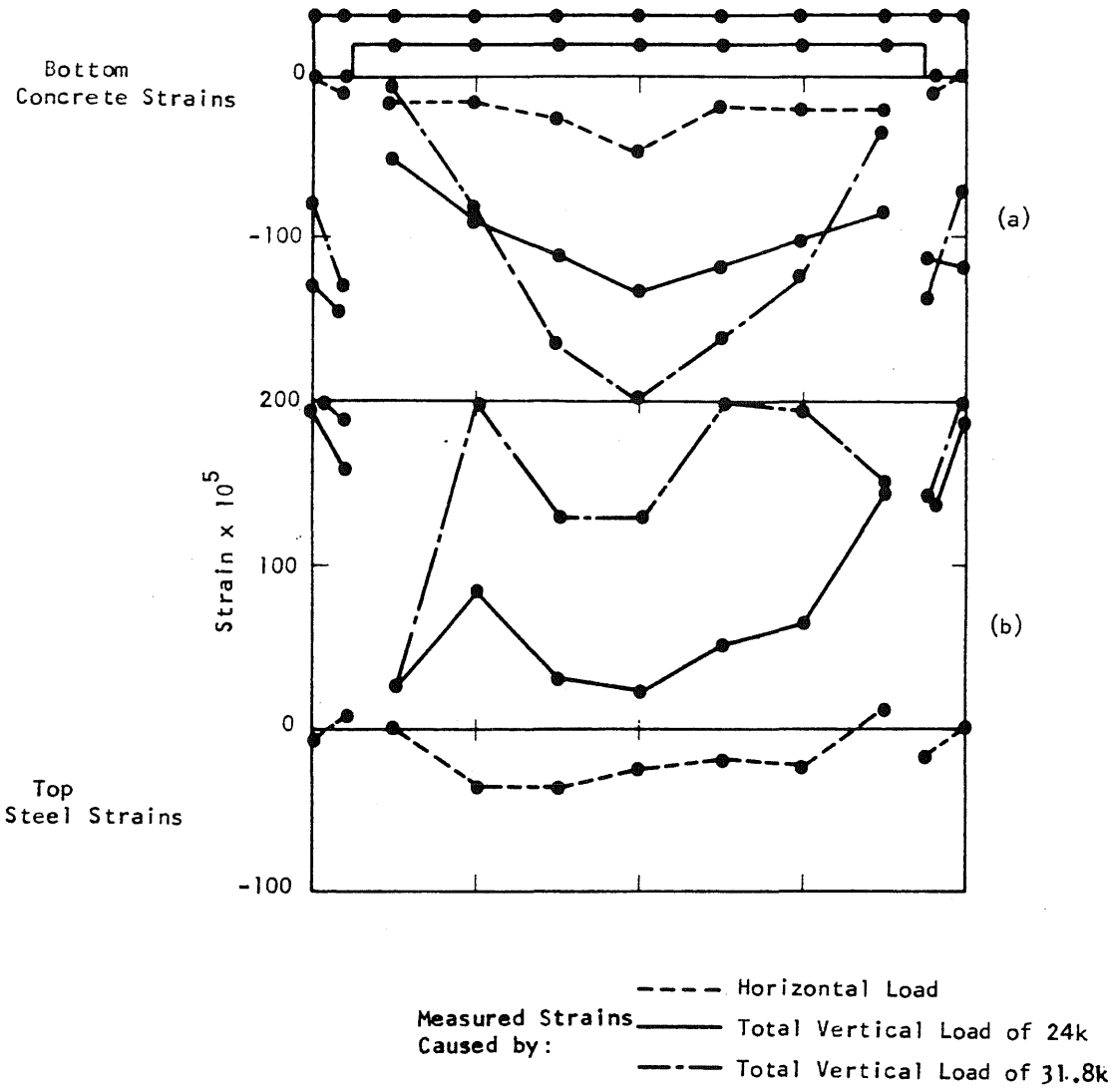

FIG. 20 STRAIN DISTRIBUTIONS AT NEGATIVE MOMENT SECTION, TEST SPECIMEN FS2

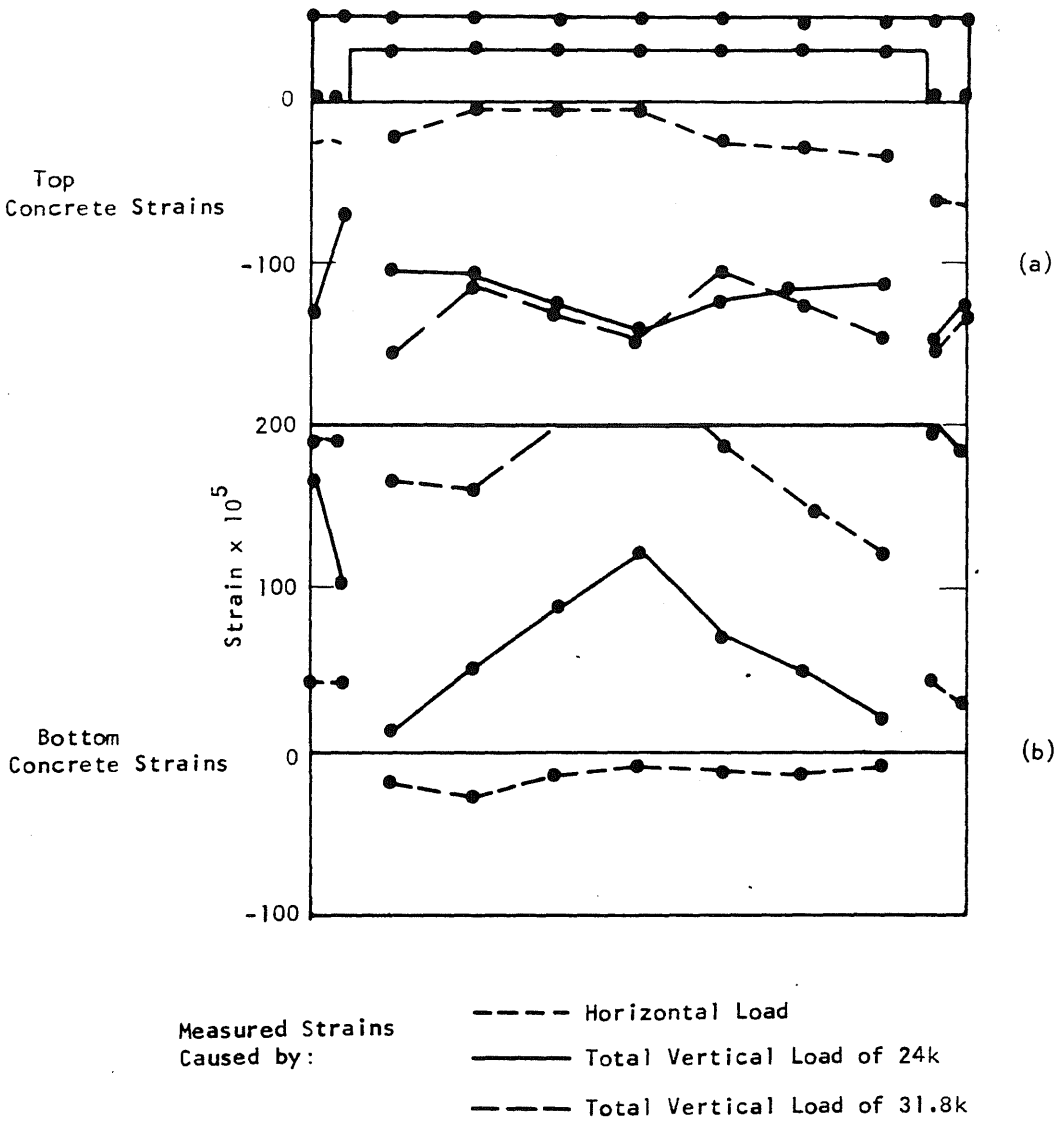

FIG. 21 STRAIN DISTRIBUTIONS AT POSITIVE MOMENT SECTION, TEST SPECIMEN FS2

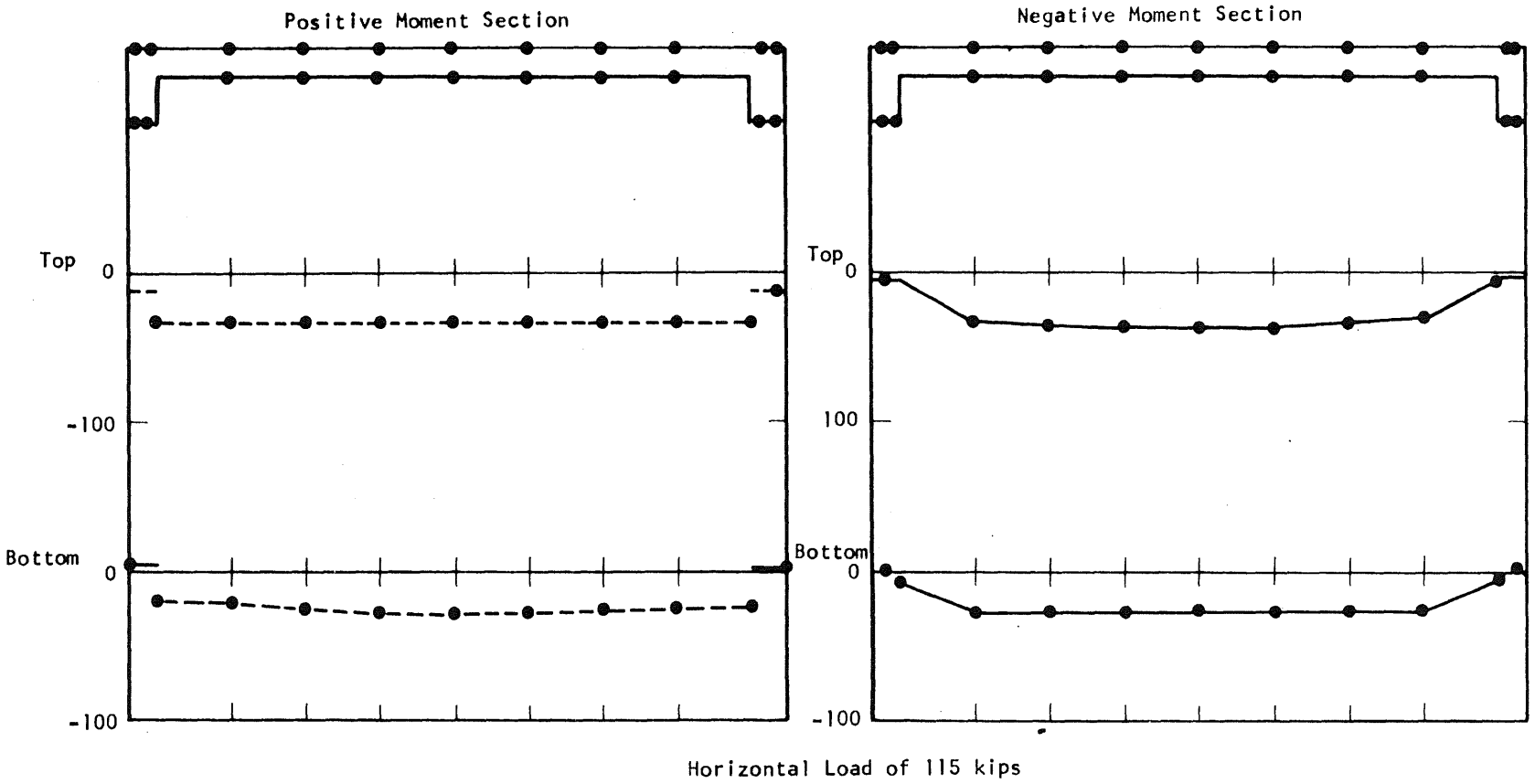

FIG. 22 THEORETICAL STRAIN DISTRIBUTION, FINITE ELEMENT SOLUTION

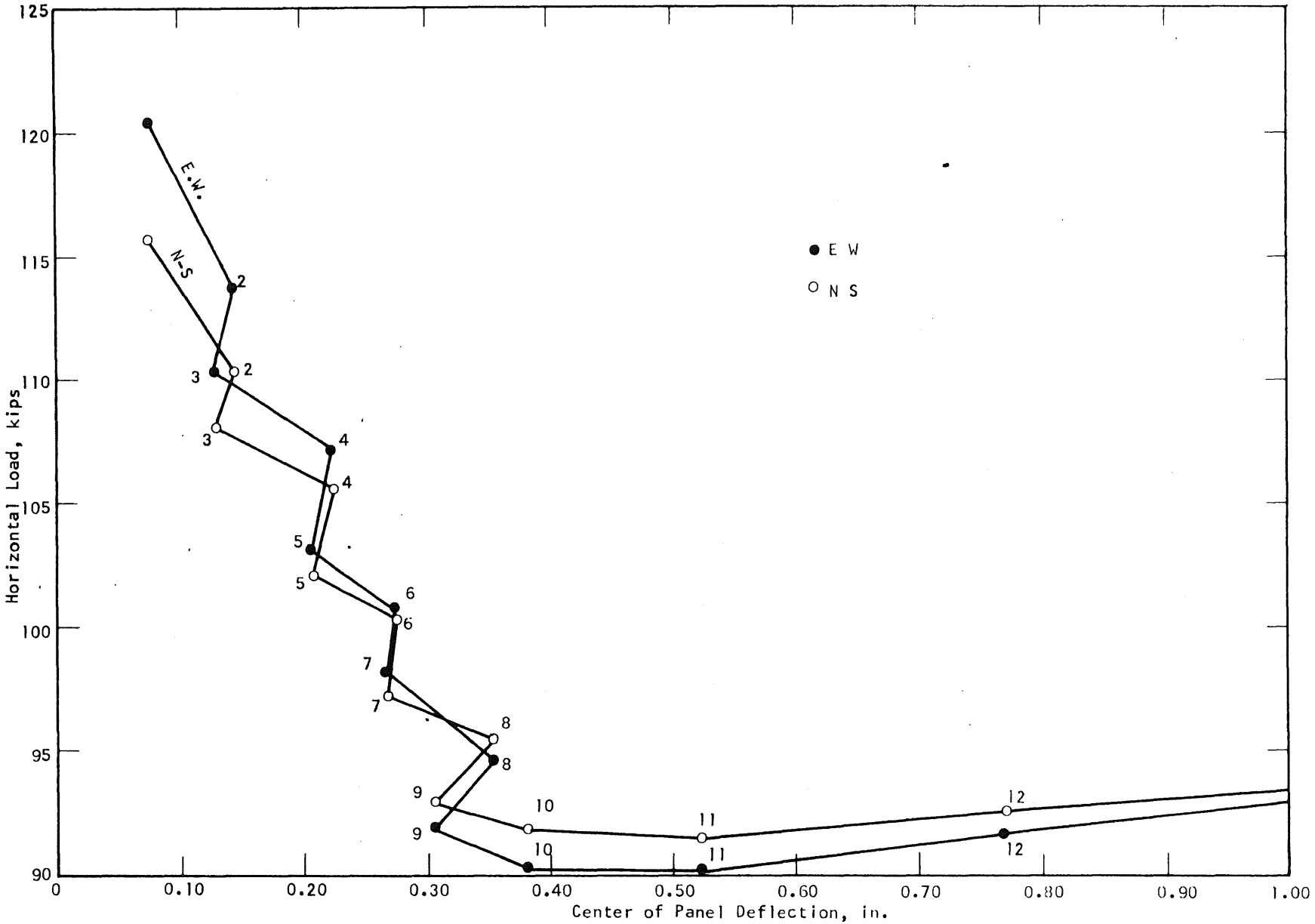

FIG. 23 HORIZONTAL LOAD-DEFLECTION CURVE FOR SPECIMEN FS2

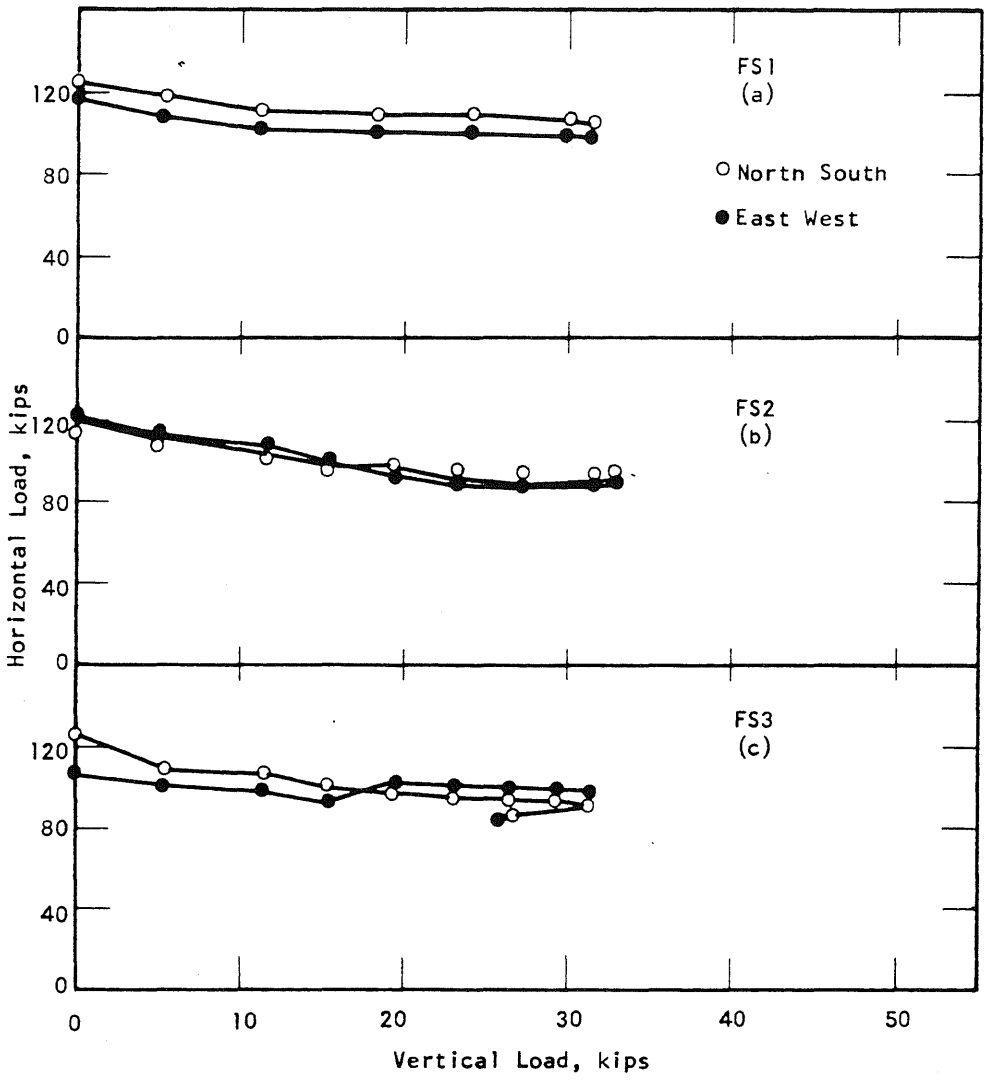

FIG. 24 HORIZONTAL vs. VERTICAL LOAD

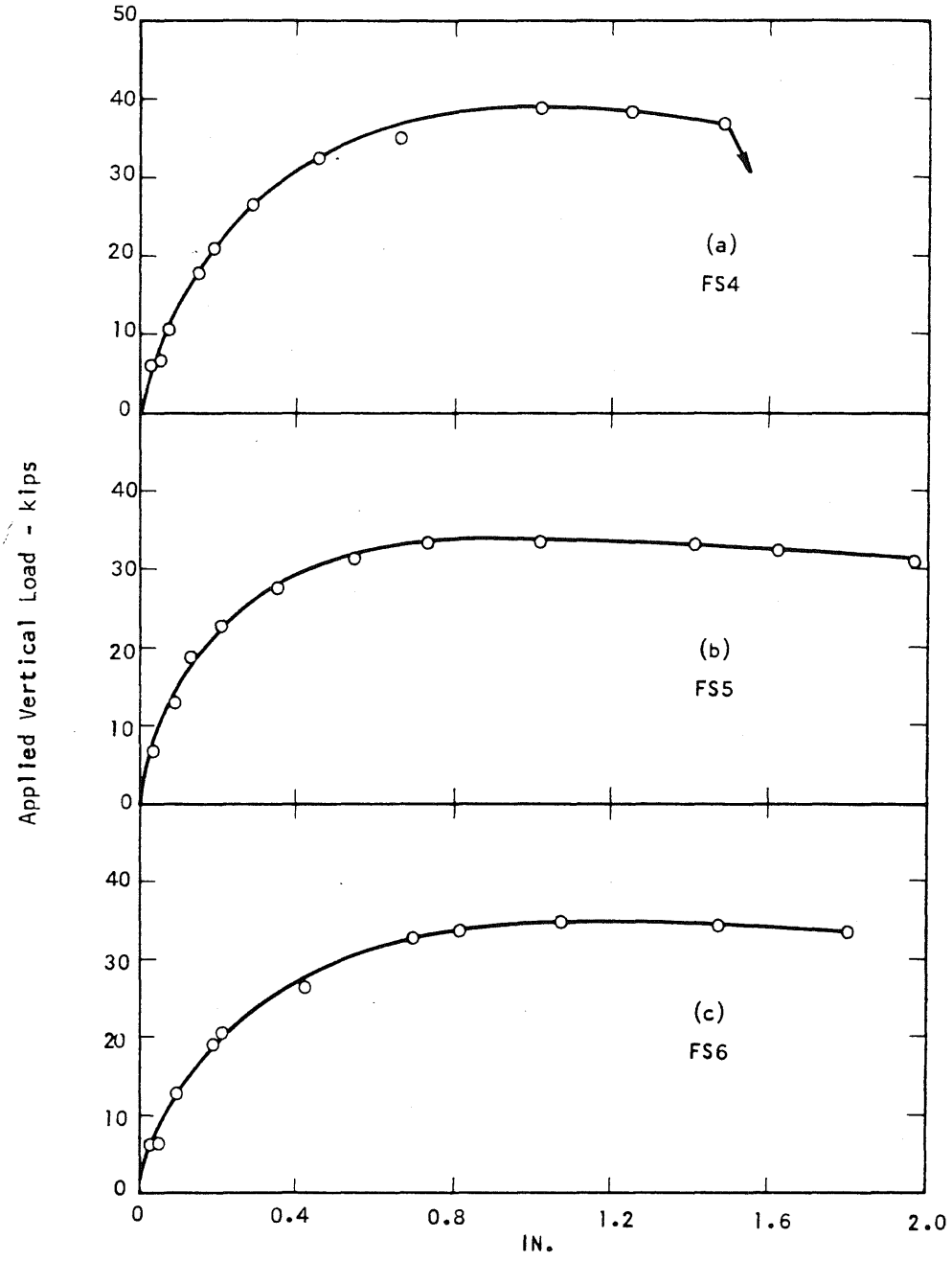

FIG. 25 VERTICAL LOAD vs. CENTER DEFLECTION

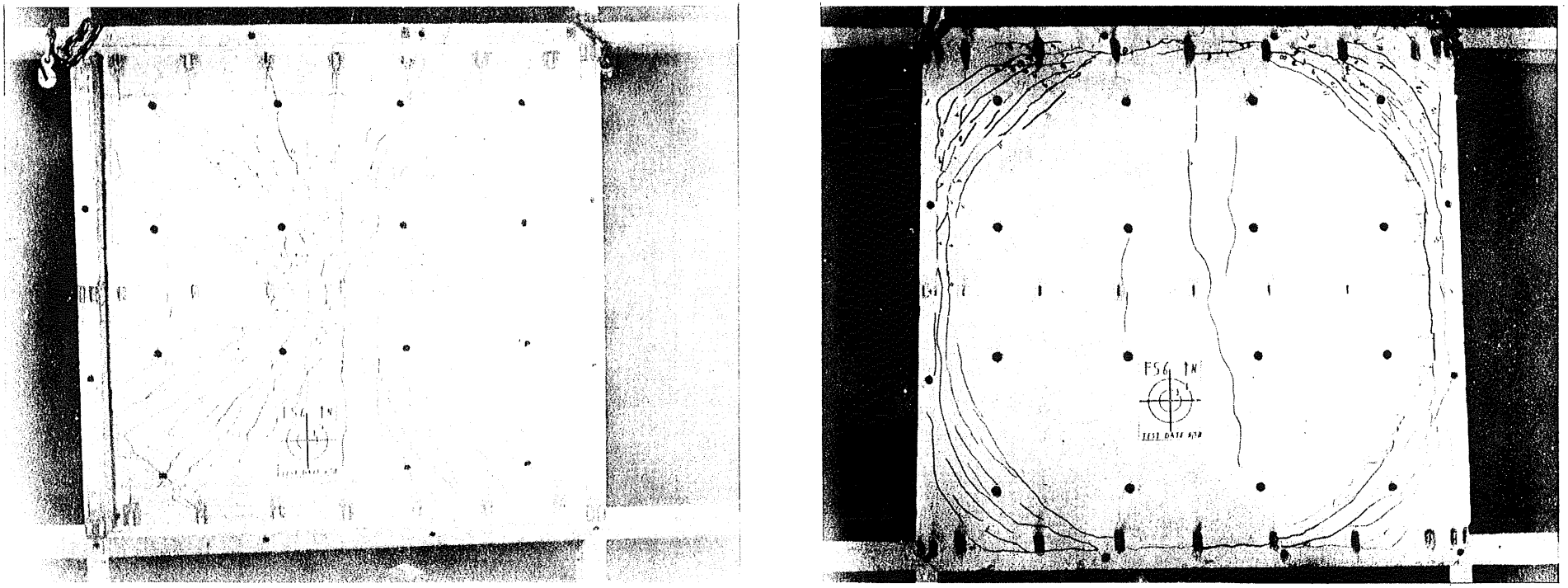

FIG. 26 TOP AND BOTTOM VIEWS OF FS6

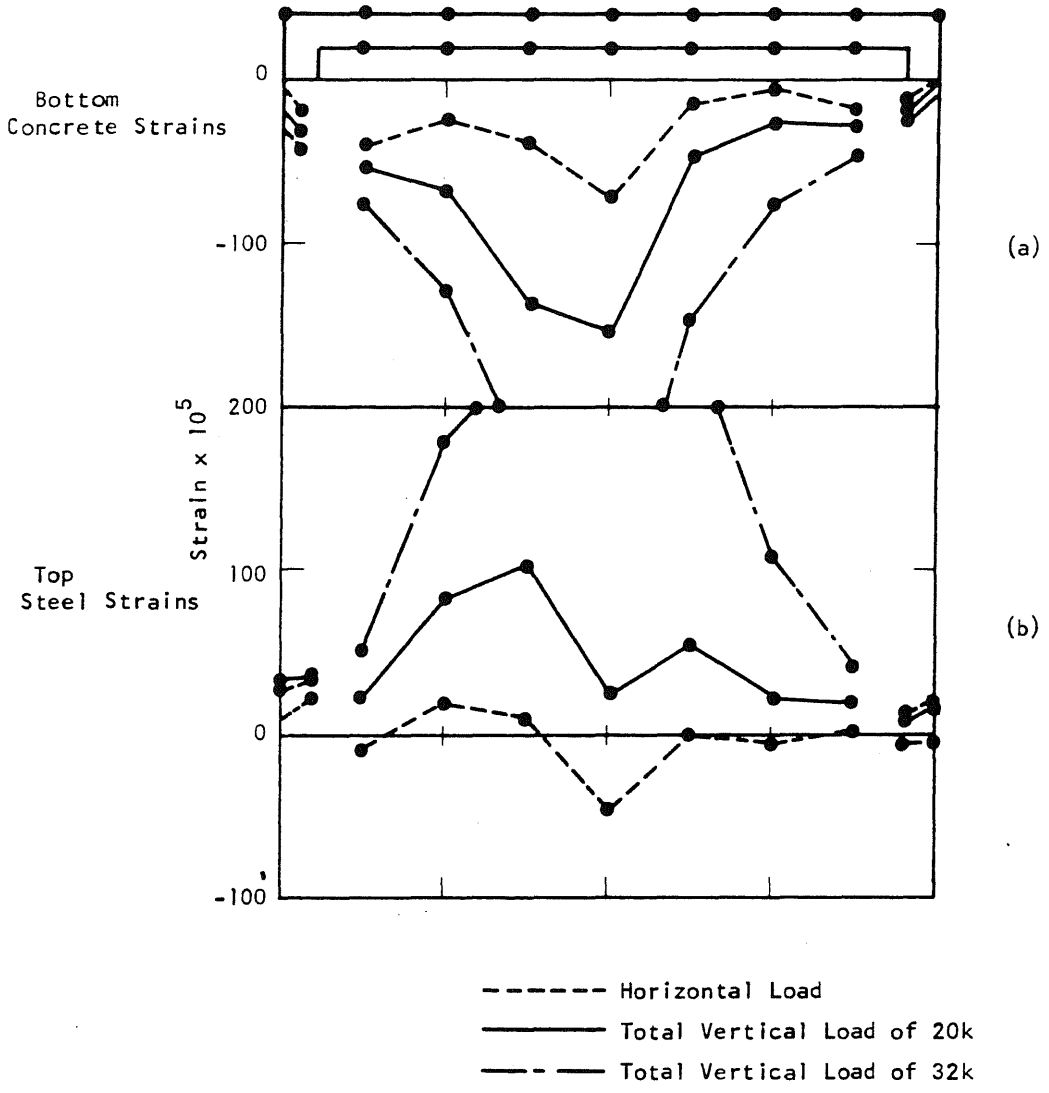

FIG. 27 STRAIN DISTRIBUTIONS AT NEGATIVE MOMENT SECTION
TEST SPECIMEN FS6

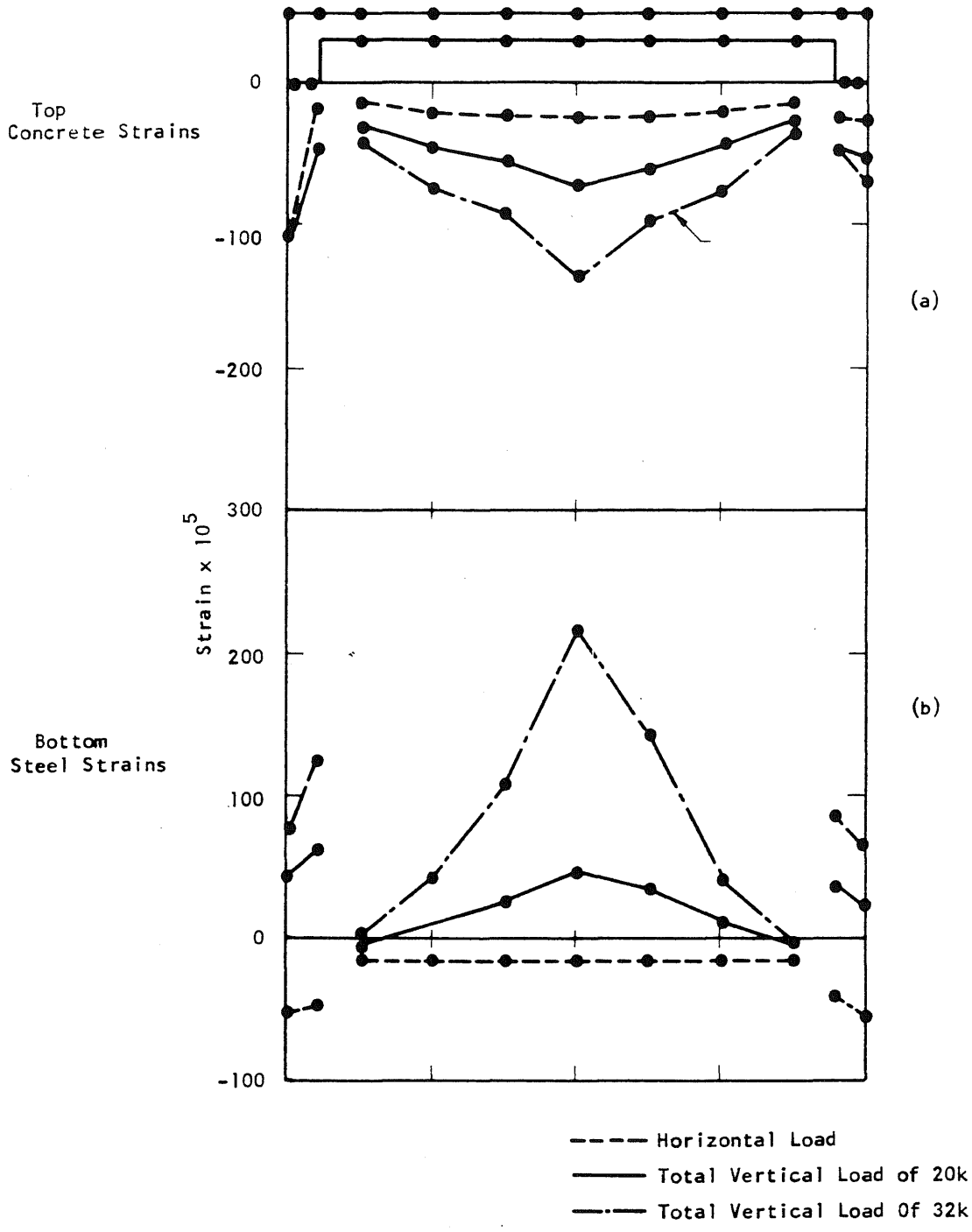

FIG. 28 STRAIN DISTRIBUTIONS AT POSITIVE MOMENT SECTIONS, TEST SPECIMEN FS6

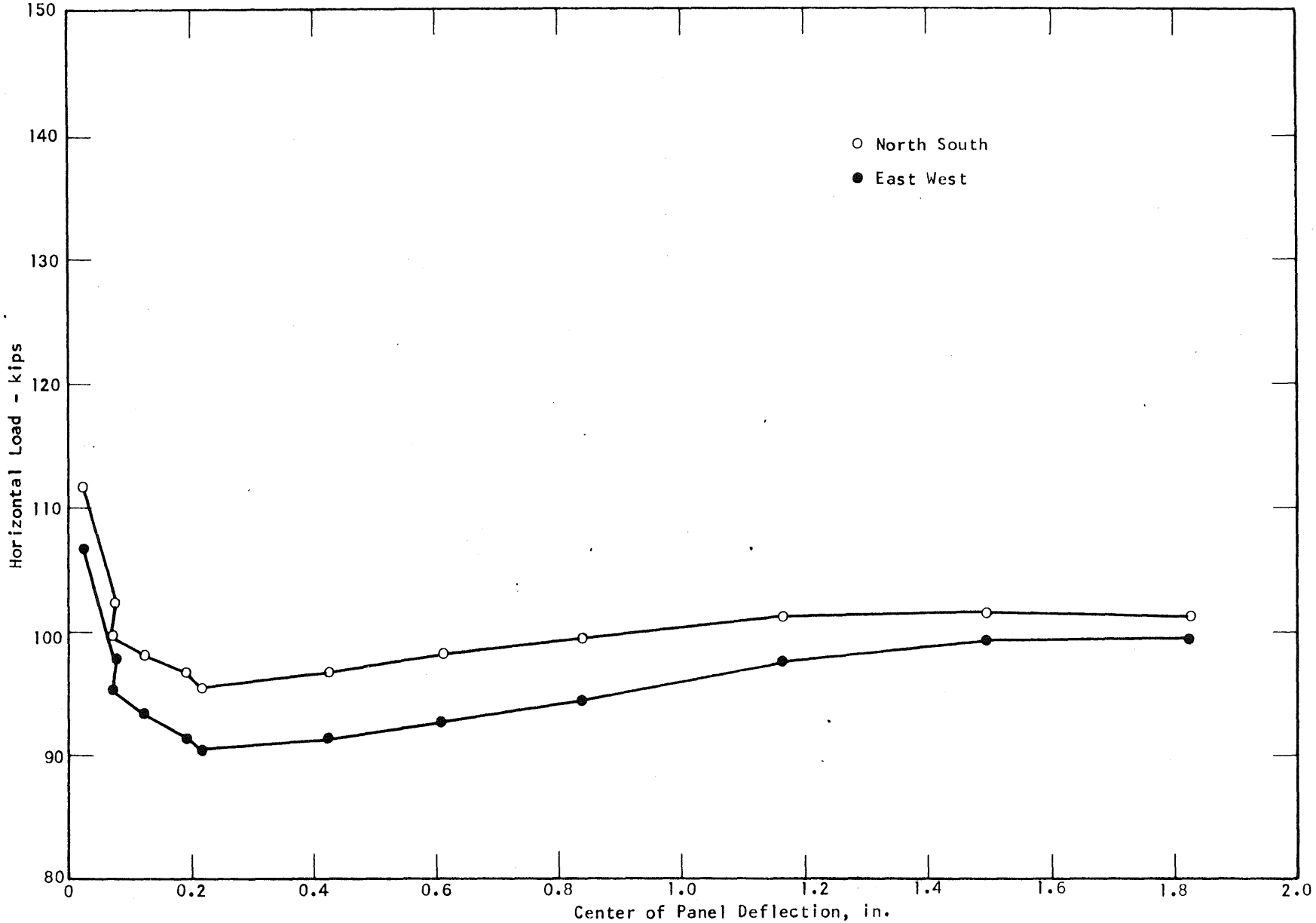

FIG. 29 HORIZONTAL LOAD-DEFLECTION CURVE FOR SPECIMEN FS6

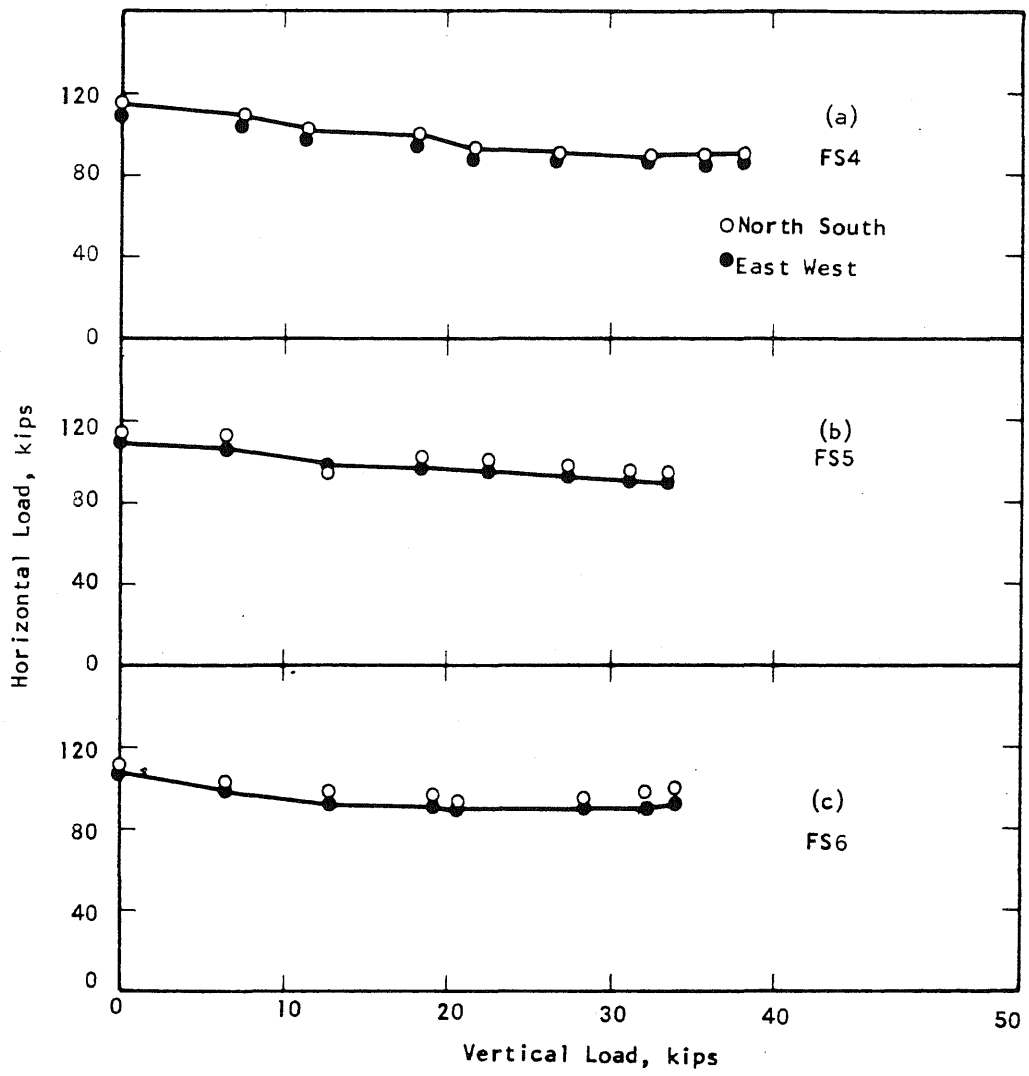

FIG. 30 HORIZONTAL vs. VERTICAL LOAD

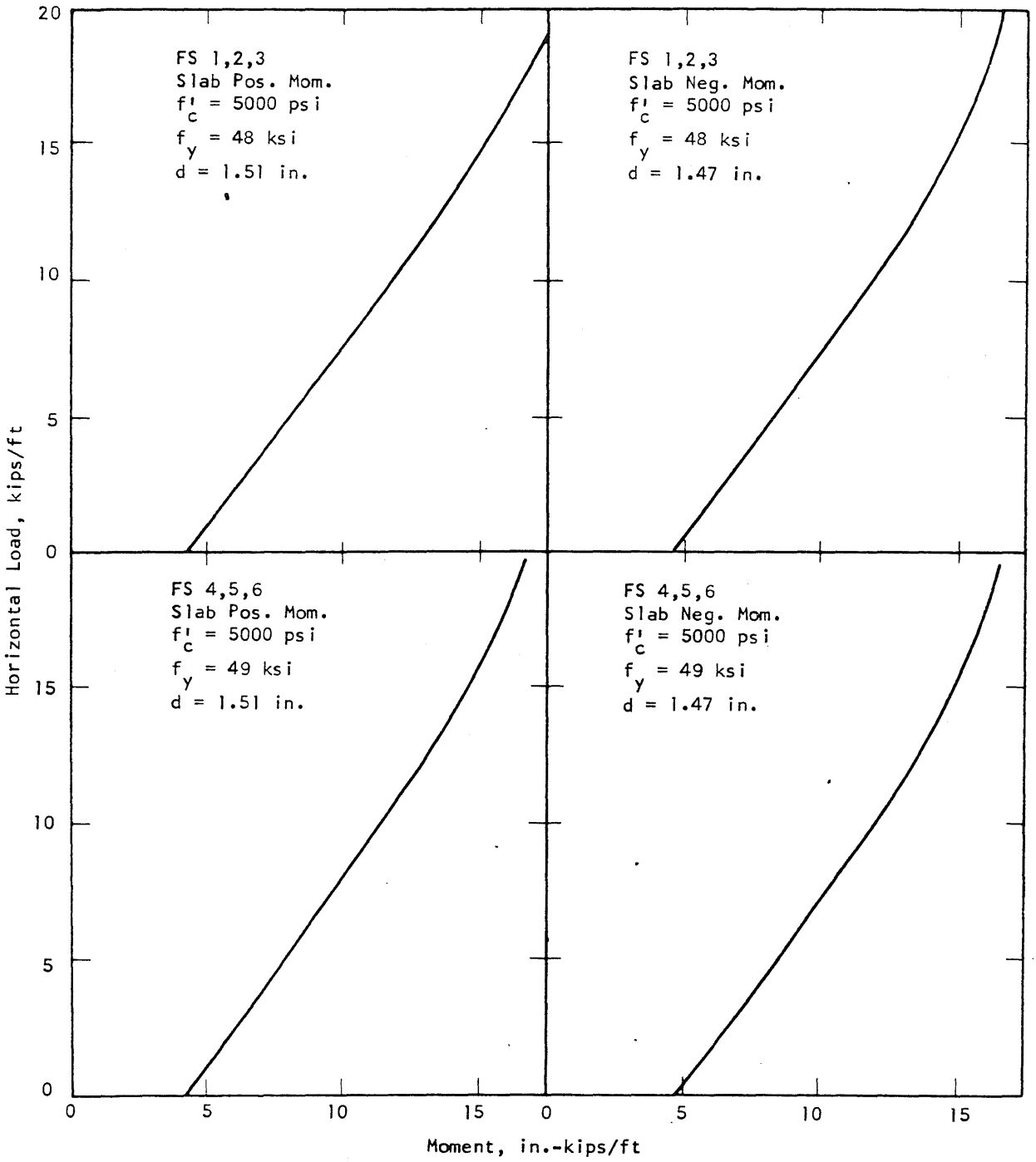

FIG. 31 INTERACTION DIAGRAM FOR CRITICAL SLAB SECTIONS

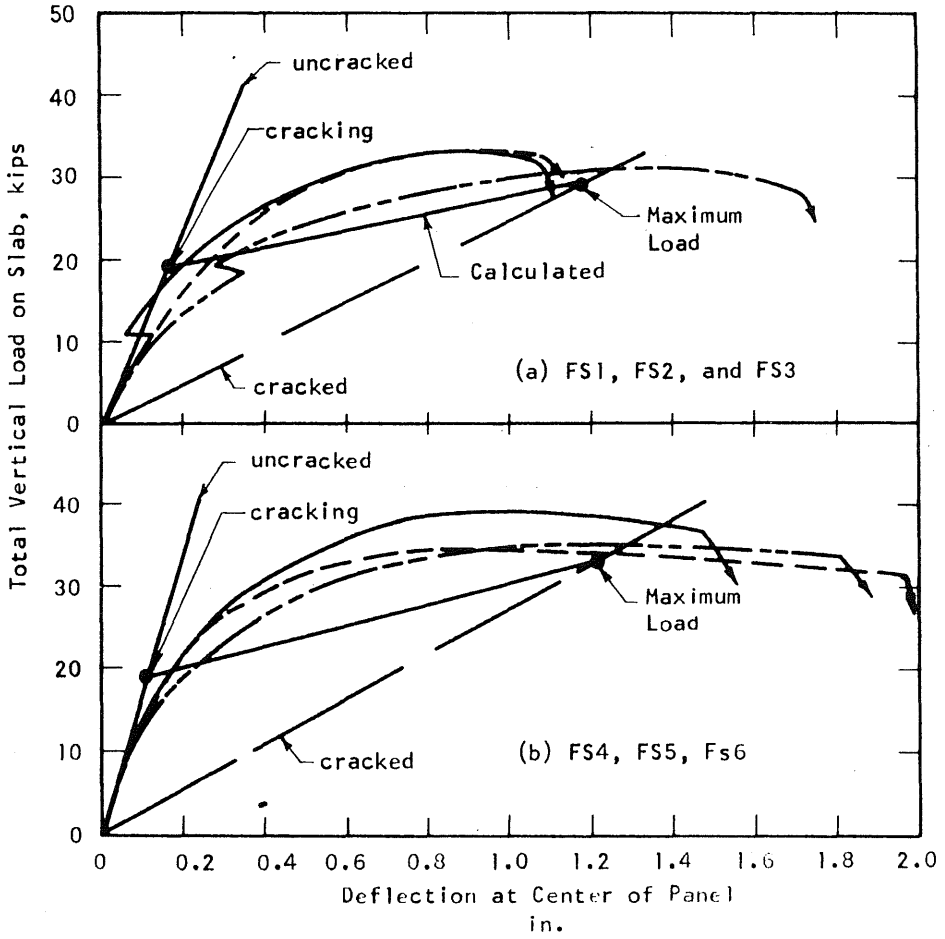

FIG. 32 APPROXIMATION TO LOAD-DEFLECTION CURVES FOR FS1 - 6

STRENGTH OF SLABS SUBJECTED TO MULTIAXIAL BENDING AND COMPRESSION

by

W. L. Gamble
H. Flug
M. A. Sozen

Technical Report to the
DEPARTMENT OF DEFENSE
OFFICE OF THE SECRETARY OF THE ARMY
OFFICE OF CIVIL DEFENSE
Contract DAHC 20-67-C-0136
Subcontract 12472 (6300 A-030)US
OCD Work Unit 1127D

DEPARTMENT OF CIVIL ENGINEERING
UNIVERSITY OF ILLINOIS
URBANA, ILLINOIS
October 1970

TABLE OF CONTENTS

		Page
1.	INTRODUCTION	1
	1.1 General	1
	1.2 Acknowledgements	1
2.	DESCRIPTION OF SPECIMENS	3
	2.1 Dimensions	3
	2.2 Materials	4
	2.3 Formwork, Casting and Curing	6
	2.4 Instrumentation	8
3.	TEST APPARATUS AND PROCEDURE	11
	3.1 Loading and Supporting Systems	11
	3.2 Test Procedure	12
4.	TEST RESULTS	14
	4.1 Determination of Applied Forces	14
	4.2 Determination of Curvatures	15
	4.3 Behavior of Test Specimens	16
	4.4 Measured Moment-Curvature Relationships	19
	4.5 Measured Strains in Reinforcement and Concrete	20
5.	COMPARISONS OF THEORETICAL AND MEASURED RESULTS	22
	5.1 Introductory Remarks	22
	5.2 Theoretical Moment-Curvature Relationships	22
	5.3 Discussion of Test Results	22
6.	SUMMARY AND CONCLUSIONS	28
7.	REFERENCES	30
TABLES		31
FIGURES		34

1. INTRODUCTION

1.1 General

Tests to failure of slab structures have shown, on many occasions, that the available load capacity may be much greater than would be indicated by the results of conventional yield-line analyses. Two tests may be referred to in order to demonstrate the problem. Ockleston (5)* reported the test of a large reinforced concrete building in which a single interior panel supported a load of 753 psf, while the computed capacity was 295 psf. Gamble (6) reported that the interior panel of a nine-panel test structure failed at an applied load of 829 psf while the theoretical capacity was 426 psf.

In each case the parts of the structure surrounding the loaded panel were able to restrain the lateral movements of the edges of the panel, and consequently, significant forces were developed in the plane of the slab. In the first instance the deflections were small and in-plane compression forces were developed. In the second case, the deflections were very large and in-plane tension forces were developed.

The work in this report is concerned with the influence of known in-plane compression forces on the response of the slab cross-section, and was undertaken as a phase of an investigation into the strength of reinforced concrete floor slabs which are loaded into the inelastic phase of behavior. Six slab specimens were constructed and tested in order to provide quantitative checks on the influence of in-plane compression forces on the strength and behavior of slab sections which are subjected to multiaxial bending forces.

---

* Numbers shown in parentheses refer to entries in the References.

The specimens, shaped as shown in Fig. 2.1, were loaded to produce uniform bending moments in all directions in the central portion of the specimens. Two different reinforcement ratios, 0.01 and 0.005 were used to represent the normal range of reinforcement ratios in slabs, and three different levels of externally applied compressive force were applied to the slabs for each reinforcement ratio.

The principal aim of these tests was to demonstrate that the strengths of the slab sections could be satisfactorily predicted on the basis of calculated bending moment-thrust interaction diagrams for the appropriate concrete sections. This was necessary to provide a tool for predictions in cases in which the axial compression forces were developed as a result of inelastic deformations rather than being directly applied.

1.2 Acknowledgements

The work reported here was part of an investigation of the Structural Interaction of Building Members carried out in the Structural Research Laboratories of the University of Illinois, Department of Civil Engineering, under the sponsorship of the Department of Defense, Office of the Secretary of the Army, Office of Civil Defense, under contract DAHC 20-67-C-0136, Subcontract 12472 (6300 A-30)US, OCD work unit 1127D.

Acknowledgement is extended to J. J. Salinas-Pacheco, A. E. Fiorato, and A. E. Girolami, Research Assistants in Civil Engineering, for their invaluable aid in the conduct of the tests and the study of the data.

2. DESCRIPTION OF SPECIMENS

2.1 Dimensions

The "circular" specimen has been successfully used in an earlier investigation (1) in obtaining a uniform moment over the test area.

Since the object of this investigation was to determine the effects of in-plane axial compression forces on the behavior of the slab, in-plane compression forces, in addition to the bending moments, were imposed on four of the test specimens. These forces were applied by means of cables which passed through ducts in the slabs.

The specimen is shown in Fig. 2.1. The test area is within the 3 ft diam circle in the center of the specimen. The test slabs were supported along the 3 ft 6 in. diam inner circle and loaded with downward forces on the 6 ft diam outer circle. The loading area contained six evenly placed slots to minimize the membrane forces outside the test area.

The thickness of the specimens was approximately four inches. The thicknesses were measured at 15 points within the test area of each slab. Average values for the thickness were used in computations, and are listed in Table 2.1.

The reinforcement ratio was one of the variables considered in the tests. Three specimens, marked FC1, had reinforcement ratios of 0.01. The other three, marked FC5, had reinforcement ratios of 0.005, as shown in Table 2.1. The reinforcement consisted of tension steel only. Figs. 2.2 and 2.3 show the placement of steel for specimen FC1C. Bars in specimens with the higher steel percentage were placed in pairs to facilitate fabrication and improve conditions for casting and vibration of the concrete.

The steel consisted of two layers of No. 2 deformed bars placed in perpendicular directions within the test area, as shown in Fig. 2.3.

The loading areas of the wings were reinforced with supplementary U-shaped No. 3 bars to prevent failure of the specimens in the loading area, as can be seen in Fig. 2.2.

Ducts which were 5/8 in. diam were formed in the slab to permit installation of the 1/2 in. prestressing strands used for applying the axial compression forces. Running from diametrically opposite wings, the cables crossed in the center of the slab, as shown in Figs. 2.1 and 2.2. Although it was desired to place these openings, (and hence the axial load) at the plastic centroid of the section, it was necessary to place one opening above and one below this position, as is shown in Fig. 2.4. The ducts were straight.

The horizontal forces were applied through ducts through the slab rather than by external means, such as large horizontal clamps, so that there would be no changes in eccentricity of the force as the slabs deflected.

2.2 Materials

a) Concrete

Since it was desired to obtain results which could be compared with previous works, the mix was the same as used in other investigations (1) conducted in the laboratory. Atlas brand, Type III, high-early strength cement was used. Wabash River sand and pea gravel was used in all specimens. The maximum size of the gravel was 3/8 in. These aggregates have been used in this laboratory for many previous investigations. The origin of the aggregates is an outwash of the Wisconsin glaciation. The major constituents of the gravel were limestone and dolomite. The sand consisted mainly of quartz.

No attempt was made to obtain the moisture content of the aggregates before each casting. Reductions were made in the mix water when the moisture content of the aggregate was excessive.

Table 2.2 lists the average compressive strength, average tensile strength from split cylinder tests, slump, and age of specimen at time of testing. The mix proportions were approximately 1:2.7:3.0, cement;sand:gravel, by weight, for all specimens, and the water-cement ratios were about 0.6 in each case.

The mix was designed for a nominal 7-day compressive strength of 5000 psi; the actual strengths at the time of testing varied from 5420 to 7370 psi. The compressive strength was determined from tests on 6 by 12 in. control cylinders. Splitting strengths were found from tests on 6 by 6 in. control cylinders. Strips of stiff fiber-board of 1/8 in. thickness were placed between the sides of the cylinder and heads of the testing machine to distribute the load evenly along the length of the specimen during the splitting tests. The control cylinders were taken from each of the concrete batches to give representative samples of the concrete placed throughout the specimen.

b) Reinforcing Steel

No. 2 deformed reinforcing bars were used. This steel was purchased from the Triangle Steel and Supply Company of Los Angeles, California and was annealed at 1200^{o}F for two hours by the Fred A. Snow Company of Chicago.

The yield stress and approximate stress-strain diagram were obtained from tension tests of samples with five in. effective lengths, performed on a Tinius Olsen testing machine with an attached load-time plotter. The elongation indicated by the charts included the slippage of the specimen in

the grips. The stress-strain relationship, including modulus of elasticity and initiation of strain hardening, were obtained using a mechanical strain indicator with a two in. gage-length. Several values obtained by this means substantiated results on specimens from the same shipment performed by R. Lenschow (1). This steel gave a nearly elasto-plastic stress-strain relationship to a strain of about 0.02, as shown in the representative stress-strain curve of Fig. 2.5.

A significant variation in the yield stresses was observed between bundles of steel and between ends of a given bundle. A representative sampling was made for each specimen and an average yield stress found. An attempt was made to use, for any one specimen, a bundle of steel with a constant yield stress. Tests indicated a modulus of elasticity of 30×10^6 psi. The yield stresses are tabulated for each specimen in Table 2.2.

2.3 Formwork, Casting and Curing

The test specimens were cast in forms with a plastic-coated plywood bottom and steel sides. Holes were formed in the specimen for the loading and supporting rods by screwing 4-in. long pieces of steel pipe to the form bottom. Plates welded to these 1-7/8 in. diam pipes formed tear-drop shaped holes in order to permit greater deformations of the specimen than circular holes alone would allow.

The reinforcement was placed in the form and supported on short pieces of No. 3 bars which provided the minimum cover of 3/8 in.

Wooden triangular-shaped blocks were clamped into the apex of each wing to block off this point. This provided a flat surface against which the axial jacking force could be applied. Holes were drilled through these blocks to permit the insertion of greased 5/8 in. cold-rolled steel rods through diametrically opposite wings. These holes were at a depth corresponding to

either the plastic centroid or 5/8 in. above or below it. These rods were removed before the final setting of the concrete and eventually replaced by cables before testing of the specimens. The rods and blocks can be seen in Fig. 2.2.

The concrete for slabs FC1A and FC1B was mixed in a non-tilting drum-type mixer. The first two specimens were cast using three batches of concrete. Three wings were cast first, then the test area, and finally the remainder of the loading areas. Three 6 by 12 in. cylinders for determining compression strength and two 6 by 6 in. cylinders for splitting strengths were cast from each batch.

A 1/2 cu yd capacity pan-type mixer was used for the remaining specimens, permitting casting each specimen with one batch of concrete. Six compressive strength control cylinders and five tensile-splitting strength control cylinders were cast for each of these specimens. The concrete in the test specimen as well as in the control cylinders was vibrated with a high frequency internal vibrator. The top surfaces of the test specimens were troweled smooth, and the pipe inserts and the steel rods forming the horizontal ducts removed two to four hours after casting. The cylinders were capped with either neat cement or Hydrocal before testing. The forms for the specimens were struck the day after casting and the specimens were then covered with wet burlap and polyethylene film. The control specimens were also stripped at this time and placed under wet burlap and polyethylene film. The specimens were kept under the wet burlap for at least two days. The specimens were cast with the reinforcement near the lower face, and were turned over before testing.

2.4 Instrumentation

a) Electrical Strain Gages on Reinforcement

One reinforcing bar in each layer of reinforcement was instrumented with electric strain gages placed within the test area. Five gages spaced at 7 1/2 in. intervals along each bar gave the strain distribution along a diameter of the test specimen. Budd HE-111 Metal-foil gages were used.

The surface of the reinforcing bar was prepared for the mounting of the gage by grinding down one rib of the deformed bar. The surface was then cleaned using emery cloth and acetone. Before mounting the gage with Eastman 910 cement, the bar was treated with a metal conditioner. The lead wires were soldered to the gages before the gages were waterproofed with an air-curing silicone-rubber caulking compound applied over a thin coating of wax which was brushed onto the gage while melted.

The gages were located as shown in Fig. 2.6.

b) Electric Strain Gages on Concrete

Concrete strains were measured on the compression face of the specimens with SR-4, Type A1-S6 bonded-wire paper gages. Thirteen gages were placed on the concrete surface in the locations shown in Fig. 2.7.

The concrete surface at the location of a gage was smoothed with sand-paper and then cleaned with acetone. Eastman 910 cement was used to bond the gages to the concrete.

c) Mechanical Dial Gages

The curvatures of the specimens were obtained from deflections along a gage line using equally spaced dial gages which were supported on a light-weight steel bridge. Two types of bridges were used; 5 dial gages spaced 7.5 in. apart, and 3 dial gages 3 in. apart.

The larger two bridges were used to obtain curvature in two directions. The bridges "hung" under the specimen from diametrically opposite "notches" and gave deflections relative to the edges of the slab. The location of the gages was as shown in Fig. 2.8. Gages 1 through 5 were supported from the same steel bar, and gages 6 through 9 were supported from a second bar. The deflections relative to the edges of the slab were thus measured at five points along one diameter and at four points along the second diameter.

Three small bridges were welded together to form a triangle. This moveable triangular bridge was placed in the center of the top surface and curvatures in the central portion of the slab, in three directions, could be obtained. These deflections were measured relative to the fixed corners of the triangle which were 12-in. apart. Deflections were measured in 0.001 in. divisions in both types of bridge.

d) Slope Measurements

The slopes of the wings were monitored during the tests by means of a machinist's level which had the bubble mounted on a rotatable protractor. The sensitivity was about 0.5 degree rotation.

e) Load Measurements

Electrical load-cells were used to measure the loads. The vertical loads, producing bending in the slab, were measured by load-cell consisting of a steel ring between two steel plates. In each load-cell, the central torodial steel ring, of T-1 steel, was supported on three steel balls spaced at 120 degrees. The ring was loaded on the opposite face by 3 steel balls which were located midway between the supporting balls. The applied load produced bending and torsional moments in the ring element. The resultant strains were measured with electrical-resistance strain gages connected as 4-arm bridge circuits and calibrated against known loads. The load-cell sensitivity

was about 40 lb per division of deviation on a strain indicator. The load-cells were placed between the jacks and the reaction frame or test floor.

The load-cells for measuring the axial compressive forces were axially loaded thick-walled cylinders at 6061-T6 aluminum. These load-cells were instrumented with four SR-4, Type A-7, strain gages, connected as 4-arm bridges. The sensitivites were about 40 lbs per division and capacities were 30 kips. Load-cells were placed at each end of each pre-stressing strand passing through the slab.

3. TEST APPARATUS AND PROCEDURE

3.1 Loading and Supporting Systems

The loading system was adapted from a test setup developed by Lenschow (1). The slab specimen was suspended about six ft above the floor from an overhead steel frame on long high-strength steel rods, and was loaded by similar rods extending below the slab to jacks located below or near the floor of the laboratory. This arrangement was adopted in order to minimize the in-plane forces that could be induced in the test specimen from the supporting and loading equipment. Known axial forces could be imposed on the test specimens by means of cables passing horizontally through the slabs.

Figs. 3.1, 3.2 and 3.3 show the supporting and loading systems for the slabs. The specimen was suspended from the three corners of a triangular frame placed on top of the steel frame. Three spreader beams distributed the supporting forces to six steel blocks placed in a circle of 3 ft 6 in. diameter. A one-in. thick rubber pad was placed between the 15 by 3 in. steel blocks and the concrete. The blocks formed a hexagon around the test area.

Three spreader beams under the specimen transferred the vertical forces from three hydraulic jacks to the six loading "wings" along a circle at 6 ft diameter. A 20 by 3 in. loading block with a rubber cushion under it was placed on each wing.

Each spreader beam consisted of two steel channels placed back-to-back. The channels were held 2.5 in. apart by three pins, one at the center and one near each end of the channels. The pins were fitted through holes in the channel webs with sufficient clearance to permit easy rotation, and were loosely secured with nuts on the outside faces of the channels. Each pin was drilled with a vertical hole to permit the passage of a loading rod and counter-sunk with a spherical seat to accomodate a spherical washer.

The loading system was statically determinate, and the arrangement of the pins and spherical bearings equalized the forces in various parts of the system and minimized the friction forces.

Three 30-ton center-hole Simplex jacks, connected to a single electric pump, were used to apply the loads. It was possible to utilize the structural floor system at the laboratory directly for two of the loading forces by passing rods through holes in the floor and jacking against it. It was necessary to construct a steel frame to transmit the third loading force to the floor, as can be seen in Figs. 3.1 and 3.2.

The axial loads were applied through three internally placed 1/2 in., seven-wire prestressing strands. These strands were coated with grease to minimize friction forces. The strands were placed in the ducts formed in the slab when the 5/8 in. rods were withdrawn.

Strand-vises, load-cells, 1/2 in. steel plates, and cork tiles were placed at each end of the strands. Three 30-ton Simplex jacks, connected to one hand hydraulic pump, were used to apply the axial compressive force. Valves were installed on all lines leading to and from jacks so that individual loads could be altered if needed.

3.2 Test Procedure

In each test, zero readings for the strain gages, deflection gages, and load cells were taken and then the axial load was applied, with all jacks being loaded simultaneously. The same axial load was applied to all the strands; this load was maintained throughout the test. After any adjustments necessary to equalize the loads, readings of forces, strains, deflections, and slopes of wings were taken. Then bending moment was then applied to the test specimen. The yield load was ordinarily reached in 10 to 12 increments, the ultimate after 14 to 18 increments. Up to yield,

equal load increments were applied. After yield, increments of deflection were imposed on the structures.

Immediately after each increment of load or deformation, force readings were taken, strain and deflection measurements were read, and the moment arms for the loads were measured. The slab was examined for cracks, which usually appeared after the third or fourth load increment. At the completion of the readings the loads were re-checked and any adjustments in the axial load made. All specimens were loaded to failure. In each case failure occurred when concrete crushed across the width of a loading wing, as can be seen in Fig. 4.2b. Each test took from five to eight hours. Concrete control specimens were tested concurrently with or immediately after the test.

4. TEST RESULTS

4.1 Determination of Applied Forces

The moments considered are those caused by the applied vertical loads, the dead load of the slab and loading equipment, and the moments introduced by the eccentricities of the forces applied to the plane of the slabs. The in-plane forces in the three directions had different eccentricities; the bias thus introduced precipitated failure along a particular, predetermined plane (wing A or D) rather than on a random plane. It was necessary to consider this effect in the analysis of the data.

The applied forces within the central area of the test specimens were obtained in terms of unit moments (kip-in./in.) and unit axial loads (kip/in.). The unit forces within the central hexagonal area of a test specimen were the same as the unit forces applied to the boundaries of the area, since the loading induced no shearing forces in the central region of the specimen.

When computing the unit moments caused by the vertical forces, the average of the three jack forces was used. The variation between the various jack forces was no more than 2 to 3 percent. The average jack force was then divided equally between two loading wings, and the force multiplied by the measured lever arm between the support and loading rods. The lever arm was nominally 15 in.; the measured lever arm of the wings which were forced to fail by the bias resulting from the eccentricity of the prestressing force was used in the moment computations. The lever arms changed slightly at the later loading stages because of the large deformations of the test specimen, but the small changes were not taken into account in the computations.

The average unit forces at the minimum section of the critical wing were considered as the applied forces.

4.2 Determination of Curvatures

Deflections were measured at nine locations on the lower surface of the slab, as shown in Fig. 2.8. Curvatures were determined from the deflections measured along the gage line which was rotated 30 degrees from the diameter connecting the centers of loading wings A and D. The data were reduced using a numerical procedure which is illustrated in Fig. 4.1. The procedure assumes constant curvature along the span between three adjacent deflection gages. The equation for curvatures was

$$\phi = \frac{1}{h^2} (\Delta_1 - 2\Delta_2 + \Delta_3), \text{ where} \qquad (4.1)$$

ϕ = average curvature, in radians per inch,

h = horizontal distrance between adjacent gages, in inches, and

Δ_1, Δ_2, Δ_3 = deflections at gage points, 1, 2, and 3, respectively, in inches.

Deflections were also measured at nine locations on the top surface of the slab, using a equilateral triangular bridge arrangement. Curvatures could be determined in three directions.

The gages on the lower surface were spaced at 7.5 in., and those on the upper surface at 3 in. The lack of sensitivity of the deflection bridge on the upper surface prevented use of the data from it except to provide rough checks. The deflections were measured to the nearest 0.001 in. in all cases. The curvature sensitivity is essentially the deflection gage sensitivity divided by h^2, and for the case of $h = 3$ in., the rotation sensitivity was on the order of 15 to 20 percent of the curvature expected at yield.

Consequently, all of the curvature data presented was computed from deflections measured on the lower surface of the slab. The curvatures were computed using several different sets of three gages each in order to check

the precision of the computations. The curvatures that are presented were based on the deflections measured at gage points 1, 3 and 5, and consequently are on the basis of h = 15 in. The check values were computed from gage sets 1, 2, 3; 2, 3, 4; and 3, 4, 5. It was noted that the measured curvatures were not always distributed uniformly along the measuring line for the lower load levels, but that at loads near yield, the curvature was nearly uniformly distributed. This may have been as much an effect of the measuring precision as of the distribution of curvature, however, as the cracking curvatures were of the same order as the best measurement attainable using the gages spaced at 7.5 in.

4.3 Behavior of Test Specimens

In every case, the observed behavior of the slabs could be divided into three separate phases. Initially, the slab was uncracked, and the application of load produced only small deformations which were within the elastic range of material behavior. Cracking initiated near the bases of the loading wings, and after a transition range, the slabs reacted as cracked reinforced concrete sections which were considerably more flexible than before cracking. During this second stage of behavior cracking spread over most of the surface of the test area of the specimens. The cracks eventually were approximately evenly spaced in an orthogonal pattern, with each crack following the path of a reinforcing bar, as can be seen in the photograph in Fig. 4.2a.

Initiation of yielding of the reinforcement leads to the third stage, where relatively large deformations were developed with only small increases in applied load. This stage ended with the failure of the test specimen. In every case the failure was initiated by crushing of the compressed concrete across the base of one or more of the loading wings, and the failure

locations are listed in Table 4.1. The compression face of specimen FC1A, after failure, is shown in Fig. 4.2b.

The failures occurred at the bases of the loading wings partially as a result of the obvious stress and strain concentration conditions at those sections. There were, however, additional factors leading to failures at these sections instead of in the central portions of the specimens. The central portions of the specimens were subject to uniform bending moment in all directions, and consequently deflected to the shape of a spherical segment. This deformation increases the moment capacity slightly since the section is no longer a flat slab section, but rather a slightly curved section, as shown schematically in Fig. 4.3. Since the average moment capacity of the central portion of the specimen was slightly larger than at the bases of the loading wings, the failures had to occur at the bases of the wings.

Although the failures occurred at the bases of the wings, the moments in the central portions of the slabs without in-plane forces, FC1A and FC5A, exceeded the yield moments and relatively large deformations developed before the failures occurred, as described in the next section.

The sections at the bases of the loading wings were subjected to strain concentrations and relatively steep moment gradients. It has been observed in beam tests (2,3) that sections with stress concentration and moment gradients are often able to sustain deformations substantially larger than would be possible in a section of constant maximum moment. One of the results of this deformation is that strain-hardening of the reinforcement at these sections may be very important, and large increases in moment

capacity can occur. Such behavior in the slab specimens would help explain how enough moment could be applied at the edges of the test area of a specimen to cause yielding throughout the central test area in spite of the fact that the edge sections appear slightly weaker than the interior parts because of curvature effects.

The specimens with in-plane forces had additional effects which forced failures at the bases of either loading wing A or D, as was mentioned earlier. This can probably best be illustrated by referring to Fig. 4.4, which is a partial moment-thrust interaction for a typical slab section with a reinforcement ratio of 0.005. Only the lower portion of the curve is shown, as the balance-point thrust is nearly 9 kip/in. and the failure axial thrust in excess of 20 kip/in., and the thrusts of interest are no more than 2 kip/in.

Because of the eccentricities of two of the prestressing strands used in applying the horizontal compression loads, the application of the in-plane compression forces produced positive bending moments at the bases of wings A and D, negative bending moments at the bases of wings C and F, and only thrusts at the remaining two sections. Points representing these initial conditions are plotted in the figure.

Application of the external positive bending moment moves all of the points plotted in Fig. 4.4 to the right by the same distance, and it is obvious that when the point representing the conditions at the base of wings A and D reaches the yield or ultimate line, the other sections still have appreciable moment capacity remaining. No single eccentricity is completely representative of the conditions in the central portion of the test specimens, but the average eccentricity must be approximately zero, so that the

strength would be about the same as that at the base of wings B and E, neglecting the effects of curvature and stress concentration.

Since the central portions of the test specimens with axial forces were subjected to moments no greater than the yield capacities, the deformations within the area were still relatively small at the time the failure occurred.

4.4 Measured Moment-Curvature Relationships

Measured and theoretical moment-curvature relationships for each of the six test specimens are plotted in Fig. 4.5 through 4.10. The measured values were obtained from measured loads and deflections, as explained earlier. The derivation of the theoretical relationships is described in Sec. 5.2. The curvatures shown were determined considering deflection gages 1, 3, and 5, spaced at 15 in. intervals. In each case, the dead-load curvature before application of the in-plane compression forces is assumed to be zero, and the total moments, including dead load and those due to eccentricity of the in-plane forces are plotted. The moments correspond to those at the bases of wings A and D.

The measured ultimate moments are tabulated in Table 4.1, as are the theoretical failure moments, the measured thrust values at failure, and other information to be discussed in the next chapter.

The two specimens without axial loads, FC1A and FC5A, Figs. 4.5 and 4.8, respectively, exhibited appreciable ductility, in terms of increasing curvature at approximately constant load. The two specimens with axial loads and reinforcement ratios of 0.01, FC1B and FC1C, exhibited only very small inelastic deformations of the central test areas of the slabs, while the two with reinforcement ratios of 0.005 underwent small deformations beyond yield before failure.

These observations are consistent with the expected results, as discussed in the last section, in that large inelastic curvatures were developed only in cases where there were no axial forces.

4.5 Measured Strains in Reinforcement and Concrete

Unit moment-strain curves for various locations on the concrete and reinforcement are given in Figs. 4.11 through 4.22, giving representative data for each of the six slabs tested.

The general shapes of the moment-strain curves are similar to the moment relationships, and indicate changes in stiffness accompanying cracking of the concrete and yielding of the reinforcement. However, since the strain measurements give indications of local deformation while the curvatures measured indicate only gross deformations, it is possible to have high strains at particular locations in a slab and still have only relatively small curvatures at the same applied moment level.

Large reinforcement strains were measured at one or more strain gage locations in all of the test specimens, with the slabs with lower reinforcement ratios and lower levels of axial force tending to have the larger strains.

The exact values of the maximum reinforcement strains in each slab cannot be determined since strain gages were not installed on every bar, and also because many of the gages showing the highest strains failed before the maximum load was reached. The maximum recorded strain exceeded 0.020 in slabs FC1A, FC1C, FC5A, and FC5B, with the greatest recorded value being 0.0267 in slab FC5A. This represents a strain about 15 times the yield strain.

In the cases of slabs FC1C and FC5C, the application of the in-plane compression forces caused compressive strains in the reinforcement so large

that they were not always overcome by the moment applied during the first increment of vertical load, as can be seen in Figs. 4.15 and 4.21.

The measured concrete strains gave a better representation of the gross behavior of the specimens than did the reinforcement strains, with smaller differences between readings on adjacent gages. Large concrete strains were produced throughout the central test areas of those specimens in which large curvatures occurred before failure.

In most cases the largest strains were indicated by gages located near the tip of a slot between adjacent loading wings, as would be expected from considerations of expected strain concentrations. In each case, the strain at gage C1 on the concrete was greater than that at C2. Gage C1 was perpendicular to a diametral line connecting the tips of slots between loading wings, while C2 was parallel to the line. This is evident in the curves of concrete strain versus load in slab FC1A, Fig. 4.12, for example.

Concrete strains approaching the crushing strain, 0.003 to 0.004, were measured at least at one gage location in all slabs except FC1B. Maximum strains of 0.0026 to 0.0036 were observed in each of the other test specimens. In no case was there a strain gage in the area of crushed concrete which fell from the slab at the time of failure, so the measured strains do not necessarily represent the maximums which occurred.

5. COMPARISONS OF THEORETICAL AND MEASURED RESULTS

5.1 Introductory Remarks

The results of the tests are discussed in this chapter, and the observed loads and deformations are compared with theoretical values. The derivation of the theoretical moment-curvature relationships is described briefly in Sec. 5.2, and the comparisons between theory and measurements are made in Sec. 5.3.

5.2 Theoretical Moment-Curvature Relationships

The theoretical moment-curvature relationships were idealized as three straight line segments connecting the origin and points representing initiation of cracking, yielding of the reinforcement, and failure. The curves obtained are plotted in Figs. 4.5 to 4.11.

The points on the curves were computed using the measured values of material properties and slab dimensions as tabulated in Tables 2.1 and 2.2, except that the modulus of rupture, f_r, was taken as $7\sqrt{f'_c}$ instead of using measured values.

The strain and stress distributions assumed within the cross-sections are shown in Fig. 5.1. The moments of the forces were summed about the plastic centroid of the section.

5.3 Discussion of Test Results

The measured ultimate moments, in terms of kip in./in., are listed in Table 4.1 for each of the six test specimens. The moments tabulated include the dead load and the moment introduced by the eccentricity of the in-plane compression force at the base of wings A and D in addition to that caused by the vertical applied loading. The in-plane compression force measured in each slab at the time the maximum moment was reached is also listed for each slab.

The theoretical moment capacities, calculated as indicated above, are also given, as are the theoretical values of reinforcement strain at failure and a listing of the sections at which the failures occurred.

The ratios of measured to theoretical moment are listed, and it can be seen that the agreement between the two values is extremely good for the specimens with 0.01 reinforcement ratios. In the cases of the specimens with 0.005 reinforcement ratios, the measured moments are consistently higher than the theoretical values, by amount of 11 to 13 percent. The reasons for this discrepancy are not completely clear, although strain hardening was the most important factor.

The theoretical values of ε_{su}, the reinforcement strain at failure of the cross-section, were calculated using an ultimate concrete strain, ε_{cu}, of 0.003, and are listed in Table 4.1. The theoretical ultimate steel strain for specimen FC5A is in excess of 0.05, which is well into the strain-hardening range of the reinforcement. However, this argument cannot be used indiscriminately since the theoretical values of final steel strain for specimens FC1A and FC5C are comparable, while the failure moment capacities are 2 and 11 percent greater than the theoretical values, respectively.

The yield stress values of the reinforcement, as listed in Table 2.2, are within one kip/in.^{2} of the correct values, on the basis of the range of results obtained in the sample testing. The measured values of slab thickness, reported in Table 2.1, were used in all computations. The concrete strangth values were established by means of cylinder tests, but even if the tests were not completely representative of the concrete, the moments capacities would have been insensitive to concrete strength variations, especially in the specimens with 0.005 reinforcement ratios.

Variation in dimensions or properties from those assumed are apparently not responsible for the lack of agreement between measured and theoretical values of the FC5 slabs.

That strain-hardening in the reinforcement must have been a factor in the high moment capacities of the FC5 slabs can be seen by examination of the moment-strain diagrams for these slabs, Figs. 4.17 to 4.22. In specimen FC5A the reinforcement strains, Fig. 4.17, go off-scale too quickly, but the concrete strains, Fig. 4.18, present a reasonable picture of the behavior. Yielding of the reinforcement obviously started at a moment of about 3 kip-in./in., and the strain trace for gage C1 shows a very gradual increase in moment up to a concrete strain of about 0.0028 and a moment of 3.25 kip-in./in., after which the moment capacity increased at a somewhat higher rate until the failure occurred. The only reasonable explanation for this change in slope would appear to be initiation of strain hardening of the reinforcement.

The moment resistance increased from 3.0 to 3.25 kip-in./in. because of a gradual increase in the internal level arm as the neutral axis moved toward the compression face, and as the cross-section was distorted by the bending moment in the perpendicular direction.

If the 3.0 kip-in./in. moment is taken as the yield moment, the ultimate moment was 14 percent higher than yield. If it were assumed that strain hardening alone were responsible for the increase in moment, which is not true, and assuming that the stress-strain curve for the reinforcement shown in Fig. 2.5 is representative of the strain-hardening properties of the reinforcement, an increase in stress to 14 percent above the yield value would require a strain of less than 0.03, which is reasonable in view of the measured and calculated values of ultimate reinforcement strain.

Neither specimen FC5B nor FC5C exhibited large plastic deformations with minor changes in moment, but both showed substantial reductions in stiffness at loads corresponding to initiation of yielding of the reinforcement within the central test area of the slabs. These changes in stiffness occurred at applied moments of about 3.9 kip-in./in. for FC5B and 5.0 kip-in./in. in FC5C. The value for FC5B is comparable to the theoretical ultimate moment, ignoring the influence of strain hardening, while that for FC5C is about five percent larger than the calculated value for failure.

In slab FC5C, yield strains in the reinforcement ($\varepsilon_y = 0.0016$) were indicated by gage S9, Fig. 4.21, at a moment of about 4.5 kip-in./in., which is slightly higher than the computed yield moment, Fig. 4.10. There was no appreciable change in stiffness at this load, so most of the reinforcement obviously had not yielded.

In most cases, the moment-strain diagrams and the moment-curvature diagrams indicated substantial reductions in stiffness at the same value of applied moment, so these measurements are in agreement. However, in most slabs at least some of the measured reinforcement strains exceeded the yield strain without causing major changes in slab stiffness. While the development of yield strains in one or two bars does not necessarily indicate that an entire cross-section has yielded, it does not seem reasonable to expect the particular bars which have strain gages mounted on them to always reach yield strains before the other bars in the section.

The measured strains from zero load to yield of the reinforcement may be larger than the expected value of f_y/E_s if the bars have been compressed before the initial strain reading was made by shrinkage of the concrete. For example, a precompression strain of 0.000400 in the reinforcement for which $\varepsilon_y = 0.001600$ would cause a strain reading of

0.002000 when the bar begins to yield. The stress at yield is not altered, and the moment capacities of sections are not changed. The moment-strain relationships would be somewhat altered because of the release of strain energy accompanying cracking. The cracking moment would be lowered because compression of the reinforcement requires tension in the concrete in order to satisfy equilibrium.

Shrinkage strains in the concrete were not measured, but some qualitative conclusions about the magnitude of the precompression of the reinforcement can be made. It can be shown, ignoring creep of the concrete under the shrinkage-induced stresses, that for a rectangular section

$$\varepsilon_s = \frac{\varepsilon_{sh}}{1 + p_g n\left(1+12\frac{e^2}{t^2}\right)}$$

where ε_s = shrinkage-induced compression strain in reinforcement,

ε_{sh} = free shrinkage of unrestrained concrete,

p_g = gross reinforcement ratio, As/bt,

n = modular ratio, E_s/E_c,

e = eccentricity of reinforcement from center of gravity of concrete,

t = thickness of concrete section, and

A_s = area of reinforcement per width of section b.

For the FC1 slabs this gives $\varepsilon_s \approx \frac{\varepsilon_{sh}}{1.16}$, and for the FC5 slabs, $\varepsilon_s \approx \frac{\varepsilon_{sh}}{1.08}$, so the precompression strains in the reinforcement are only slightly smaller than the free shrinkage strains. The effect of creep of the concrete would be to reduce the compressive strains developed in the reinforcement.

Since many of the moment-steel strain curves indicated yielding started at strains of 0.002000 to 0.002200, and the yield strains for bars tested

in air were from 0.001600 to 0.001700, precompression strains of 0.000300 to 0.000500 would be required to explain the test results adequately.

Since shrinkage strains were not measured, no positive conclusions can be drawn. However, shrinkage strains of 0.000300 to 0.000500 are not completely unreasonable (4), especially in view of the thin sections, 4 in., and the low relative humidities occurring in the laboratory, where the relative humidity seldom exceeds 50 percent and drops to 20 percent or less during the winter. Shrinkage strains of this magnitude are probably not reasonable for slab FC1B, which was tested at 7 days, but are possible for the other five slabs.

The measured ultimate moment values are also shown in Fig. 5.2, where values of thrust, in kip/in., and plotted versus values of moment, in kip-in./in. In addition, partial theoretical moment-thrust interaction diagrams for "Ideal" specimens having f'_c = 6,500 psi, f_y = 50,000 psi, and d = 3.50 in. are plotted, for conditions corresponding to initiation of yielding of the reinforcement and to failure, for reinforcement ratios of 0.005 and 0.01.

The measured values for the FC1 specimens lie close to the theoretical M-P failure curve, with the variations being explained in terms of actual values of yield stress of the reinforcement. The points for the FC5 specimens lie uniformly to the right of the theoretical line, as was discussed earlier.

This figure demonstrates the validity of the method of calculating the strength of a reinforced concrete slab section subjected to combined axial load and bending moment, as the test results and the theoretical results follow exactly the same trends as the axial forces are applied.

6. SUMMARY AND CONCLUSIONS

The fabrication and testing of six reinforced concrete slabs used in an investigation of the influence of known in-plane compression forces on the strength and behavior of slabs is described.

The slabs were hexagonal in general shape, Fig. 2.1, and were supported and loaded to produce uniform bending moments in all directions within the central test area of the slab. Horizontal in-plane compression forces were applied to four of the slabs by means of jacks acting on cables passing through ducts cast in the slab.

The variables were the amount of reinforcing steel, $p = 0.005$ or 0.010, and the level of in-plane force, 0, 0.55 kip/in., or 1.10 kip/in. width of slab section.

Loads, axial forces, reinforcement and concrete strains, and deflections were measured, and were used in determining the moments and curvatures at various stages of testing.

Since the three cables used in applying the in-plane forces could not be located at one level within the slab thickness, the locations of failure planes were biased in the specimens with in-plane forces, as shown in Fig. 4.4.

In all slabs the failure moments could be satisfactorily explained in terms of conventional reinforced concrete theory, taking into account the presence of the in-plane compression forces, although the effects of strain hardening had to be considered in the specimens with the lower reinforcement ratios.

Application of an in-plane force of approximately 0.55 kip/in., or 138 psi, caused increases in moment capacity of 16 and 32 percent for slabs with

0.010 and 0.005 reinforcement ratios, respectively. In-plane compressions of 1.1 kips/in., or 275 psi, caused increases of 37 and 57 percent, respectively, for similar slabs, relative to slabs without in-plane forces. These increases were compatible with those predicted by the use of theoretical thrust-moment interaction diagrams, Fig. 5.2, for reinforced concrete sections.

7. REFERENCES

1. Lenschow, Rolf J. and M. A. Sozen, "A Yield Criterion for Reinforced Concrete under Biaxial Moments and Forces," Civil Engineering Studies, Structural Research Series No. 311, Department of Civil Engineering, University of Illinois, Urbana, July 1966, 527 p.

2. Burns, Ned H., and C. P. Siess, "Plastic Hinging in Reinforced Concrete," Proc. ASCE, Journal Structural Division, Vol. 92, No. ST5, October 1966, pp. 45-64.

3. Corley, W. G., "Rotational Capacity of Reinforced Concrete Beams," Proc. ASCE, Journal Structural Division, Vol. 92, No. ST5, October 1966, pp. 121-146.

4. ACI Committee 435, "Deflections of Prestressed Concrete Members," J. ACI, Proc. Vol. 60, Dec. 1963, pp. 1697-1728.

5. Ockleston, A. J., "Loading Tests on a Three-Storey Reinforced Concrete Building in Johannesburg," The Structural Engineer, October 1955, Vol. 33 No. 10, pp.304-321.

6. Gamble, W. L., M. A. Sozen, and C. P. Siess, "Tests of a Two-Way Reinforced Concrete Floor Slab," Proc. ASCE, Journal Structural Division, Vol. 95 No. ST6, June 1969, pp. 1073-1096.

Table 2.1

Physical Properties of Slab Specimens

Specimen	Steel Ratio, p	Axial Load kip/in.	Slab Thickness in.
FC1A	0.01	0	4.03
FC1B	0.01	0.55	3.97
FC1C	0.01	1.10	4.04
FC5A	0.005	0	4.15
FC5B	0.005	0.55	3.99
FC5C	0.005	1.10	3.99

Table 2.2

Material Properties of Slab Specimens

Specimen	f_y (ksi)	Compressive Strength, f'_c (psi)	Young's Modulus, E_c (psi)	Splitting Strength, f_{sp} (psi)	Slump (in.)	Age at Test (Days)
FC1A	48	6800	3.85×10^6	470	2, 2.5, 2.5**	25
FC1B	50	5420	3.79	440	0.8, 2.8, 2.3**	7
FC1C	52	6260	4.06	468	2	24
FC5A	50	6260	3.63	410	4	28
FC5B	48	6570	3.82	451	...	15
FC5C	48	7370	3.77	423	1.8	17

** - 3 batches

Table 4.1

Comparison of Measured and Theoretical Moments

Slab	Meas. M_u k-in./in.	Theo. M_u k-in./in.	$\frac{\text{Meas. } M_u}{\text{Theo. } M_u}$	Meas. Thrust at M_u k/in.	Theo. ε_{su}	Failure at Wing
FC1A	5.54	5.44	1.02	0	0.0285	D&E
FC1B	6.42	6.54	0.98	0.55	0.0148	D
FC1C	7.61	7.62	1.00	1.11	0.0131	A
FC5A	3.36	2.98	1.13	0	0.0543	B
FC5B	4.43	3.93	1.13	0.64	0.0305	D
FC5C	5.27	4.76	1.11	1.12	0.0255	D

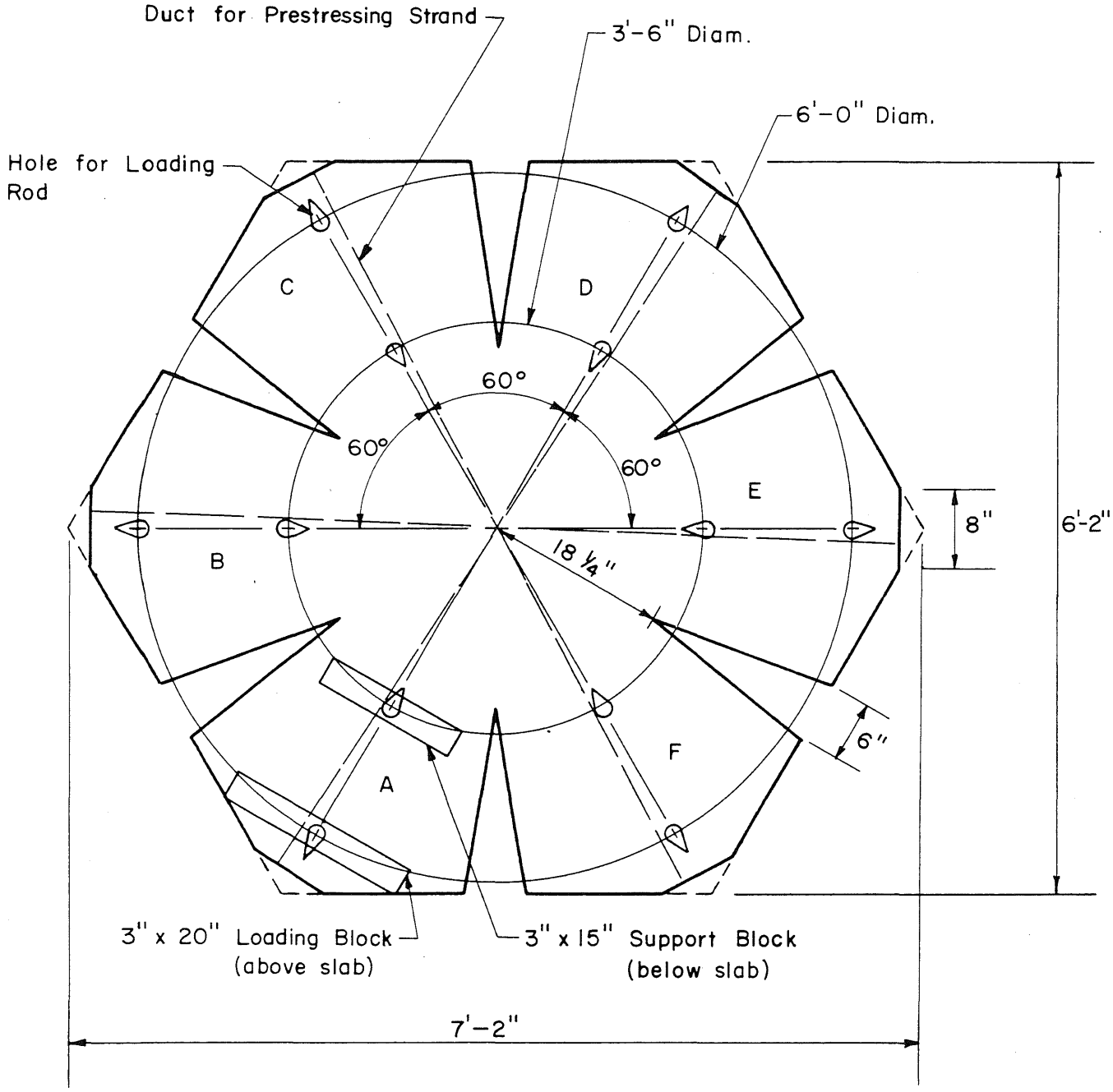

Fig. 2.1 Plan of "Circular" Test Specimen

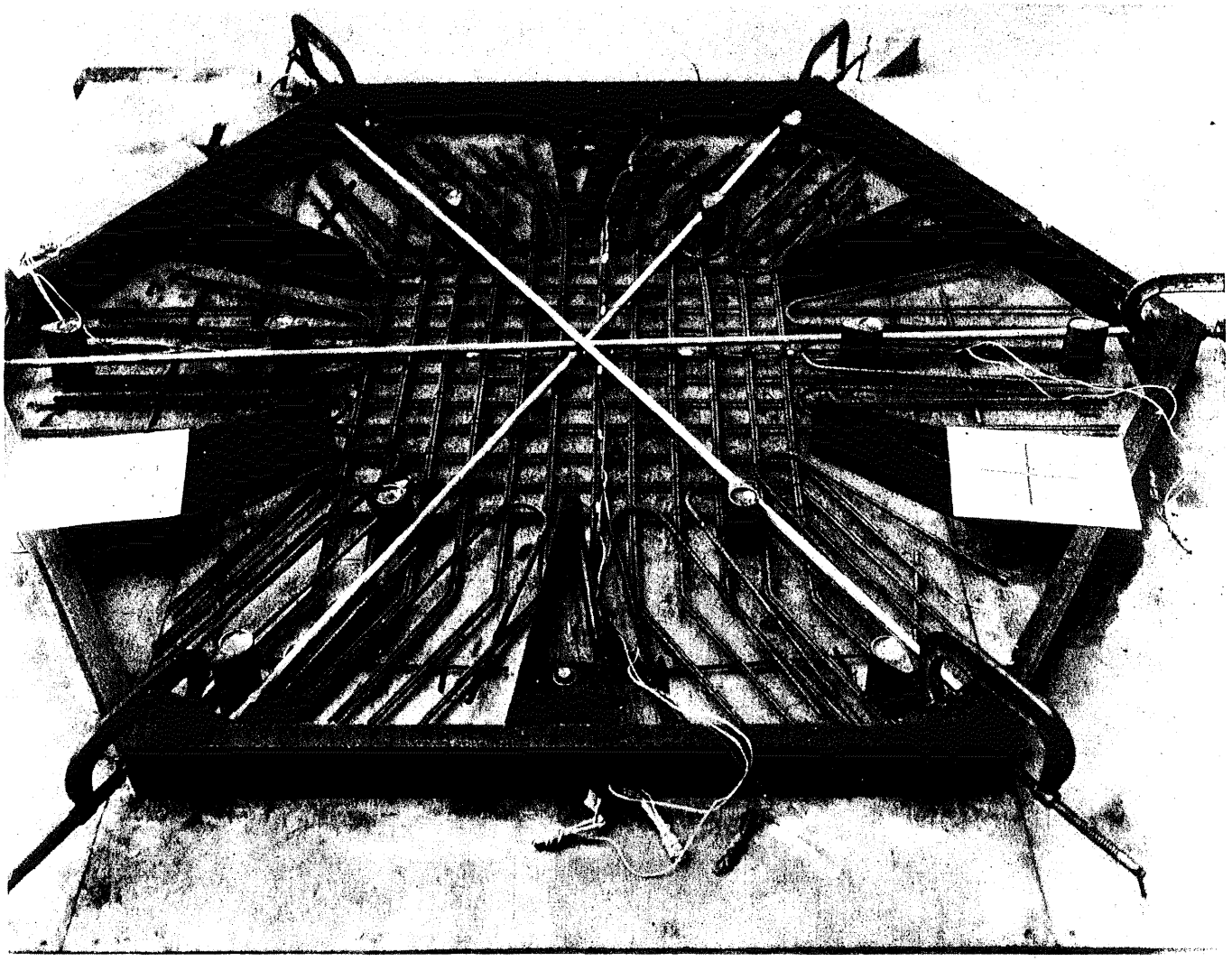

Fig. 2.2 Photograph of Reinforcement in Slab FC1C

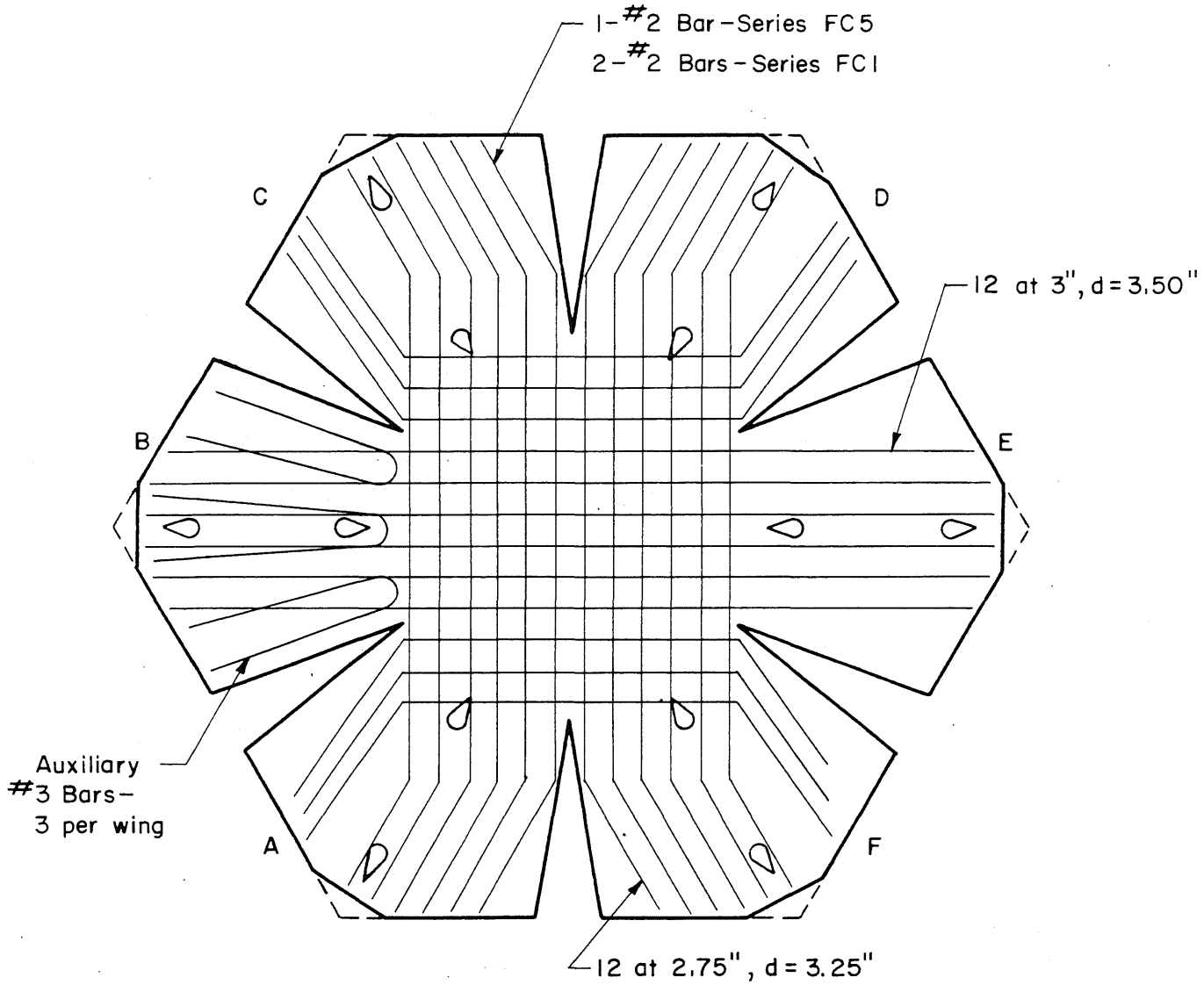

Fig. 2.3 Reinforcement in Circular Test Specimens

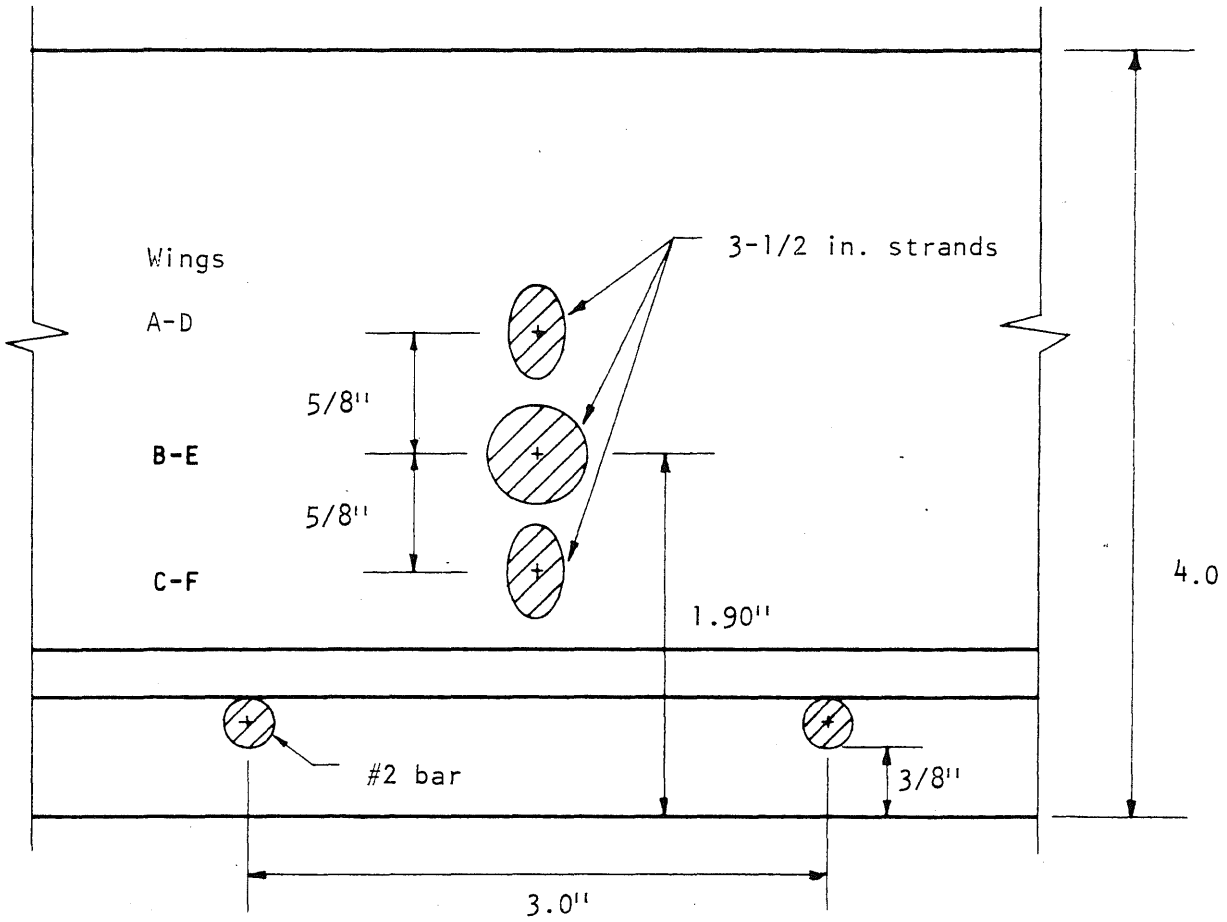

Position as Cast

Fig. 2.4 Locations of Axial Forces in Slabs

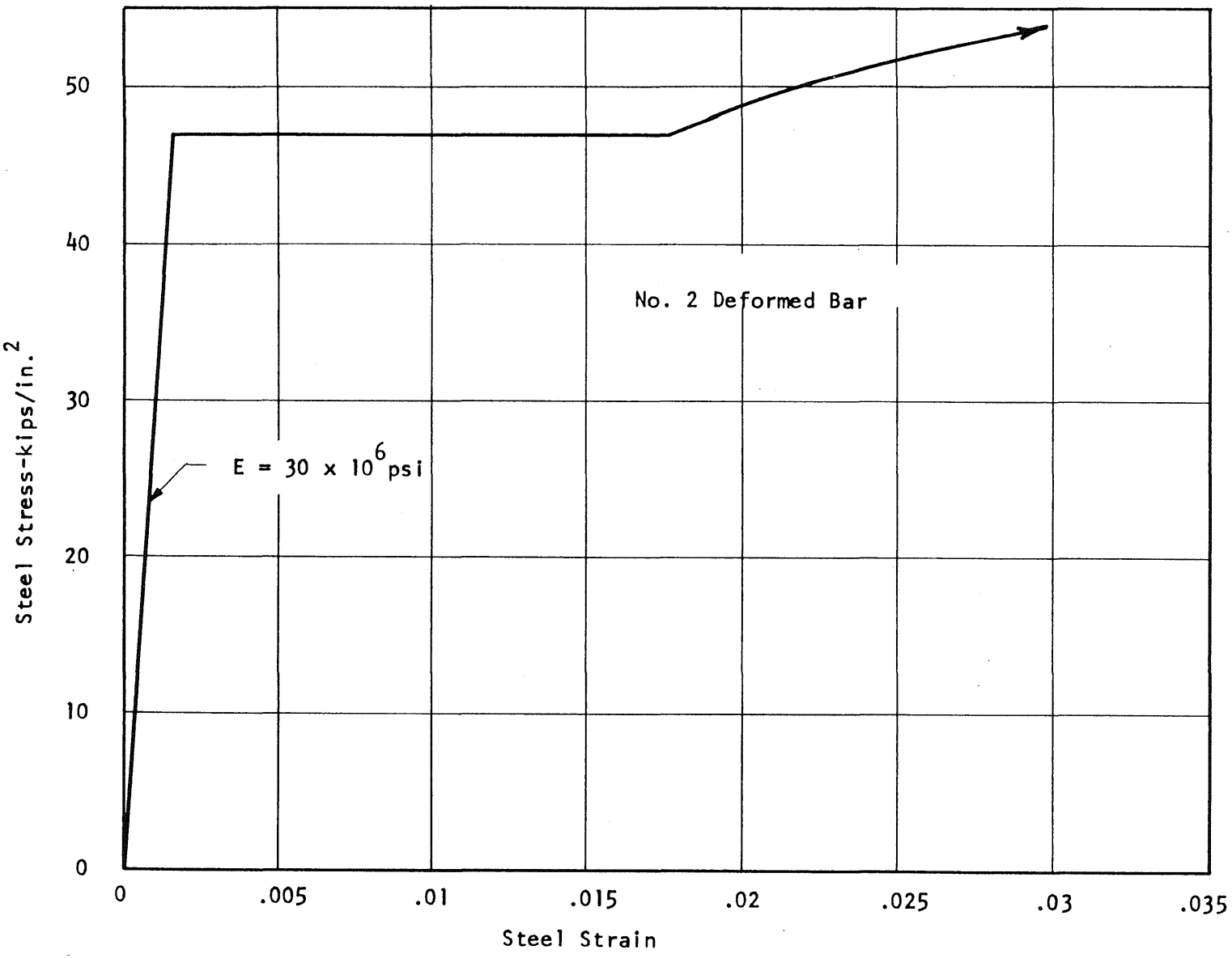

FIG. 2.5 REPRESENTATIVE STRESS-STRAIN CURVE FOR REINFORCEMENT

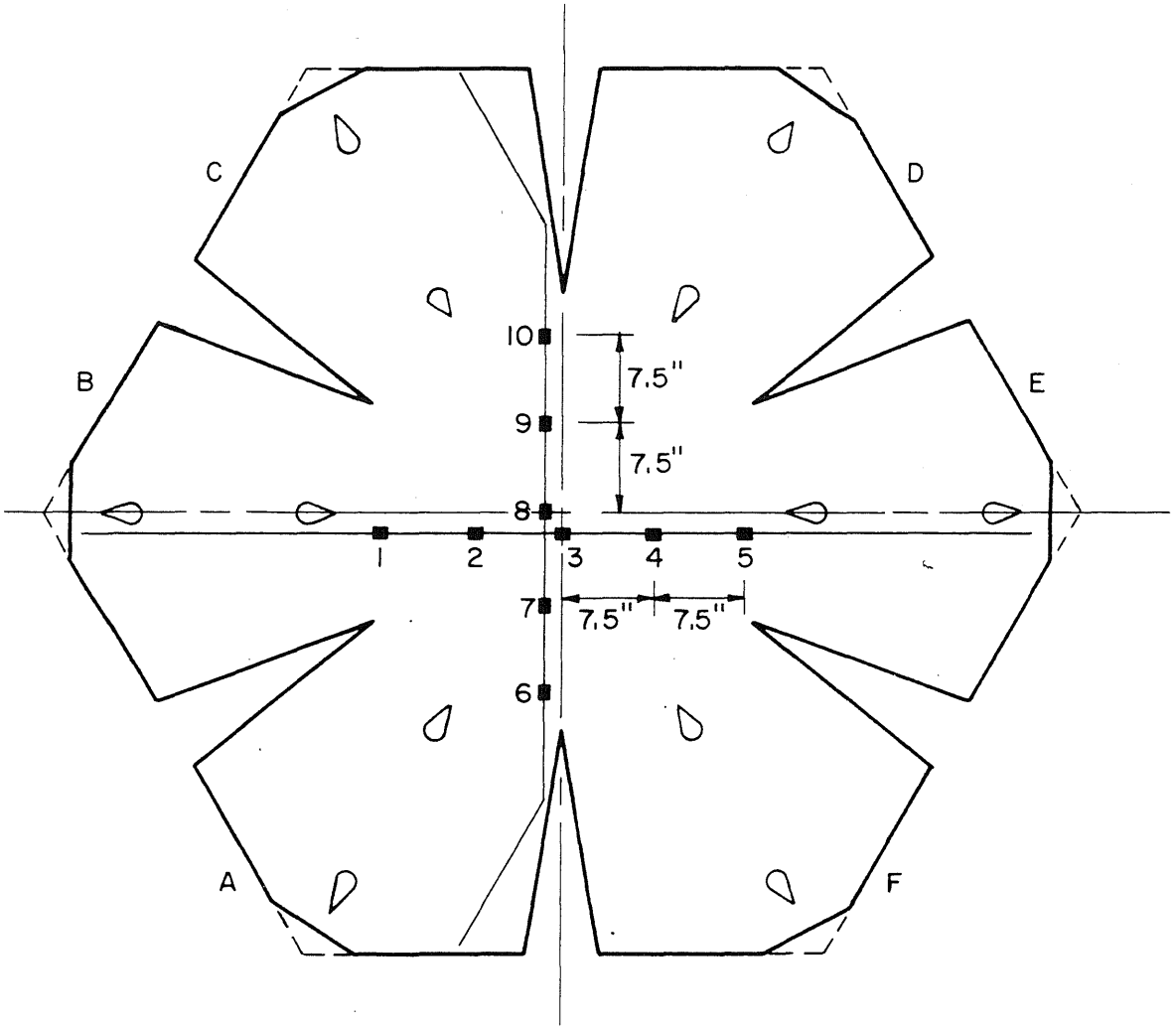

Fig. 2.6 Typical Locations and Designations of Strain Gages on Reinforcement

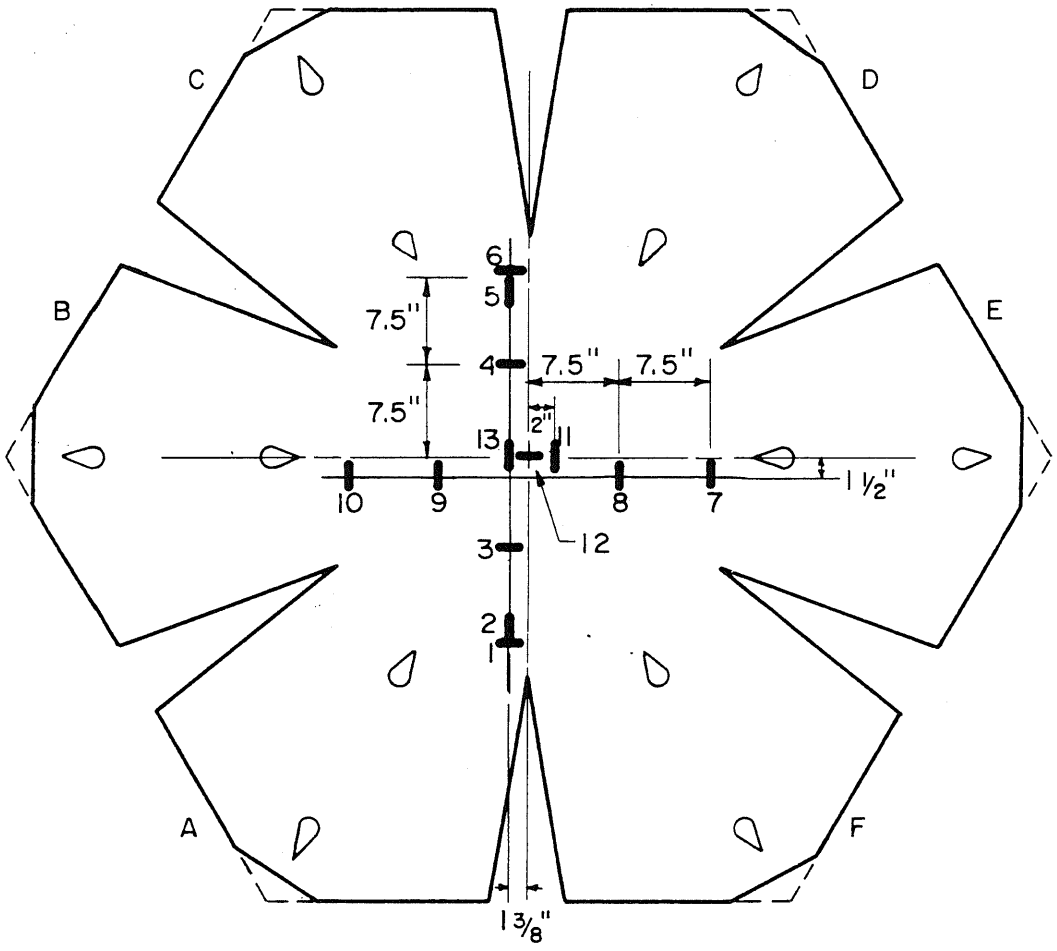

FIG. 2.7 TYPICAL LOCATIONS AND DESIGNATIONS OF STRAIN GAGES ON CONCRETE

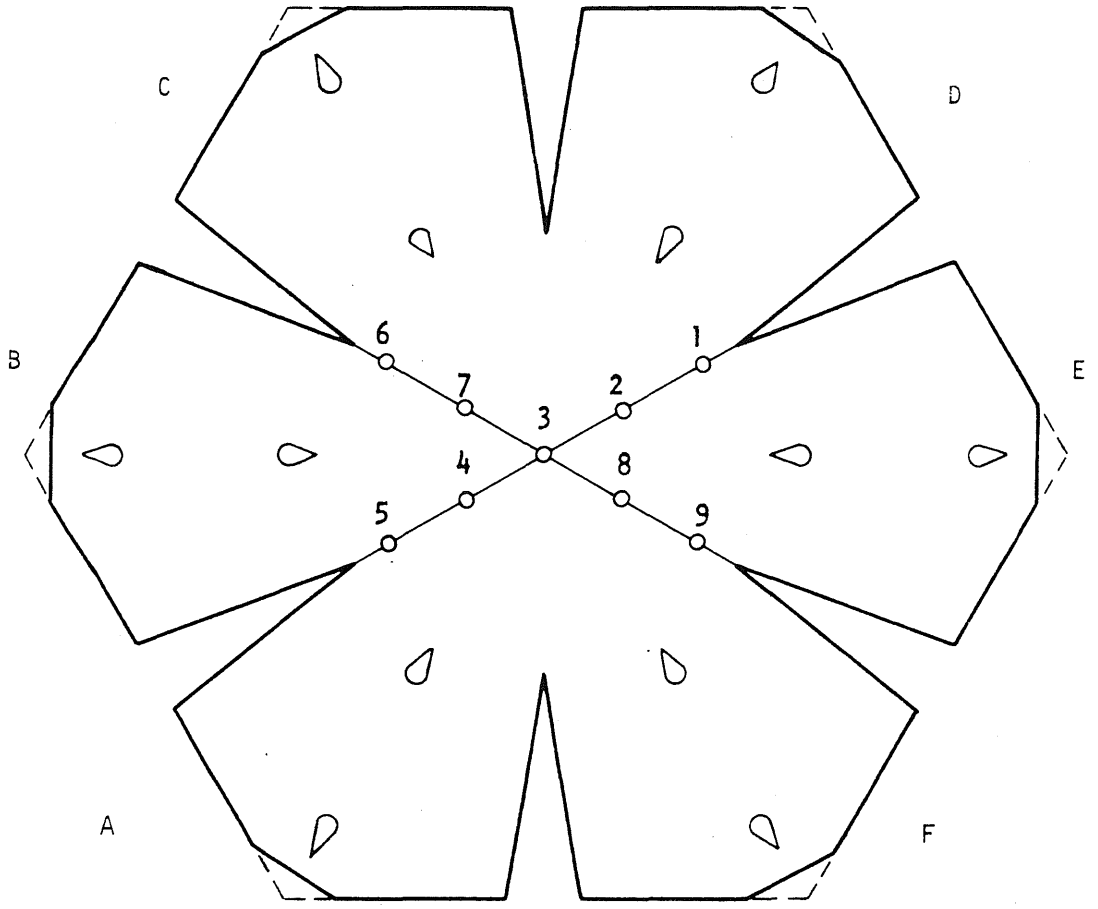

Gages Spaced at 7.50 in.
Gages 1-5 Supported on one bar
Gages 6-9 Supported on second bar

Fig. 2.8 Locations and Designations of Deflection Gages

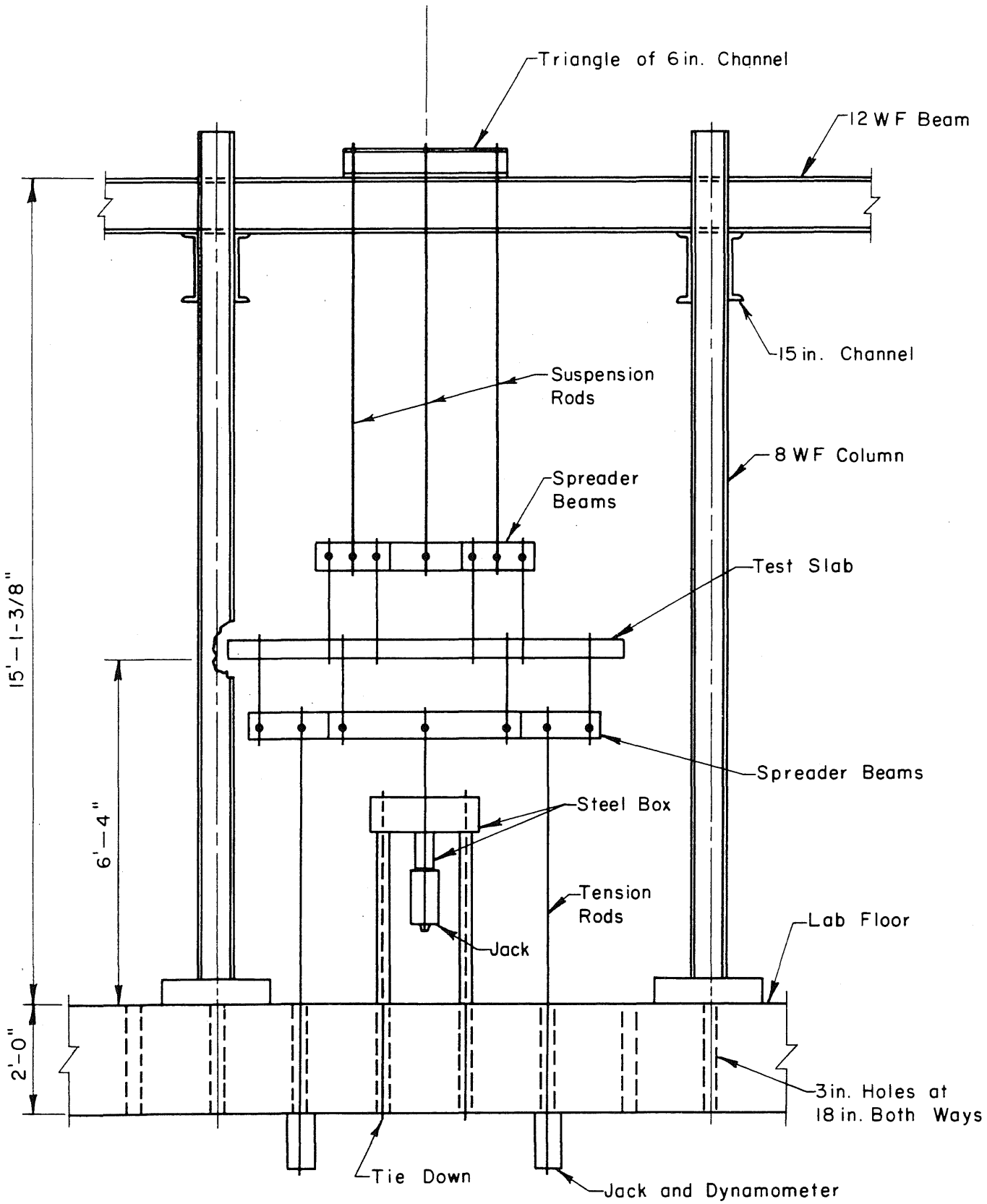

FIG. 3.1 ELEVATION OF TEST FRAME

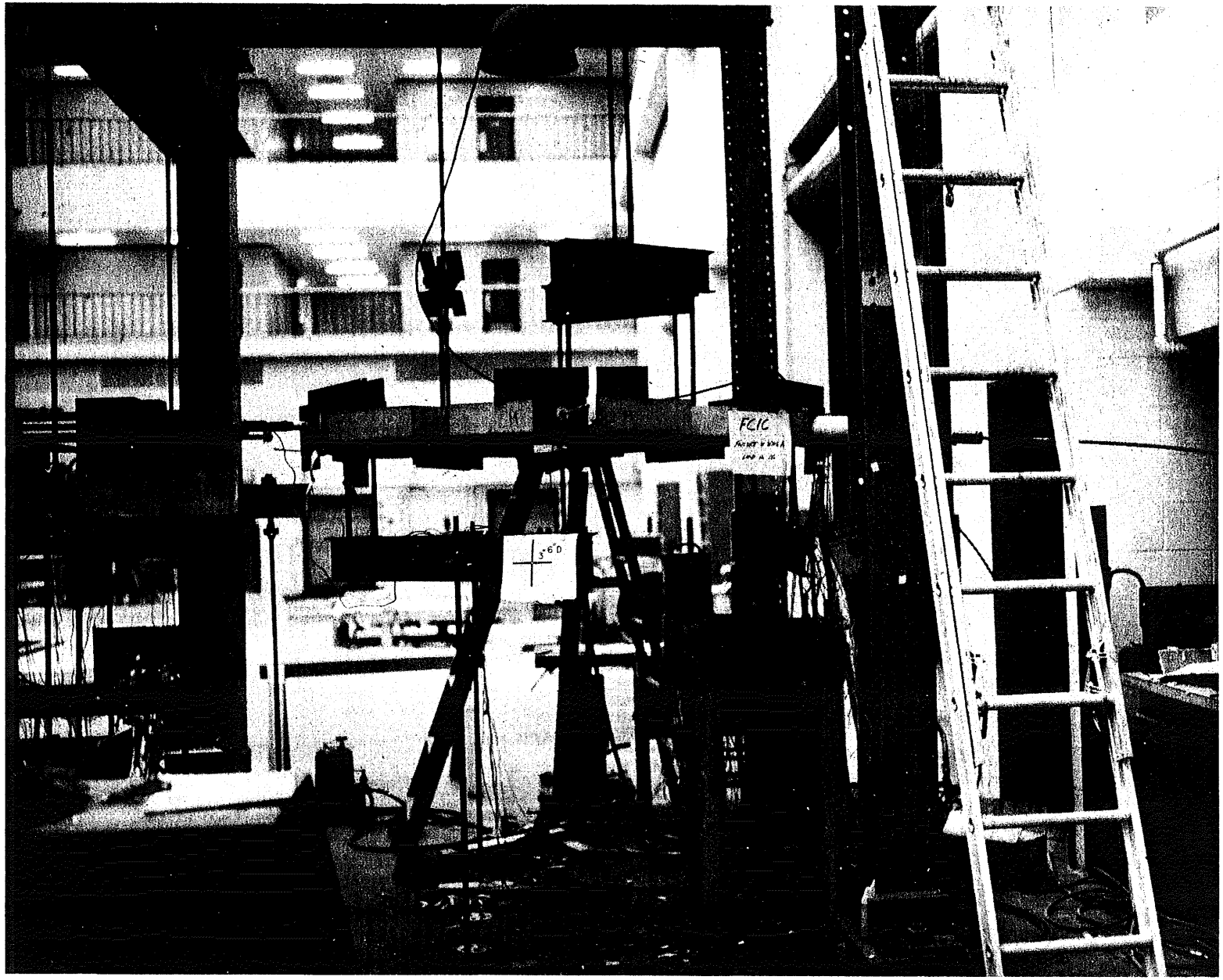

FIG. 3.2 PHOTOGRAPH OF TEST FRAME WITH SLAB IN PLACE

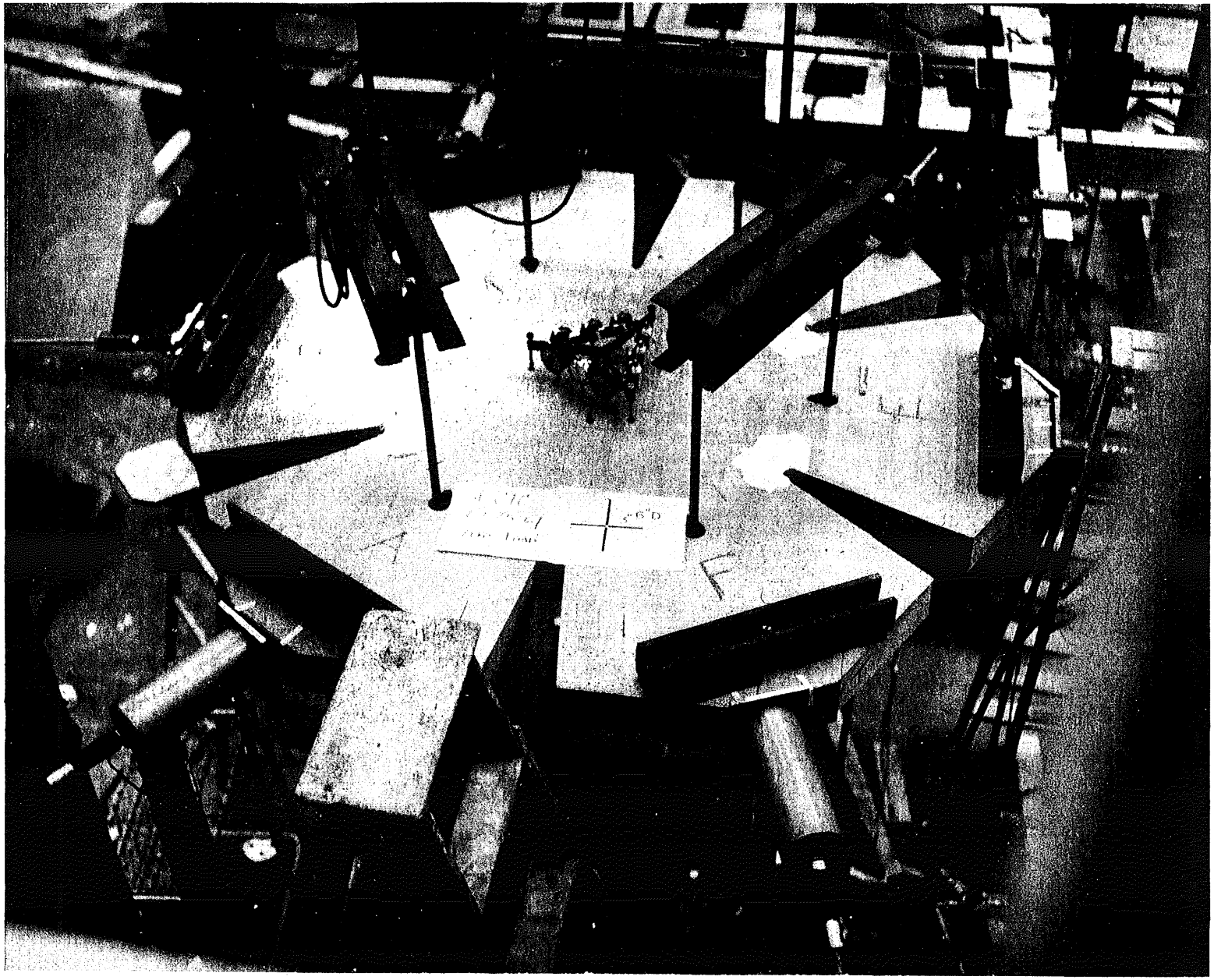

FIG. 3.3 PHOTOGRAPH OF TOP OF SLAB IN TEST FRAME

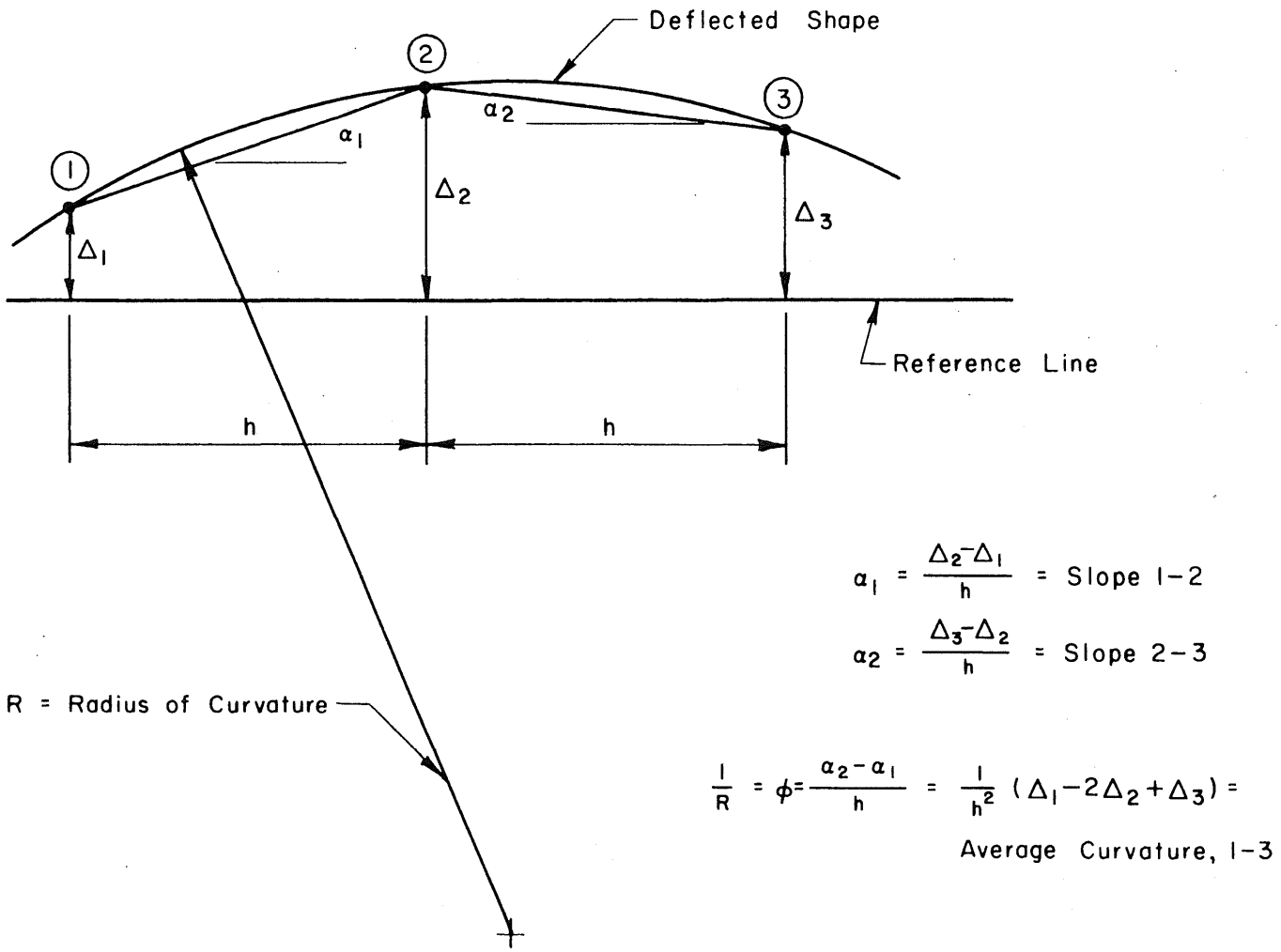

FIG. 4.1 DETERMINATION OF CURVATURES FROM DEFLECTIONS

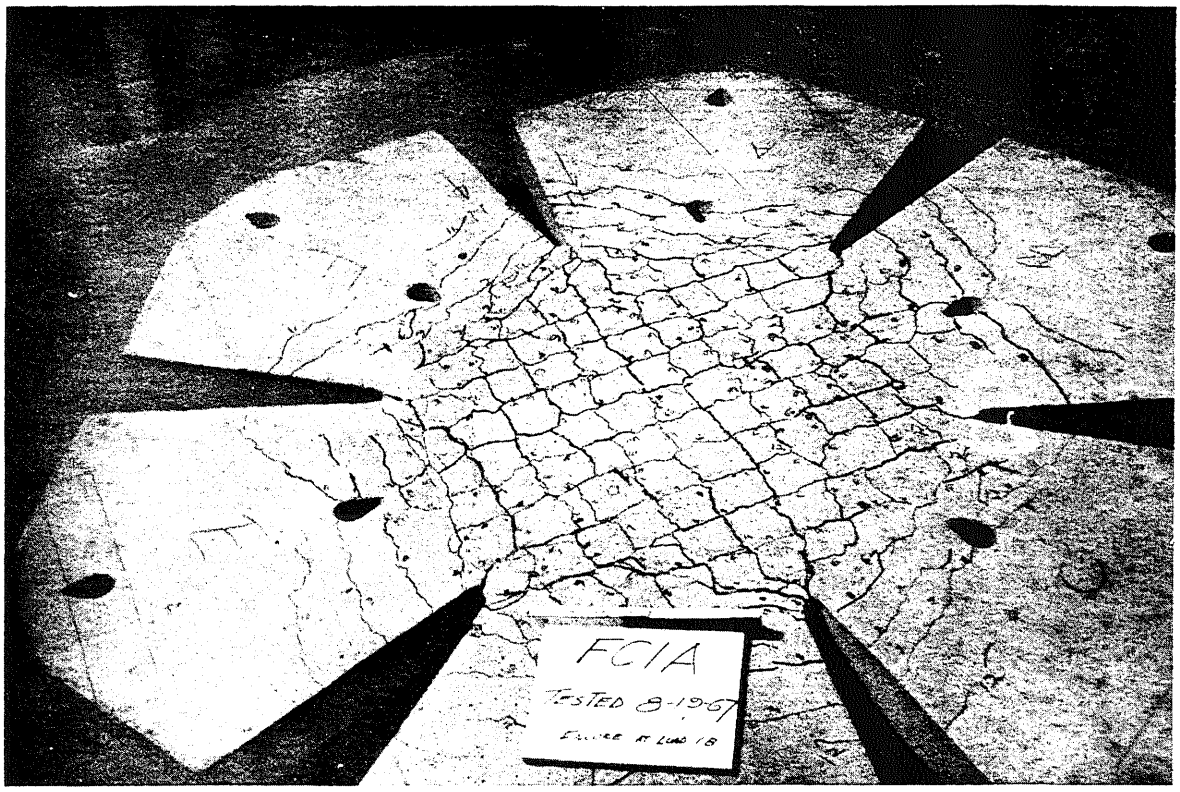

FIG. 4.2a TENSION SURFACE OF SPECIMEN FC1A AFTER TESTING

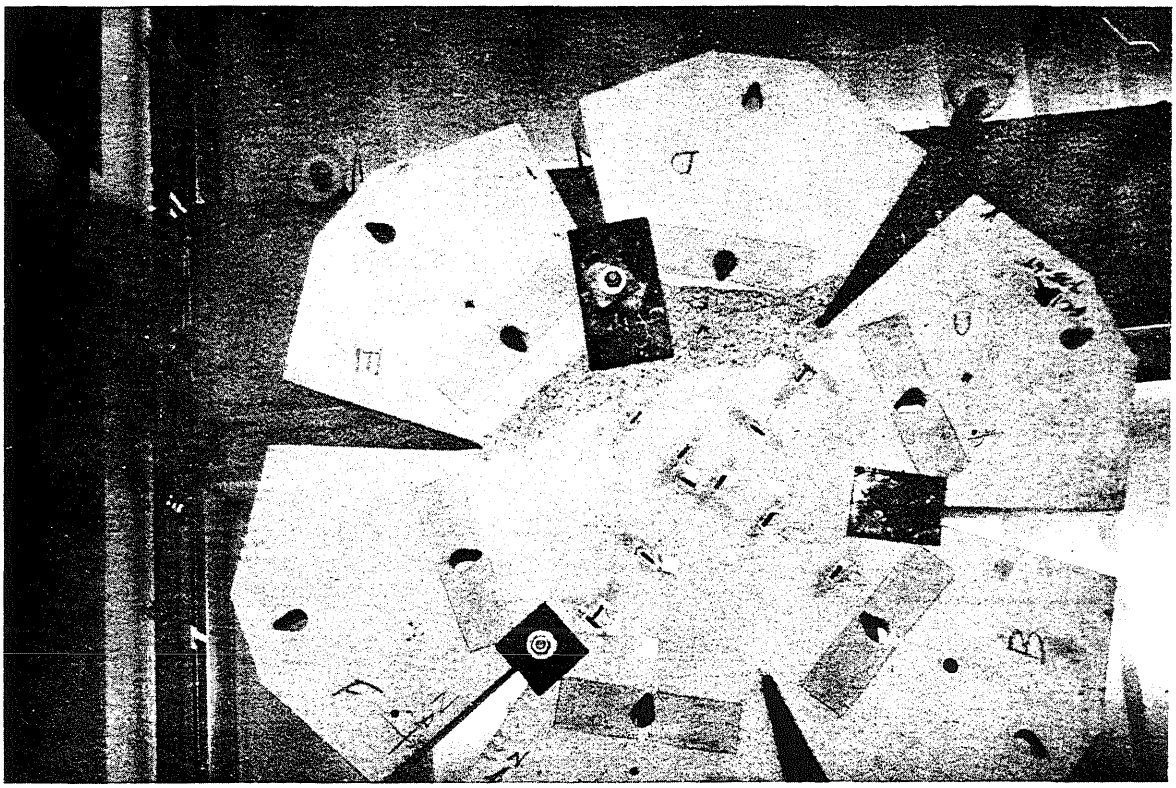

FIG. 4.2b COMPRESSION SURFACE OF SPECIMEN FC1A AFTER TESTING

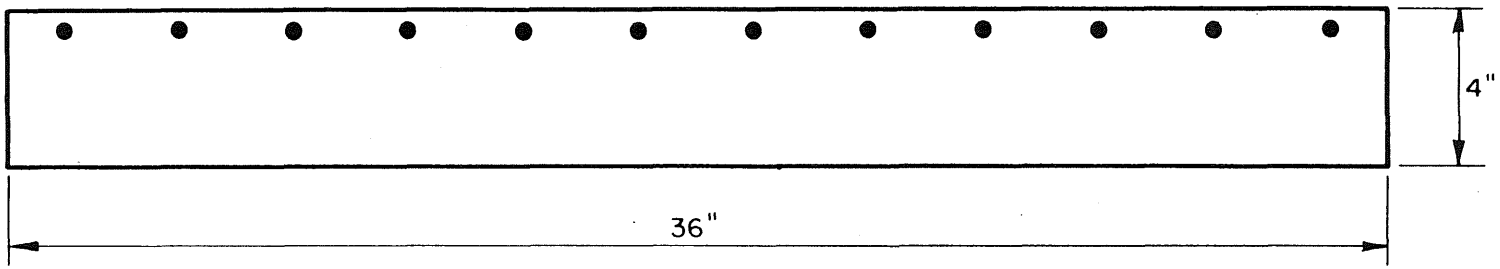

(a) Before Defomation

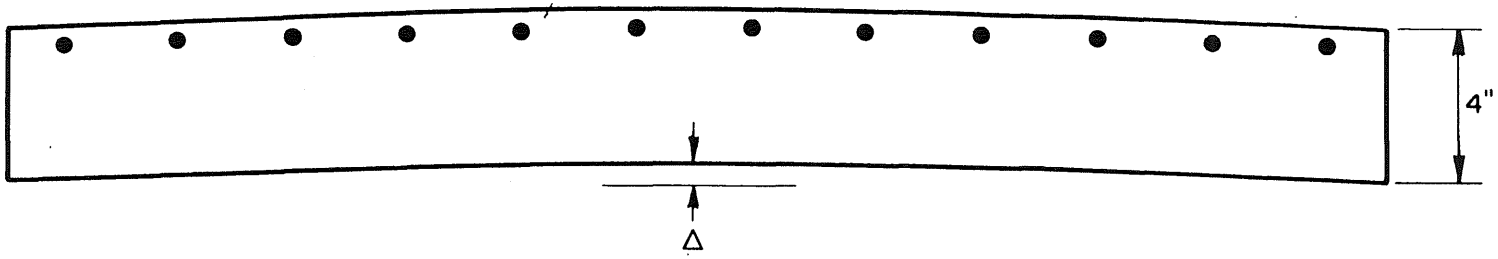

(b) After Deformation

FIG. 4.3 CROSS SECTIONS OF FLAT AND CURVED SLABS

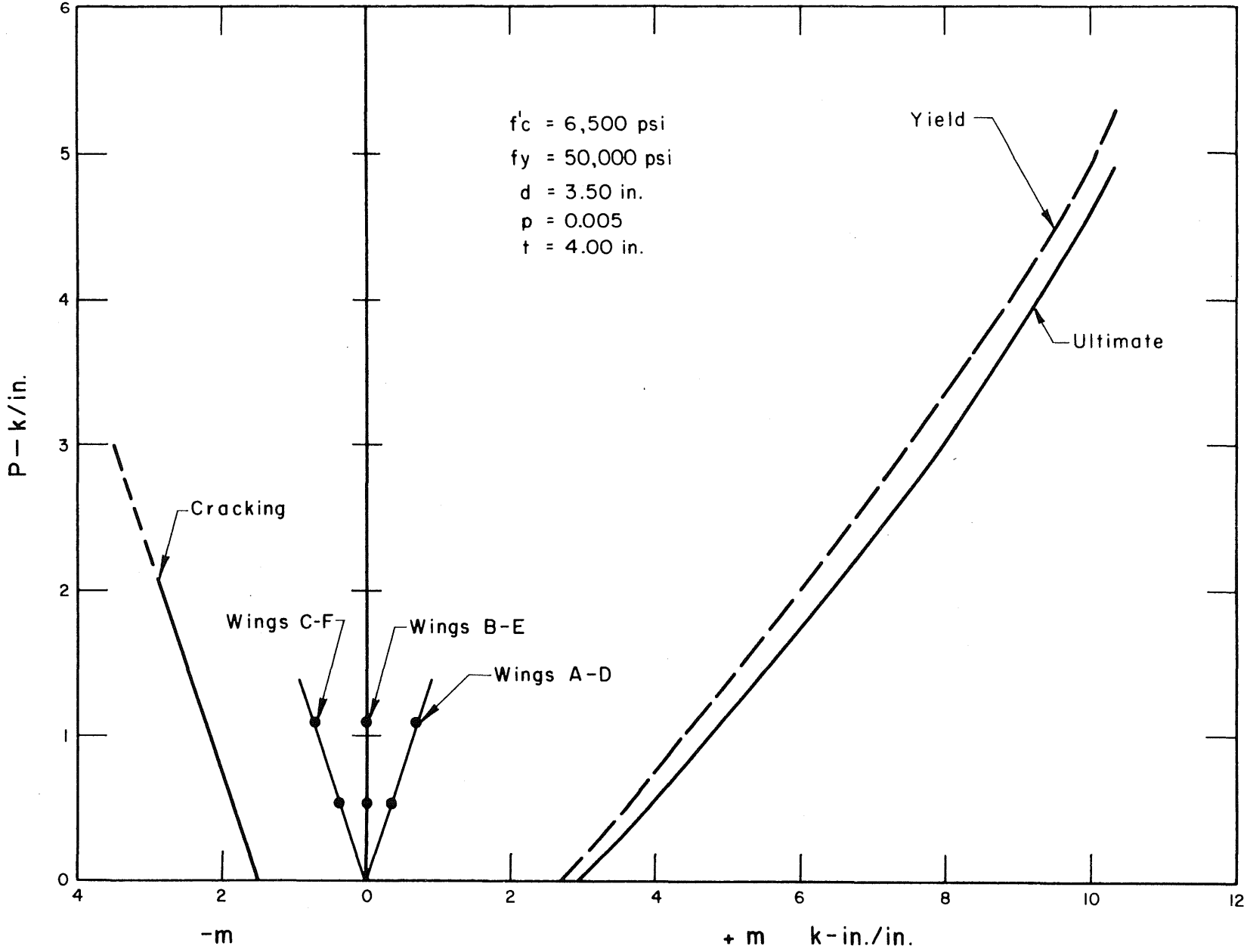

FIG. 4.4 PARTIAL THRUST—MOMENT INTERACTION DIAGRAM SHOWING INITIAL CONDITIONS

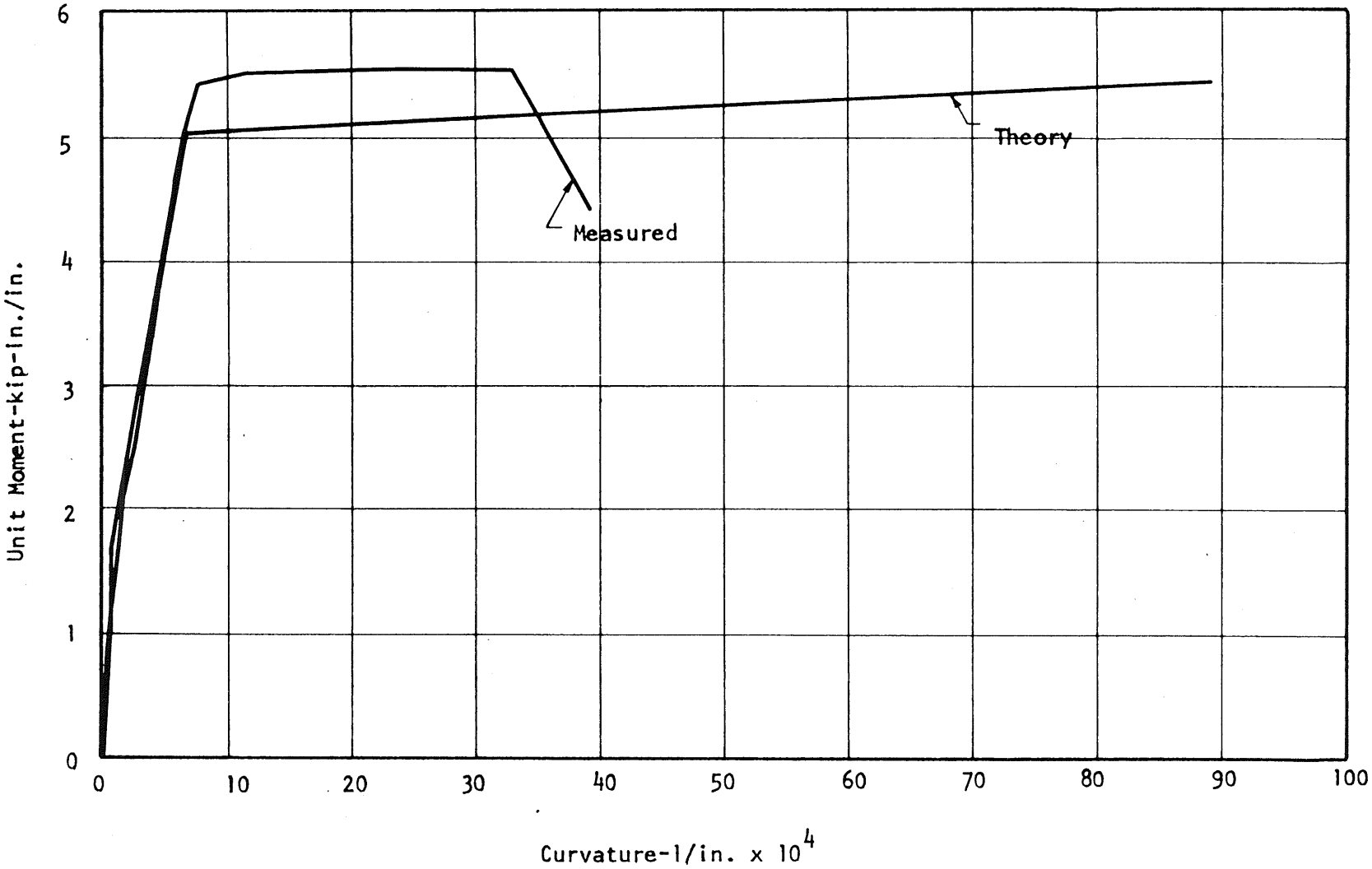

FIG. 4.5 MOMENT-CURVATURE RELATIONSHIPS FOR SLAB FC1A

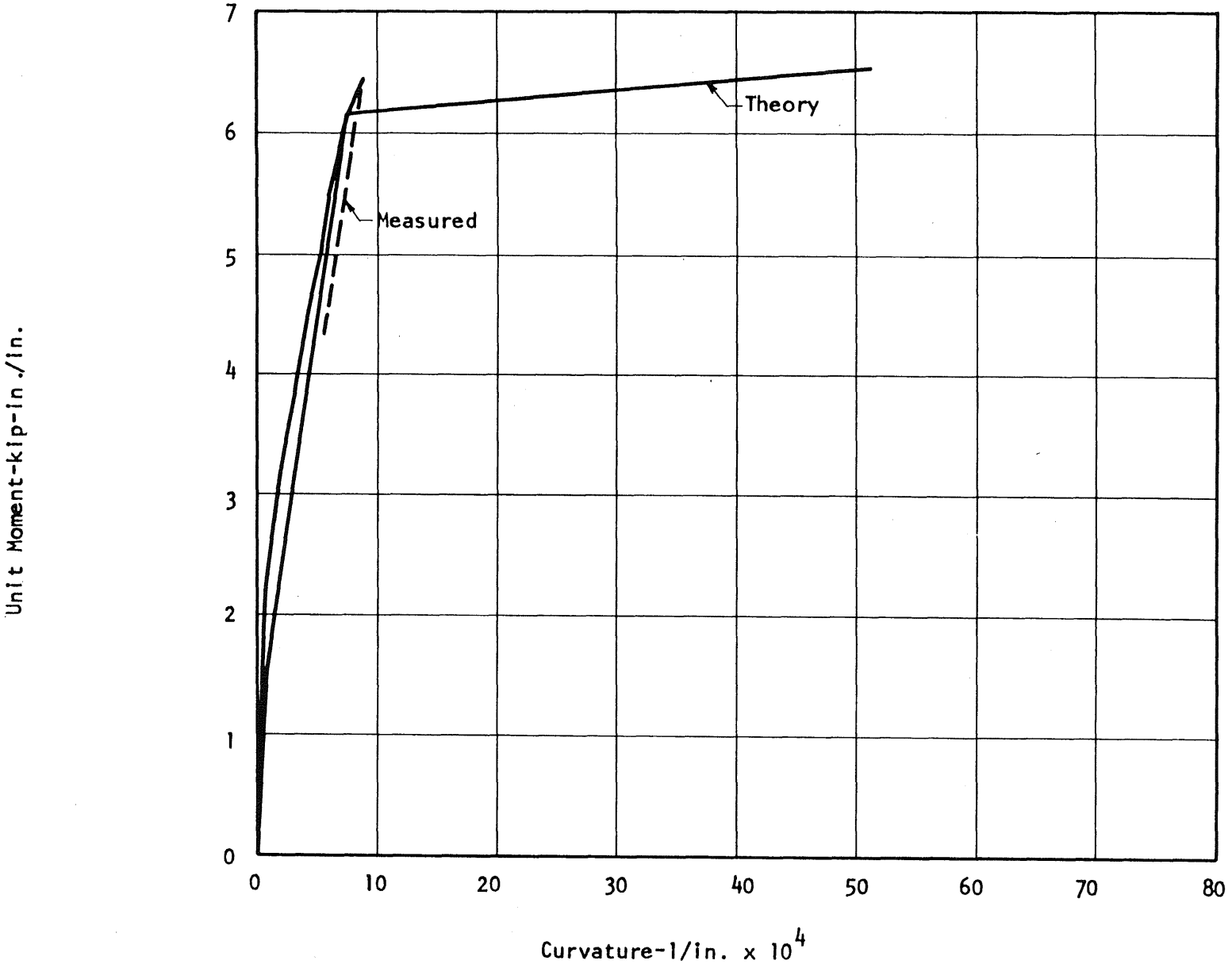

FIG. 4.6 MOMENT-CURVATURE RELATIONSHIPS FOR SLAB FC1B

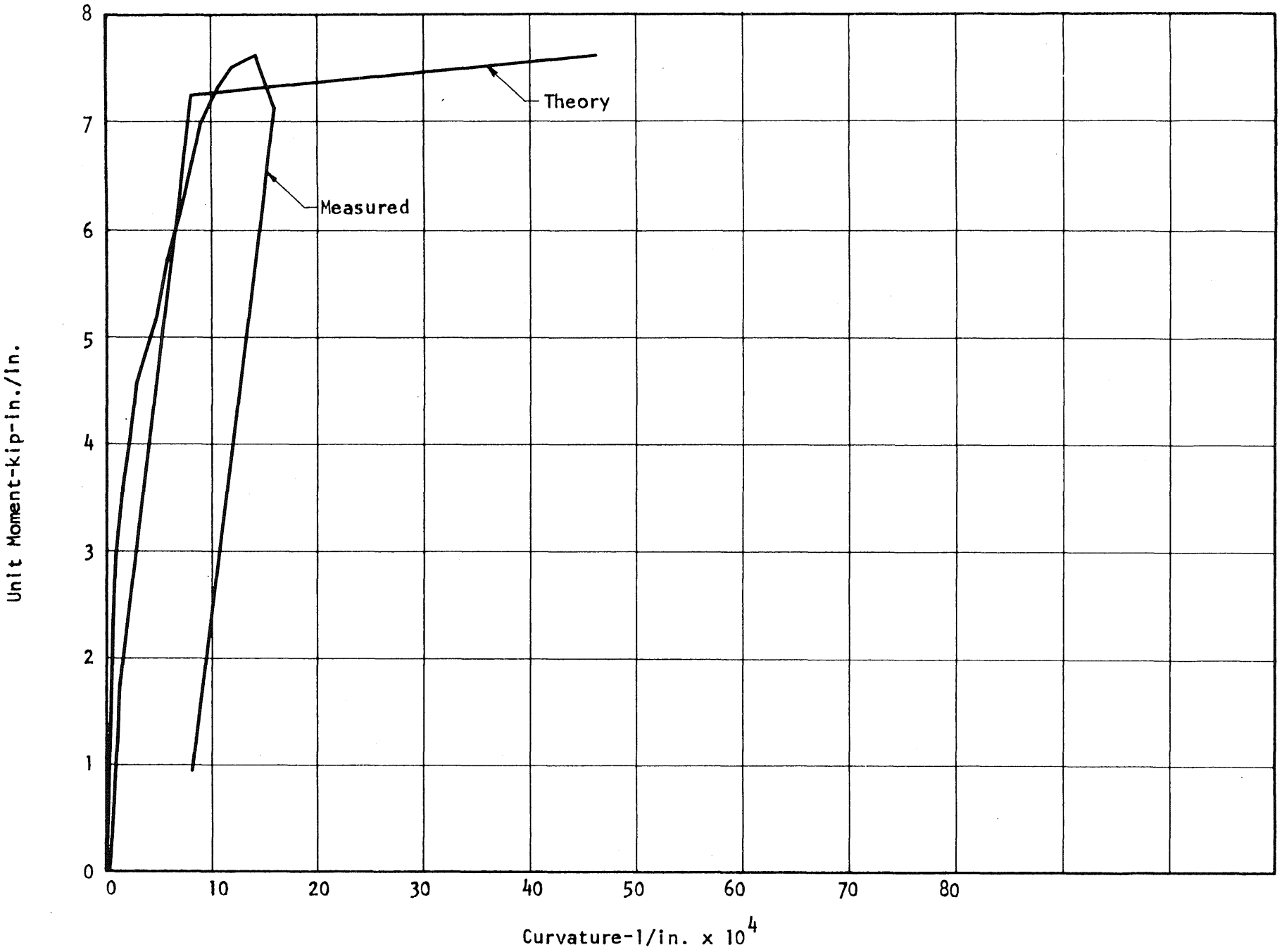

FIG. 4.7 MOMENT-CURVATURE RELATIONSHIPS FOR SLAB FC1C

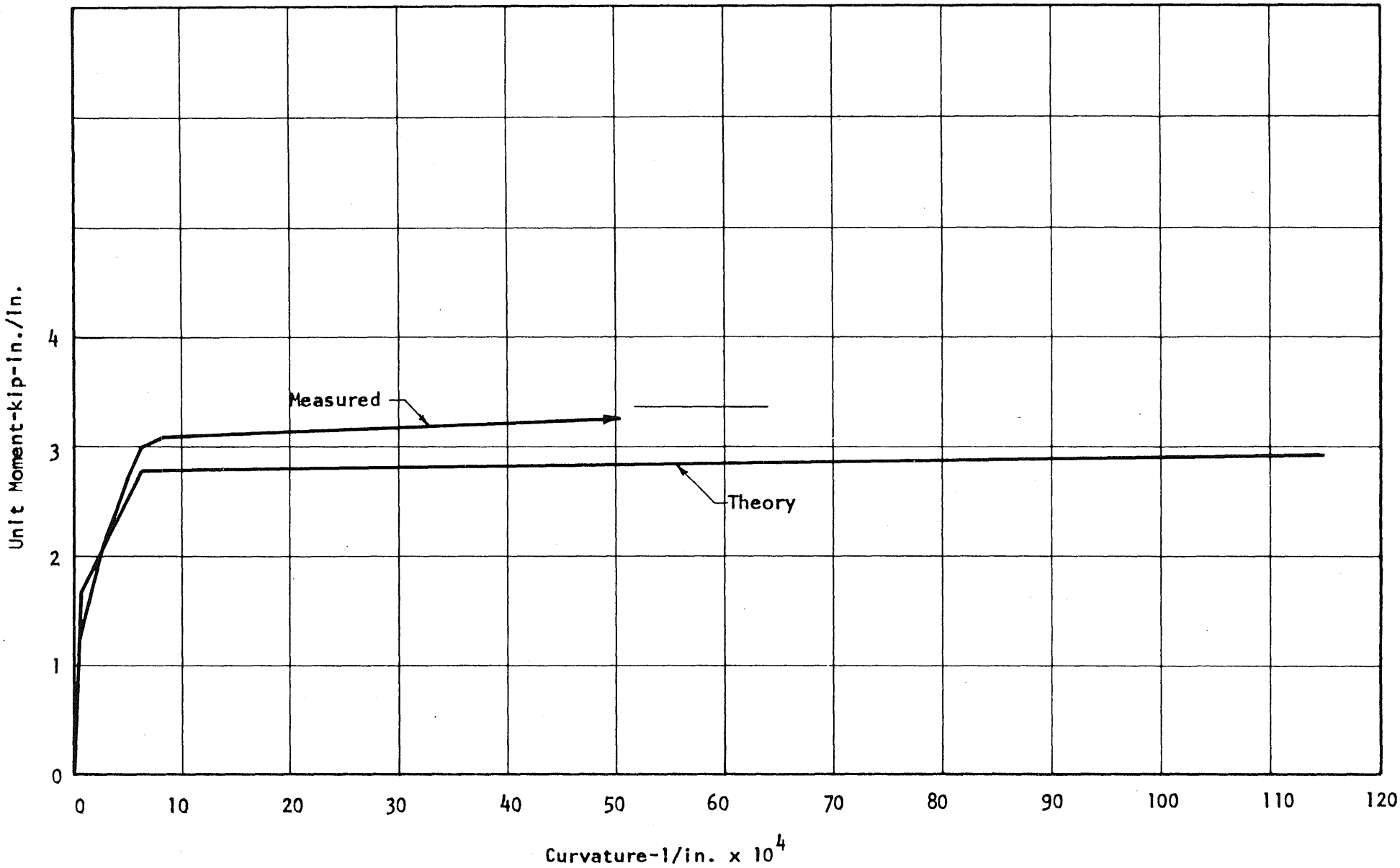

FIG. 4.8 MOMENT-CURVATURE RELATIONSHIPS FOR SLAB FC5A

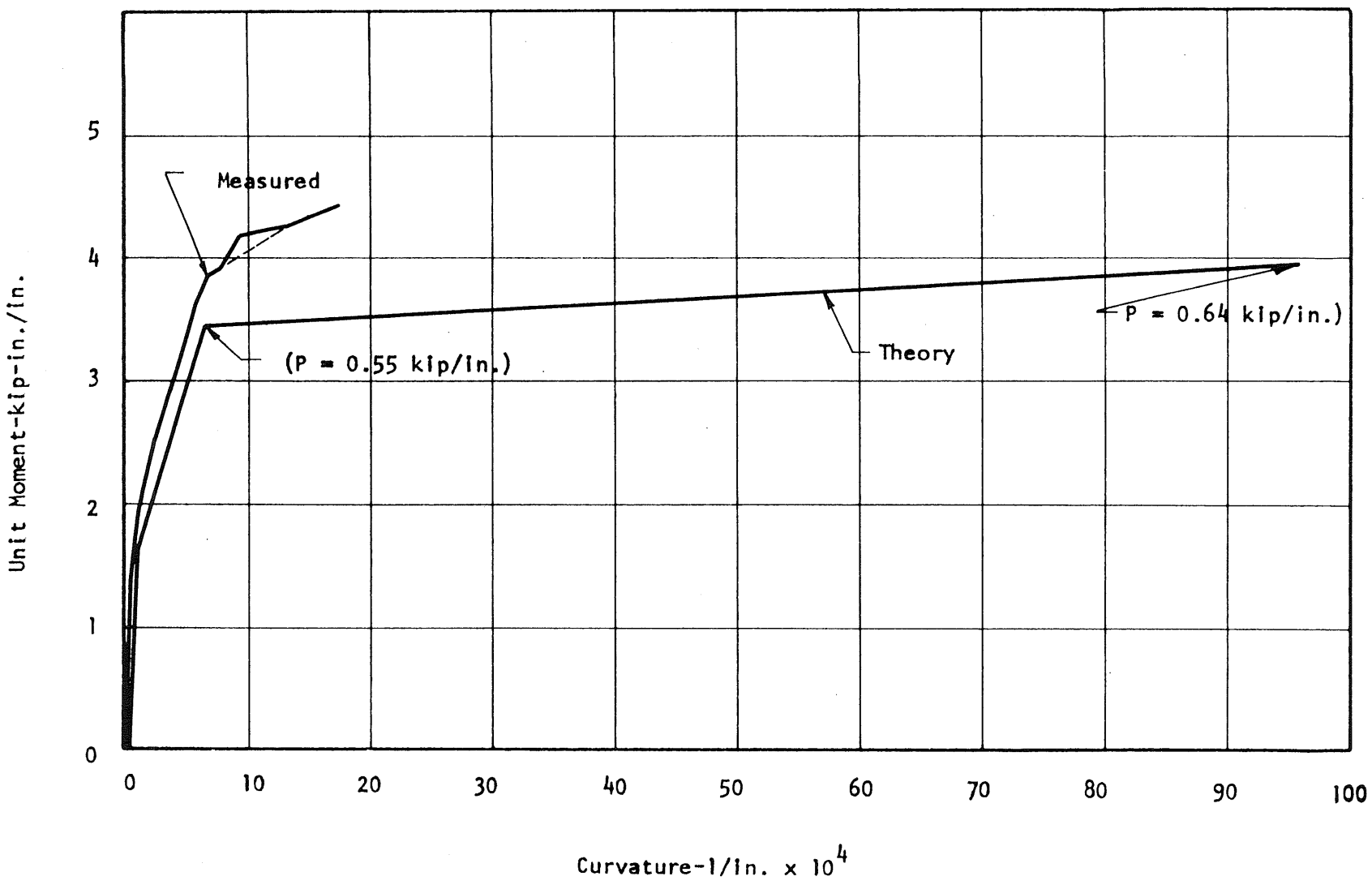

FIG. 4.9 MOMENT-CURVATURE RELATIONSHIPS FOR SLAB FC5B

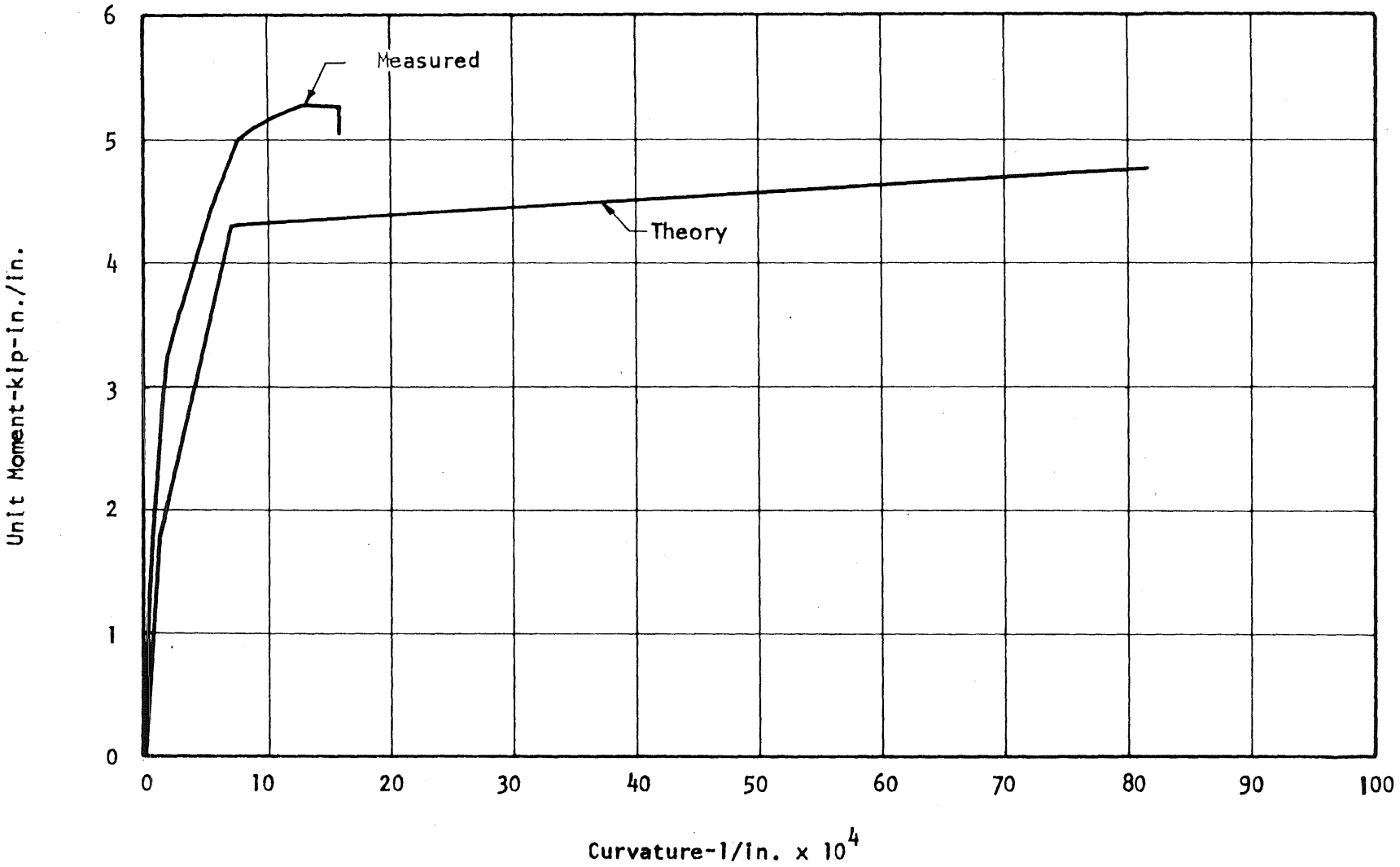

FIG. 4.10 MOMENT-CURVATURE RELATIONSHIPS FOR SLAB FC5C

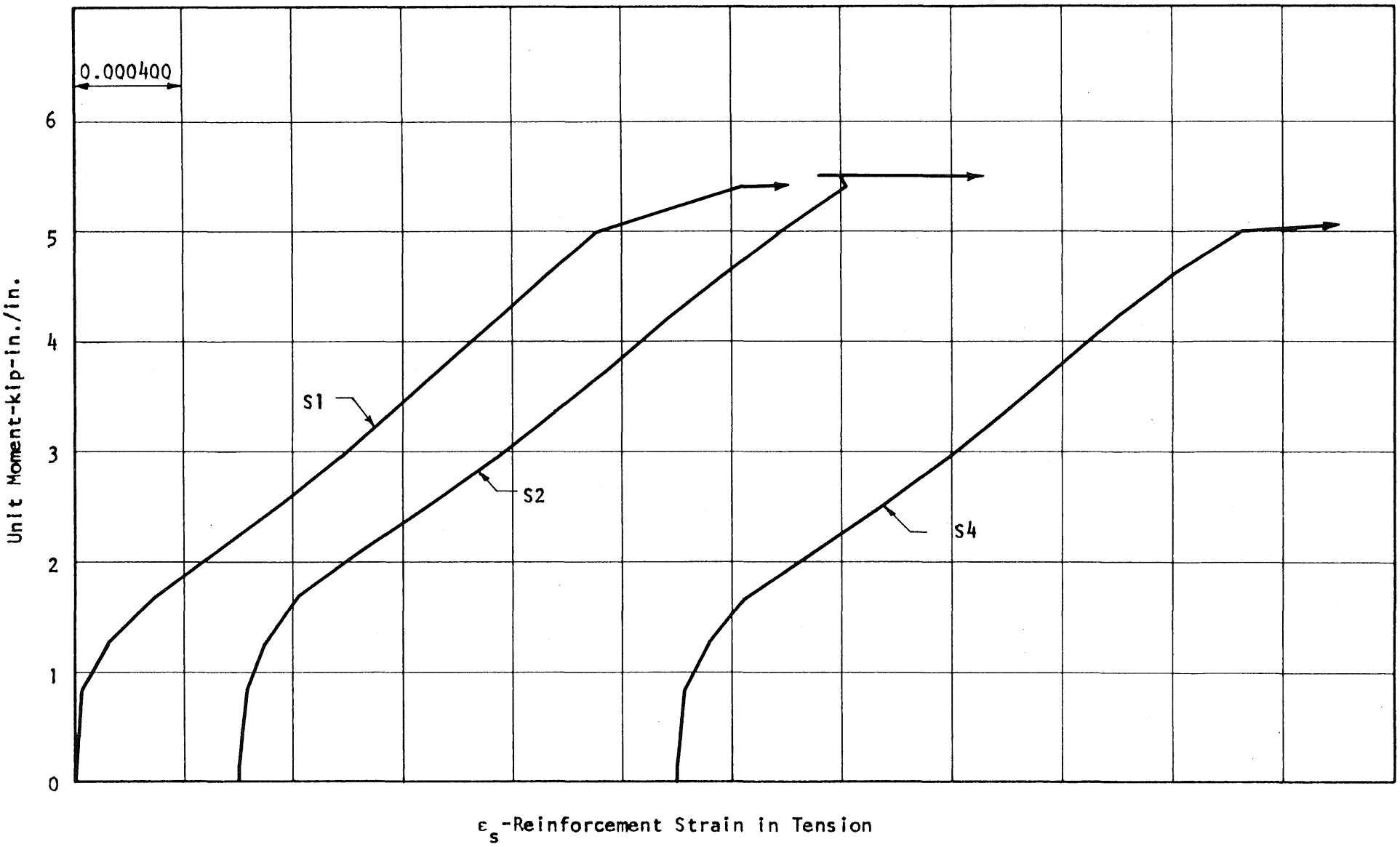

FIG. 4.11 MOMENT-REINFORCEMENT STRAIN CURVES FOR SLAB FC1A

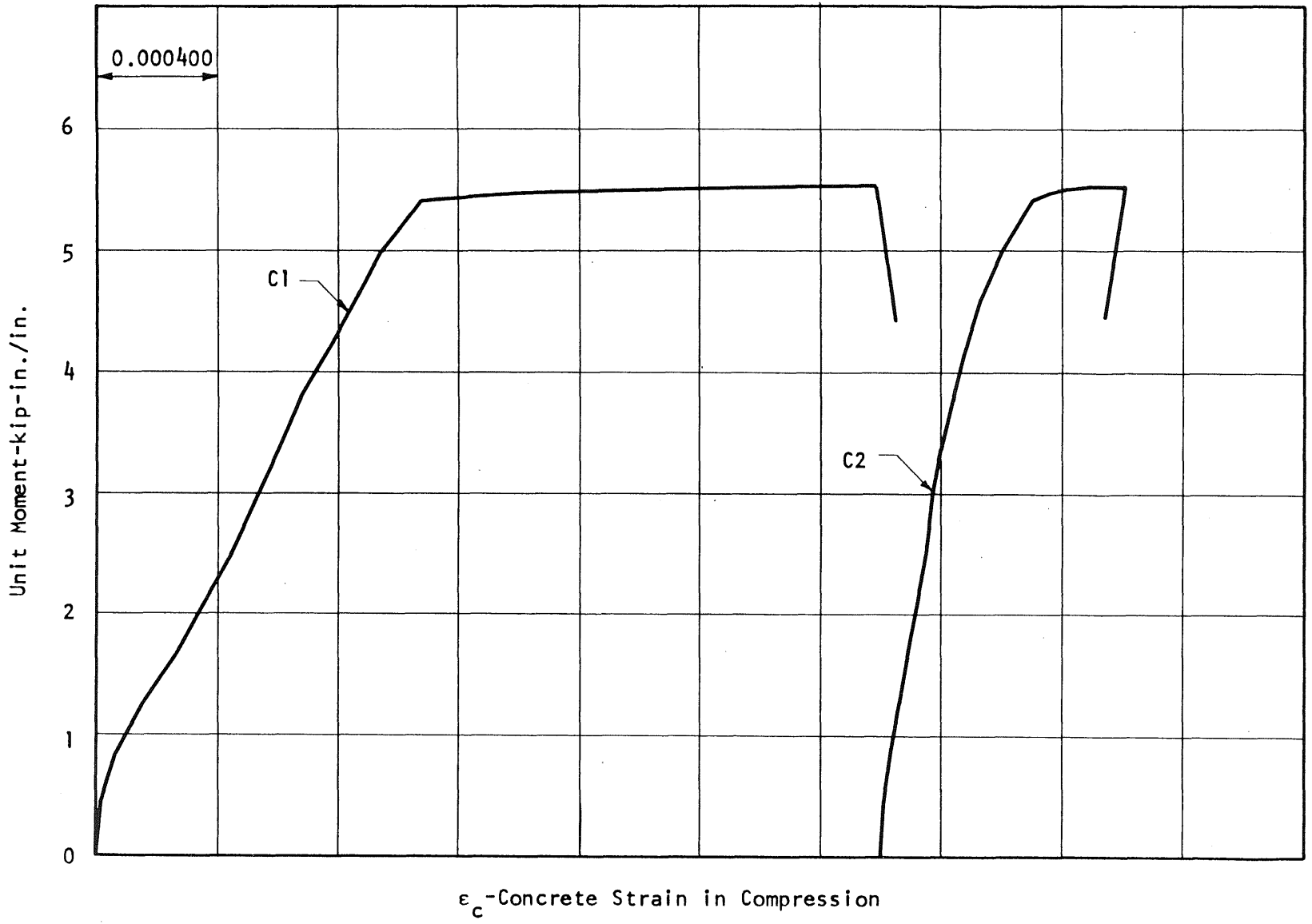

FIG. 4.12 MOMENT-CONCRETE STRAIN CURVES FOR SLAB FC1A

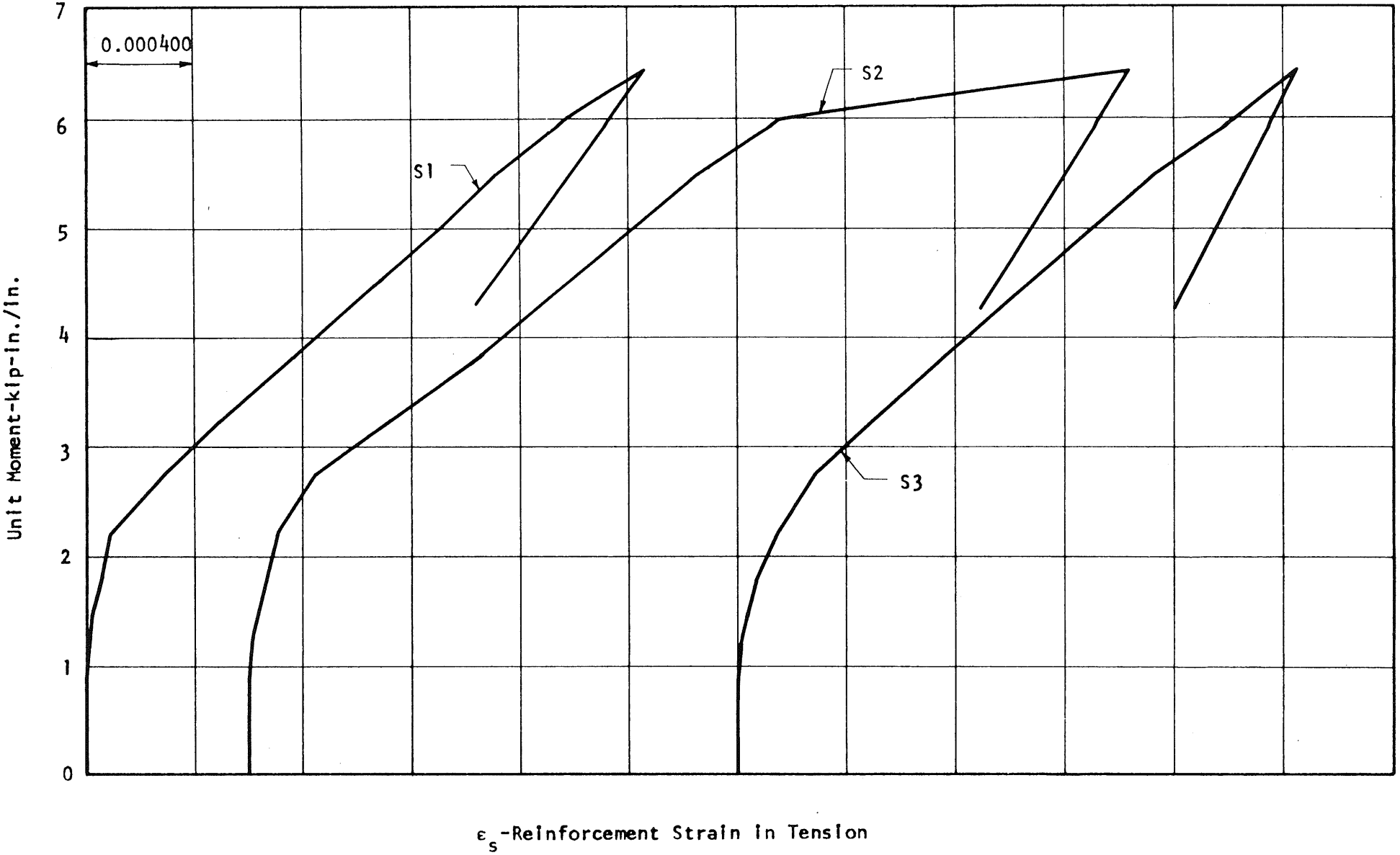

FIG. 4.13 MOMENT-REINFORCEMENT STRAIN CURVES FOR SLAB FC1B

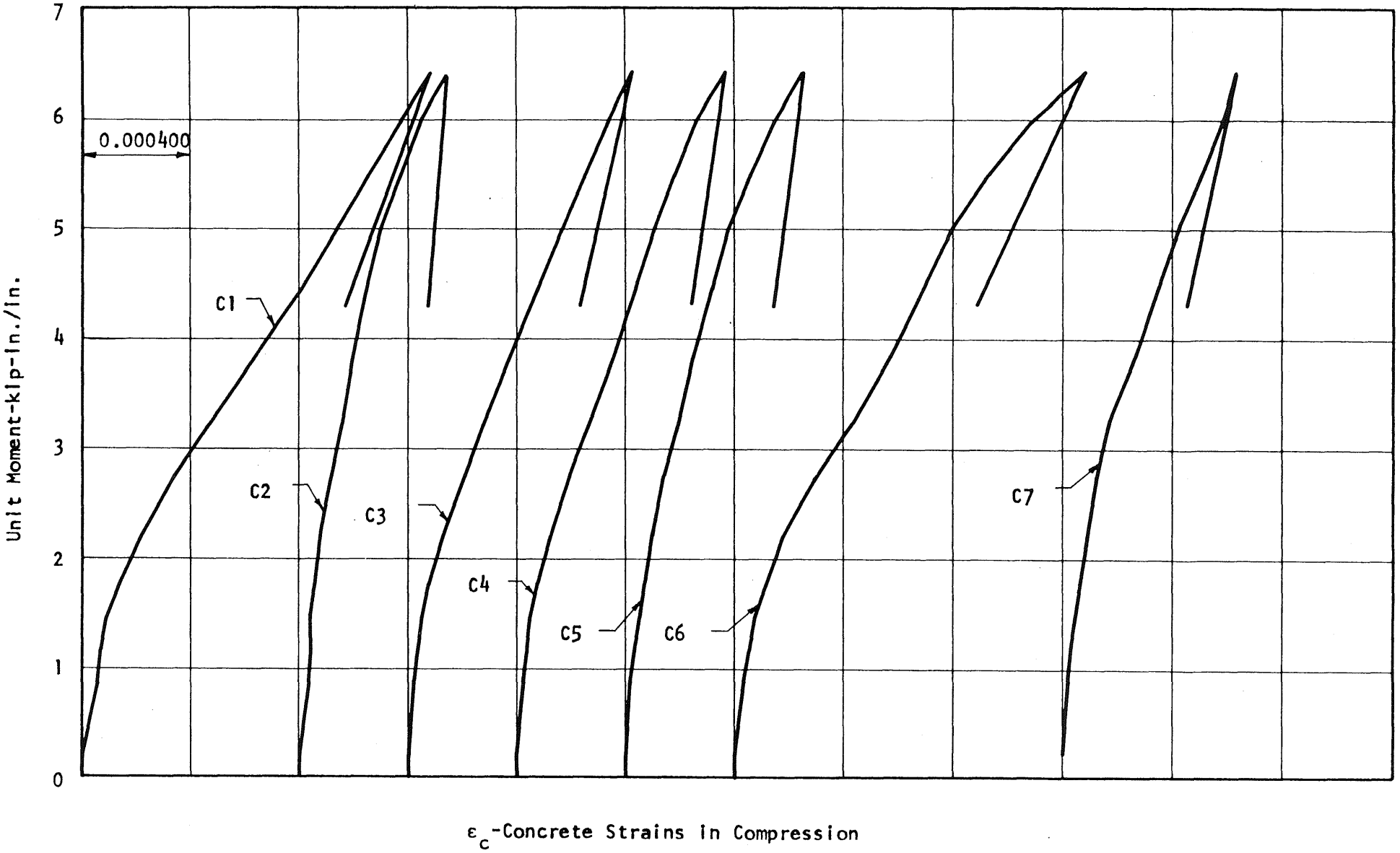

FIG. 4.14 MOMENT-CONCRETE STRAIN CURVES FOR SLAB FC1B

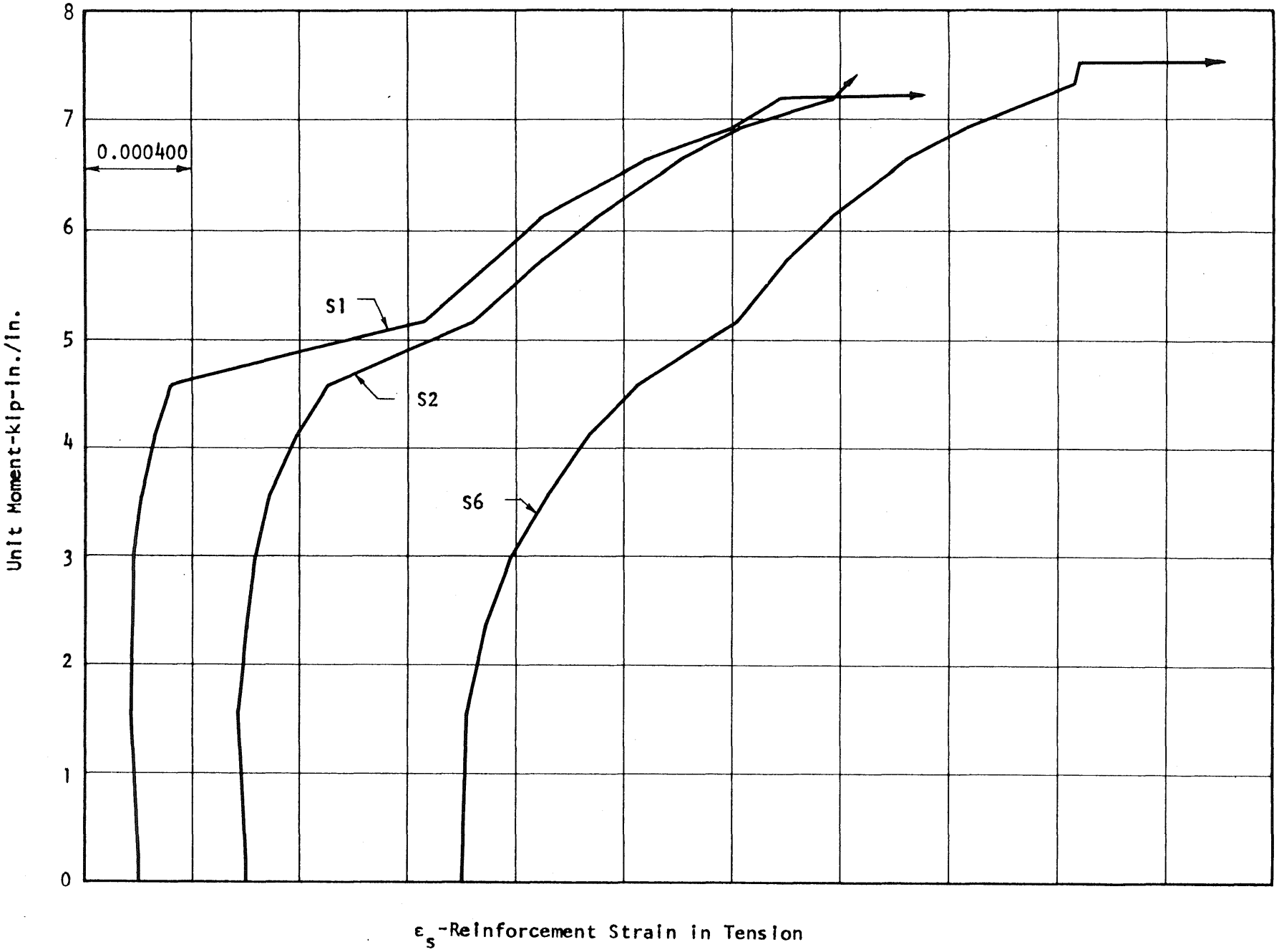

FIG. 4.15 MOMENT-REINFORCEMENT STRAIN CURVES FOR SLAB FC1C

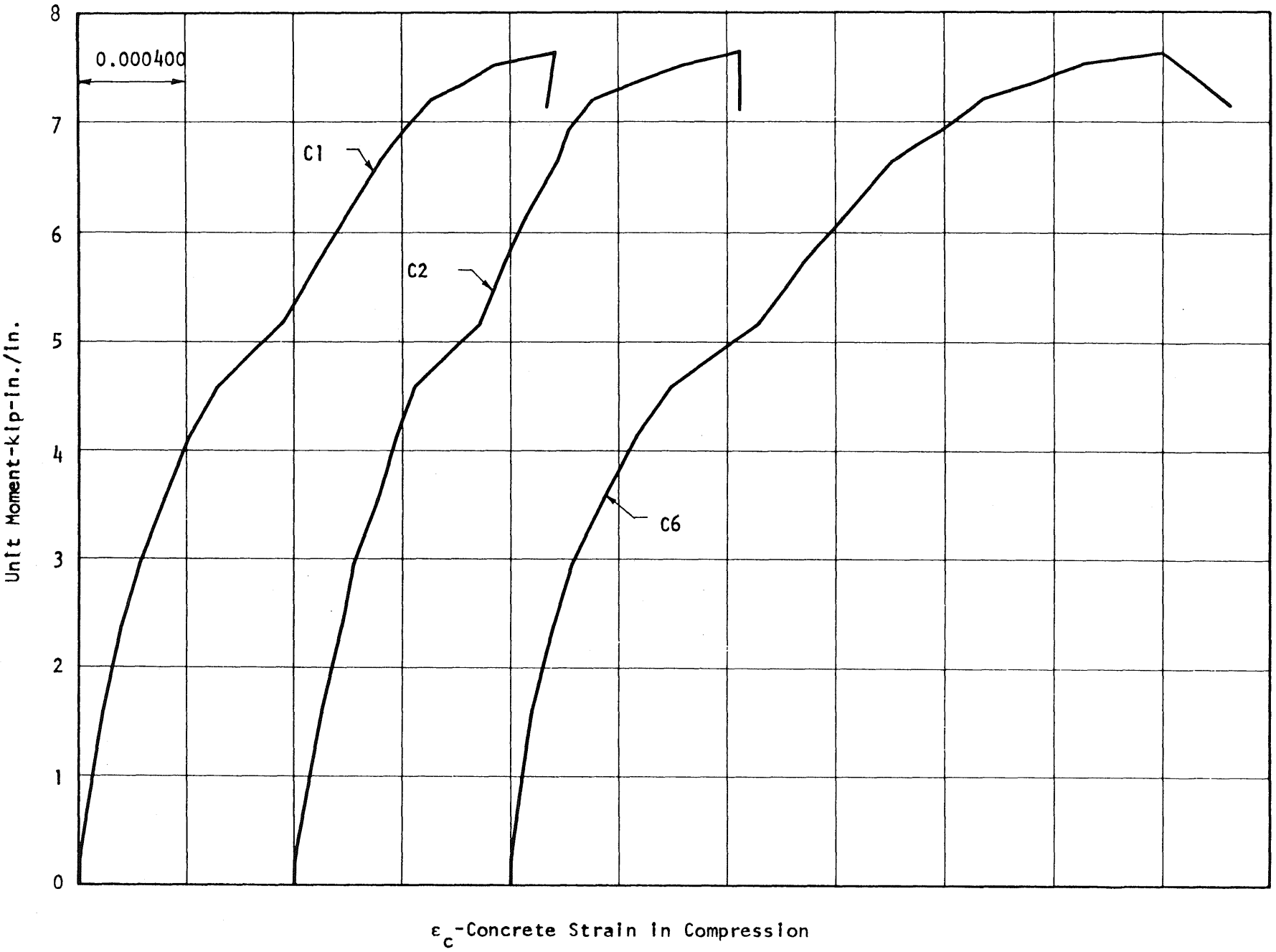

FIG. 4.16 MOMENT-CONCRETE STRAIN CURVES FOR SLAB FC1C

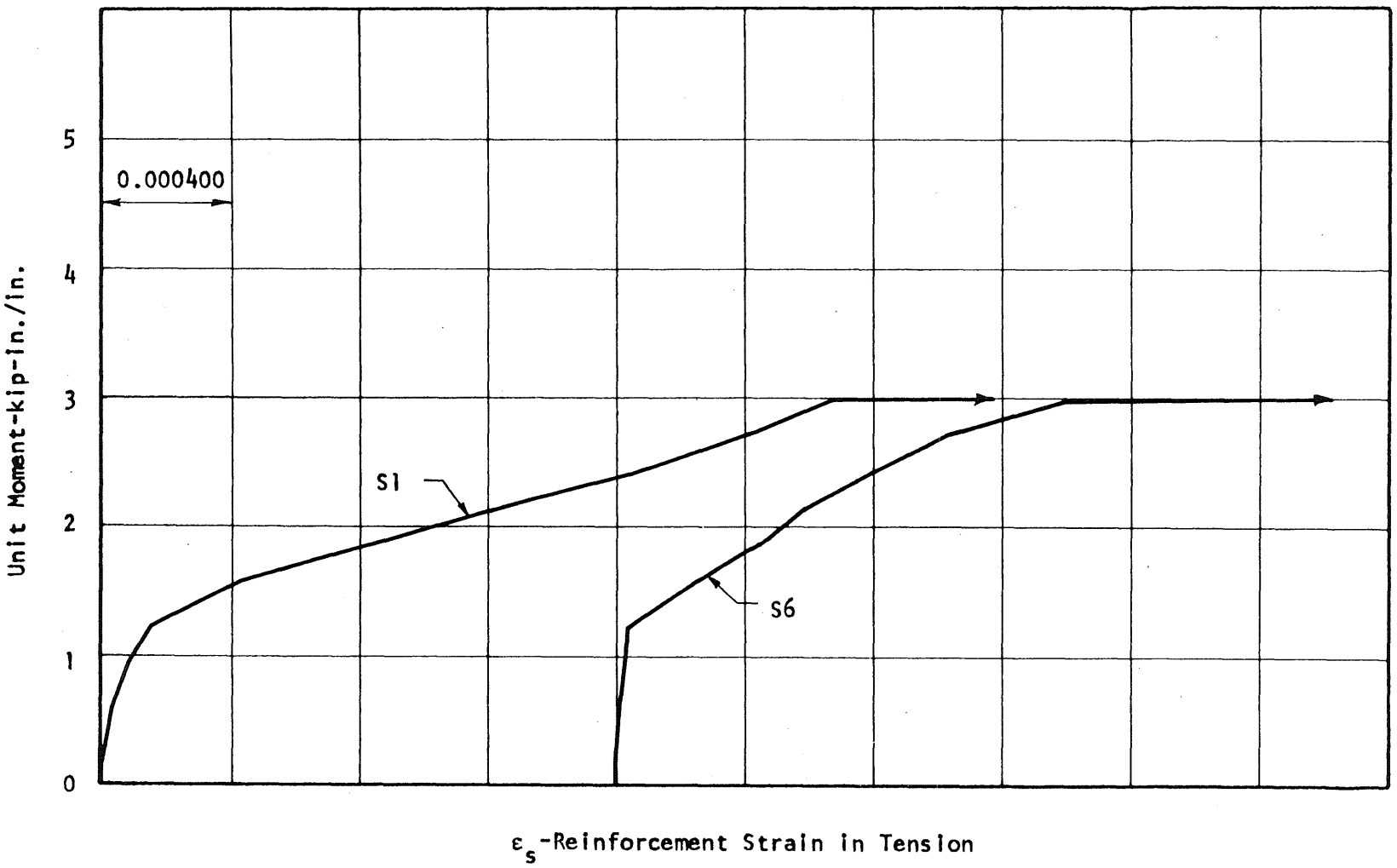

FIG. 4.17 MOMENT-REINFORCEMENT STRAIN CURVES FOR SLAB FC1C

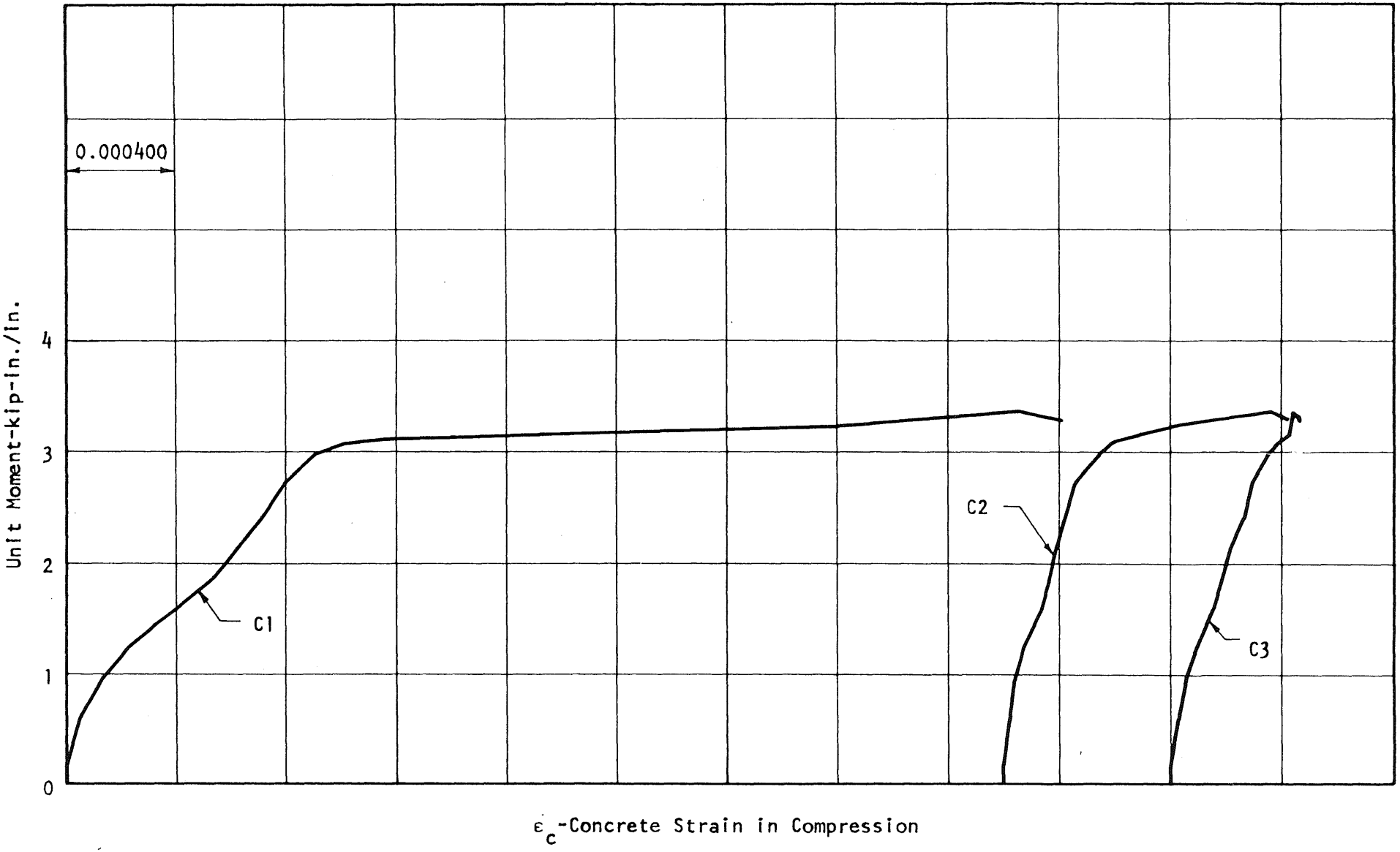

FIG. 4.18 MOMENT-CONCRETE STRAIN CURVES FOR SLAB FC5A

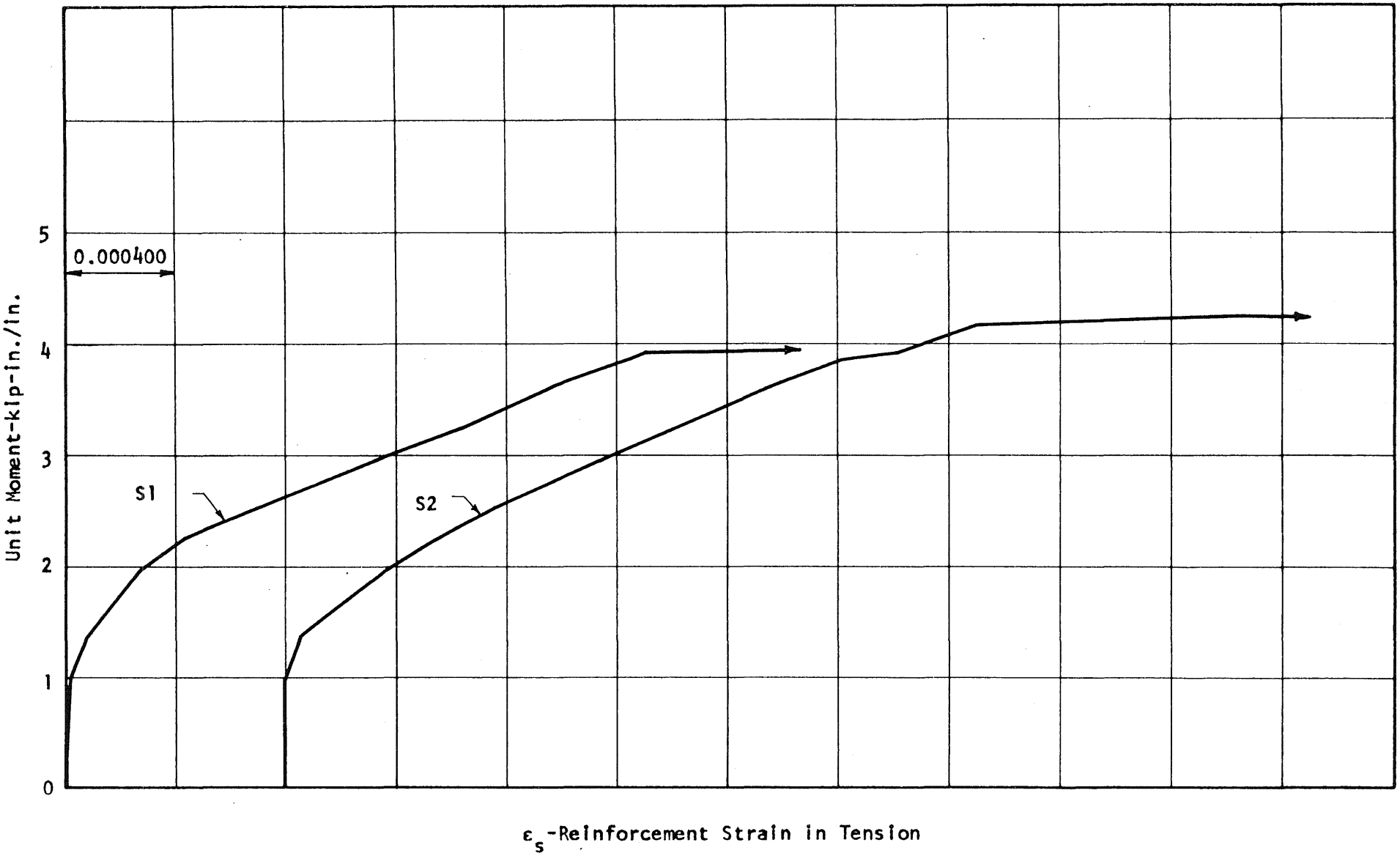

FIG. 4.19 MOMENT-REINFORCEMENT STRAIN CURVES FOR SLAB FC5B

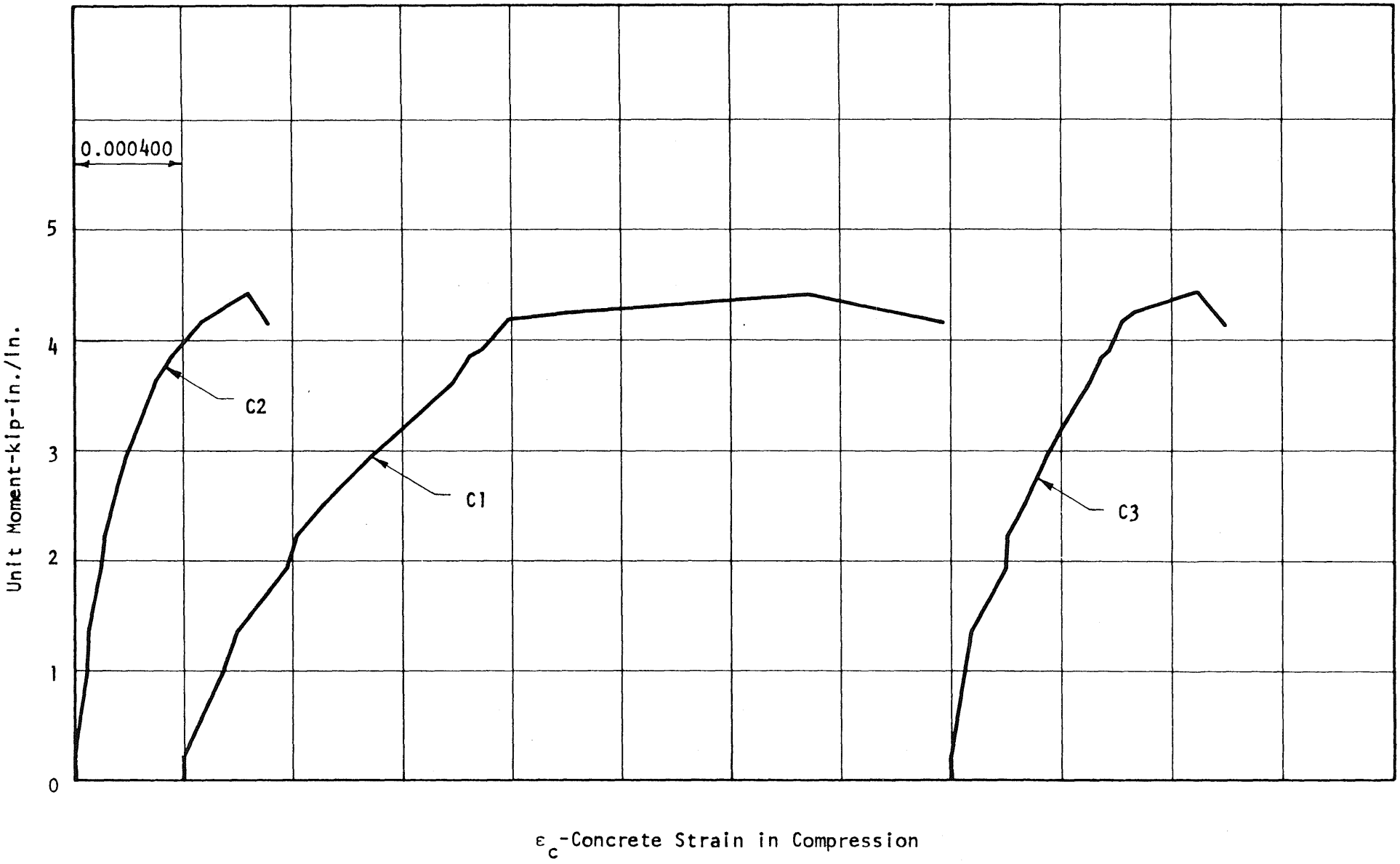

FIG. 4.20 MOMENT CONCRETE STRAIN CURVES FOR SLAB FC5B

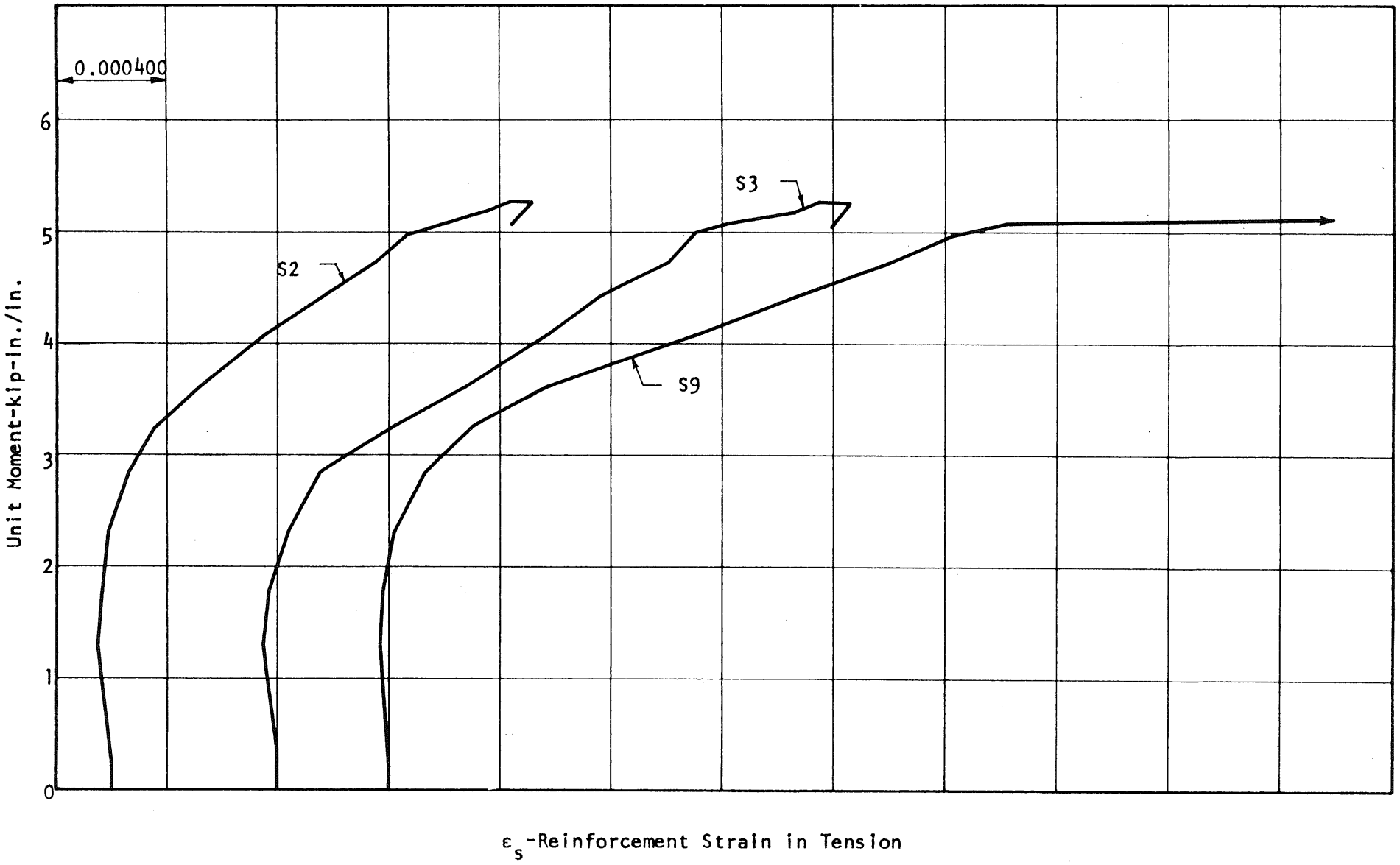

FIG. 4.21 MOMENT-REINFORCEMENT STRAIN CURVES FOR SLAB FC5C

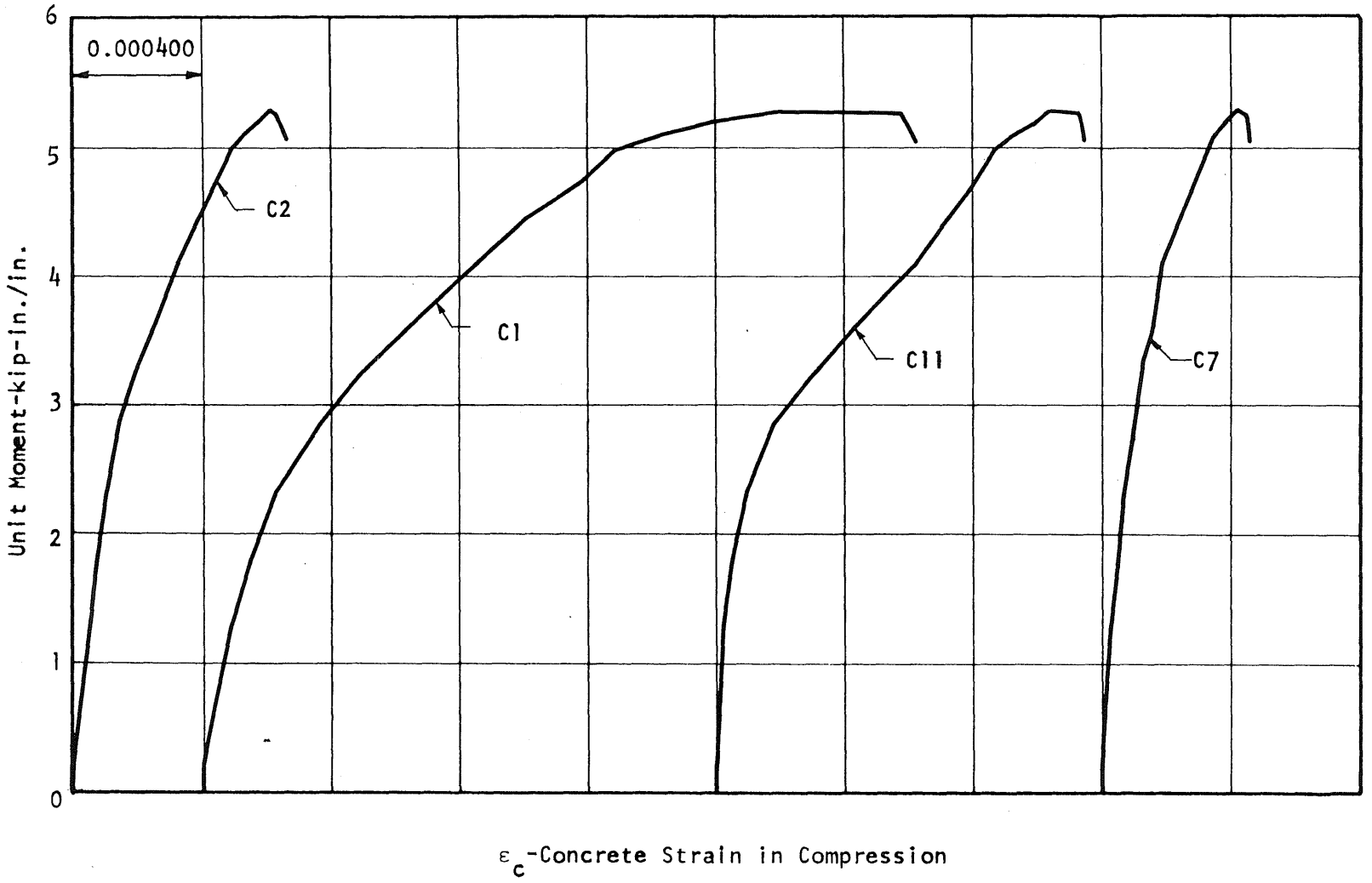

FIG. 4.22 MOMENT-CONCRETE STRAIN CURVES FOR SLAB FC5C

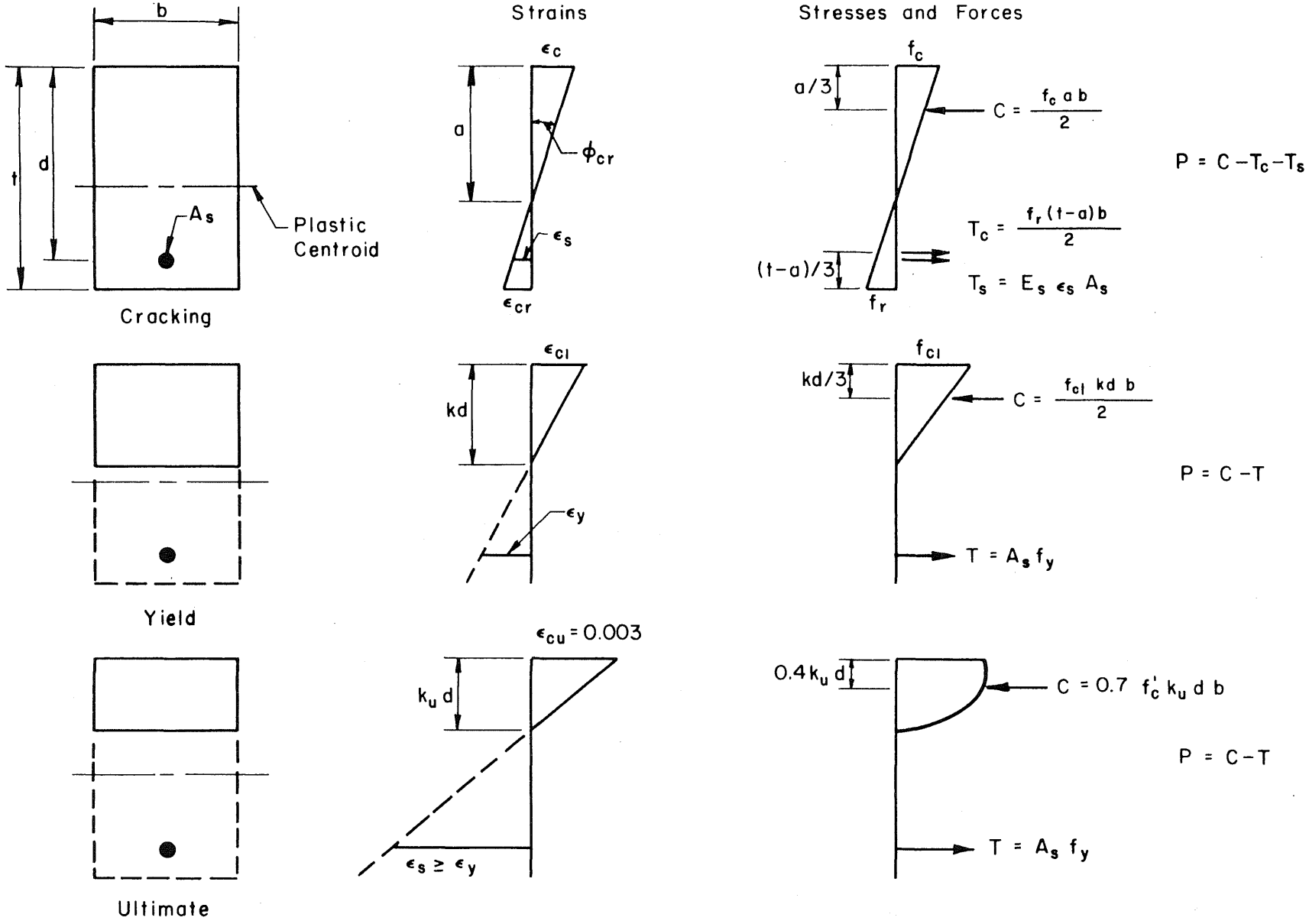

FIG. 5.1 STRAIN AND STRESS CONDITIONS FOR MOMENT–CURVATURE RELATIONSHIPS

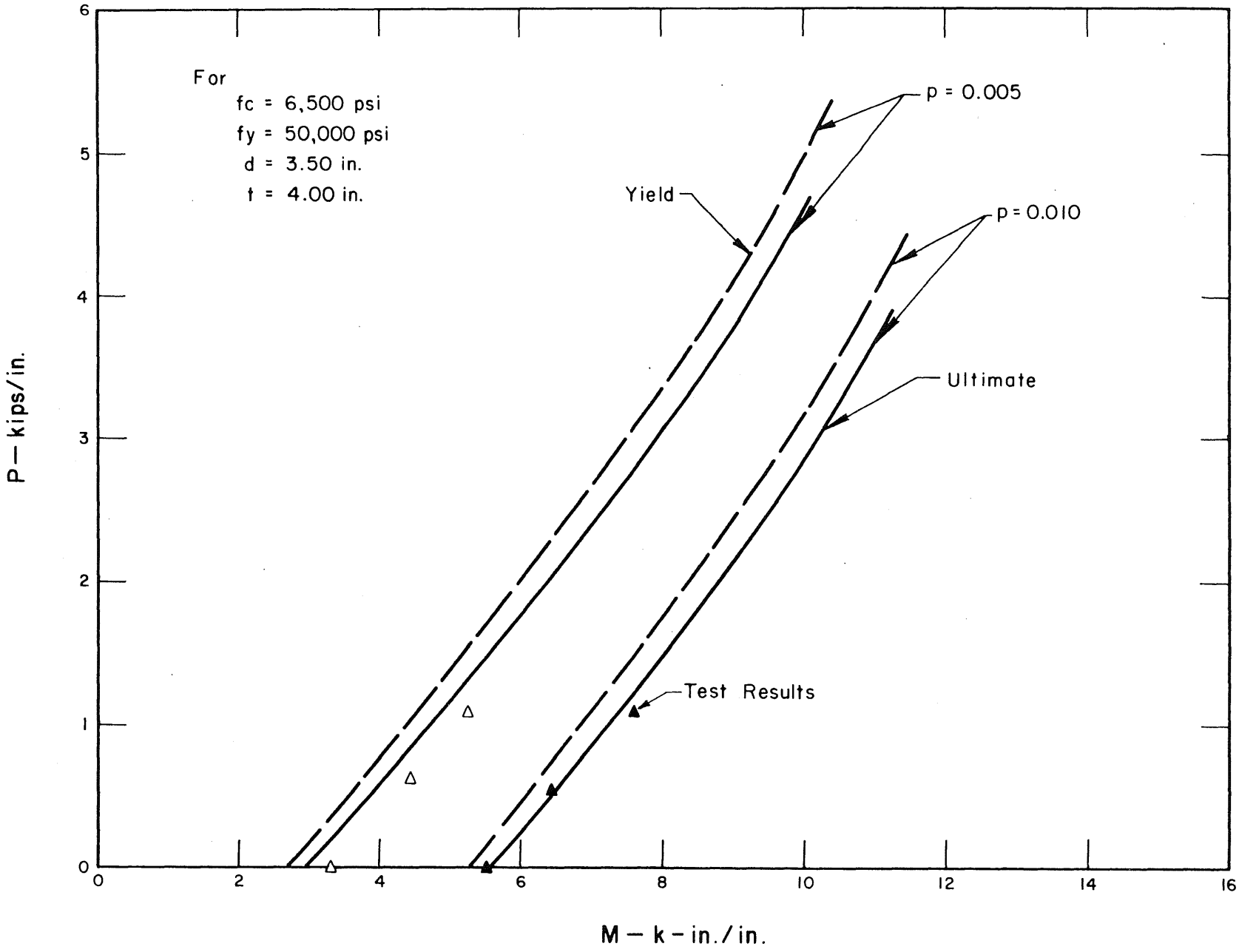

FIG. 5.2 PARTIAL MOMENT — THRUST INTERACTION DIAGRAMS

O.C.D. DISTRIBUTION LIST

Addressee	No. of Copies
Office of Civil Defense Office of the Secretary of the Army Attn: Research Administration Office Pentagon Washington, D. C. 20310	45
Army Library 1A 518, Pentagon Washington, D. C. 20310	1
Assistant Secretary of the Army (R&D) Attn: Assistant for Research Washington, D. C. 20310	1
Chief of Naval Research Department of the Navy Washington, D. C. 20360	1
Commander, Naval Supply Systems Command (Code 0611C1) Department of the Navy Washington, D.C. 20360	1
Commander, Naval Facilities Engineering Command Research and Development (Code 0322C) Department of the Navy Washington, D. C. 20390	1
Mr. Richard Park Advisory Committee on Civil Defense National Academy of Sciences 2101 Constitution Avenue, N. W. Washington, D. C. 20418	1
Defense Documentation Center Cameron Station Alexandria, Virginia 22314	20
Mrs. Joanne S. Gailar Civil Defense Research Project Oak Ridge National Laboratory P. O. Box X Oak Ridge, Tennessee 37830	1
Mr. Norward A Meador Shelter Research Division Office of Civil Defense Department of the Army - OSA Washington, D. C. 20310	1

Addressee	No. of Copies
Chief of Naval Personnel (Code Pers M 12) Department of the Navy Washington, D. C. 20360	1
U. S. Naval Civil Engineering Laboratory Port Hueneme, California 93041	1
Director, Disaster and Defense Services Staff Agricultural Stabilization and Conservation Service U. S. Department of Agriculture Washington, D. C. 20250	1
Mr. Bill Miller Department of Civil Engineering 307 More Hall University of Washington Seattle, Washington 98105	1
Professor Carl Koontz Department of Civil Engineering Worcester Polytechnic Institute Worcester, Massachusetts 01609	1
Mr. Franklin J. Agardy Department of Civil Engineering San Jose State College San Jose, California 95114	1
Professor Robert Bailey School of Civil Engineering Civil Engineering Building Purdue University Lafayette, Indiana 47907	1
Mr. John A. Samuel Department of Mechanical Engineering University of Florida Gainesville, Florida 32601	1
Professor Gale K. Vetter School of Architecture University of Colorado Boulder, Colorado 80302	1
Professor Richard E. Kummer 101 Eng. A Pennsylvania State University University Park, Pennsylvania 16802	1

Addressee	No. of Copies
Mr. George N. Sisson, Director Shelter Research Division Office of Civil Defense Department of the Army - OSA Washington, D. C. 20310	1
Director, Defense Atomic Support Agency Attn: Jack R. Kelso Washington, D. C. 20301	1
Mr. Edward R. Saunders, Jr. Deputy Director National Resource Analysis Center Office of Emergency Preparedness Executive Office of the President Washington, D. C. 20504	1
Director, Civil Effects Branch Division of Biology and Medicine Atomic Energy Commission Attn: Mr. L. J. Deal Washington, D. C. 20545	1
Air Force Special Weapons Laboratory Attn: Technical Library Kirtland Air Force Base, New Mexico 87117	2
Los Alamos Scientific Laboratory Attn: Document Library Los Alamos, New Mexico 87544	1
Miss Nancy K. Barberii OCD Professional Advisory Service Center University of Arizona Tucson, Arizona 85721	1
Chief of Engineers Department of the Army Attn: ENGME-RD Washington, D. C. 20314	1
Chief, Joint Civil Defense Support Group Office, Chief of Engineers Department of the Army Attn: ENGMC-D Washington, D. C. 20314	1

Addressee	No. of Copies
Director, Army Materials and Mechanics Research Center Attn: Technical Library Watertown, Massachusetts 02172	1
Director, U. S. Army Ballistic Research Laboratory Attn: Document Library Aberdeen Proving Ground, Maryland 21005	1
Director, U. S. Army Ballistic Research Laboratory Attn: Mr. William Taylor Aberdeen Proving Ground, Maryland 21005	1
Director, Defense Atomic Support Agency Attn: Technical Library Washington, D. C. 20301	1
Director, U. S. Army Engineer Waterways Experiment Station Post Office Box 631 Attn: Nuclear Weapons Effects Branch Vicksburg, Mississippi 39180	1
Director, U. S. Army Engineer Waterways Experiment Station Post Office Box 631 Attn: Document Library Vicksburg, Mississippi 39180	1
District Engineer, U. S. Army Engineer District, Omaha Attn: Chief, Engineering Division 6012 U. S. Post Office and Court House Omaha, Nebraska 68101	1
Mr. Carl K. Wiehle Civil Defense Technical Office Stanford Research Institute Menlo Park, California 94025	1
Mr. William L. White Civil Defense Technical Office Stanford Research Institute Menlo Park, California 94025	5
Mr. Werner Weber Director, New York State Civil Defense Commission Public Security Building State Office Building Campus Albany, New York 12226	1

Addressee	No. of Copies
Agbagin-Jacobsen Associates 8943 South Sepulveda Boulevard Los Angeles, California 90045	1
Amman and Whitney 111 Eighth Avenue New York, New York 10011	1
Mr. Arthur D. Caster Chairman, Coordinating Committee on Civil Defense American Society of Civil Engineers 2864 McFarlan Park Drive Cincinnati, Ohio 45211	1
The Dikewood Corporation 1009 Bardbury Drive, S. E. University Research Park Albuquerque, New Mexico 87106	1
General American Transportation Coporation General American Research Division 7449 North Natchez Avenue Niles, Illinois 60648	1
Hudson Institute Quaker Ridge Road Croton-on-Hudson, New York 10520	1
Bell Telephone Laboratories, Inc. Attn: Mr. R. W. Mayo Whippany Road Whippany, New Jersey 07981	1
Dr. Eugene Sevin IIT Research Institute 10 West 35th Street Chicago, Illinois 60616	1
Dr. Harold Brode The RAND Corporation 1700 Main Street Santa Monica, California 90401	1
Research Triangle Institute P. O. Box 12194 Research Triangle Park North Carolina 27709	1
Mr. Luke J. Vortman Division 5412 Sandia Corporation Box 5800, Sandia Base Albuquerque, New Mexico 87115	1

Addressee	No. of Copies
URS Research Company 155 Bovet Road San Mateo, California 94402	1
Massachusetts Institute of Technology Department of Civil and Sanitary Engineering Cambridge, Massachusetts 02138	1
Dr. Nathan M. Newmark University of Illinois 1114a Civil Engineering Building Urbana, Illinois 61801	1
Dr. William Hall University of Illinois 1108 Civil Engineering Building Urbana, Illinois 61801	1
Dr. Merit P. White University of Massachusetts School of Engineering Amherst, Massachusetts 01002	1
Dr. Abner Sachs Institute for Defense Analyses 400 Army-Navy Drive Arlington, Virginia 22202	1
The Vertex Corporation 10400 Connecticut Avenue Kensington, Maryland 20795	1
Chief of Engineers Department of the Army Attn: ENGMC-EM Washington, D. C. 20314	1
Dr. C. S. White President-Director Lovelace Foundation 5200 Gibson Boulevard, S. E. Albuquerque, New Mexico 87108	1
Dr. Charles Osterberg Acting Chief, Environmental Sciences Branch Division of Biology and Medicine U.S. Atomic Energy Commission Washington, D. C. 20545	1
Mr. J. J. Davis Effects Evaluation Division Nevada Operations Office U.S. Atomic Energy Commission Las Vegas, Nevada 89101	1

Addressee	No. of Copies
Mr. Eugene F. Witt Bell Telephone Laboratories, Inc. Whippany Road Whippany, New Jersey 07981	1
Mr. Paul Zigman Environmental Science Associates 770 Airport Boulevard Burlingame, California 94010	1
Mr. J. W. Foss Supervisor Buildings Studies Group Bell Telephone Laboratories Whippany Road Whippany, New Jersey 07981	1

UNIVERSITY OF ILLINOIS DISTRIBUTION

Metz Reference Room (2)
B106 CEB

Ross J. Martin, Director (2)
Engineering Experiment Station
112 E.H.
(Sent to Engineering Documents Center)

Engineering Library (2)
119 E. H.

TAM Library
212 TL

W. H. Munse
2129 CEB

Engineering Document Center (10) plus extra copies
208 EH
Note: Secondary distribution from Doc Center requires project officer or author release notification.

The John Crerar Library
Chief, Acquisition Dept.
35 W. 33rd Street
Chicago, Illinois

Library of Congress
Chief,
Exchange and Gift Division
Washington, D. C. 20540

The Engineering Societies Library
Order Department 345 East 47th Street
New York, New York 10017

Clearinghouse for Federal Scientific and Technical Information
5285 Port Royal Road
Springfield, Va. 22151

National Lending Library for Science and Technology
Dept. of Scientific and Industrial Research
Boston, Spa, Yorkshire, ENGLAND

National Library for Science and Invention
State Paper Room
The British Museum
London, W. C. 1, ENGLAND

National Research Council Library
Library Acquisitions Section
Sussex Drive
Ottawa, 2 CANADA

Concrete Subjects Only
Cement and Concrete Association Library
52 Grosvenor Garden
London, S.W. 1, ENGLAND

C. P. Siess
3129 CEB

M. A. Sozen
3112 CEB

C. E. Kesler
2129 CEB

W. C. Schnobrich
3525 CEB

B. Mohraz
2213 CEB

W. L. Gamble
2209 CEB

A. E. Fiorato
2214 CEB

A. E. Girolami
1867 Temple, #35
Long Beach, California 90806

H. Flug
816 College Parkway
Rockville, Maryland 20850

J. J. Salinas-Pachecho
Dept. of Civil Engineering
University of Calgary
Calgary, Alberta, CANADA

Unclassified

Security Classification

DOCUMENT CONTROL DATA - R & D

(Security classification of title, body of abstract and indexing annotation must be entered when the overall report is classified)

1. ORIGINATING ACTIVITY *(Corporate author)*
Department of Civil Engineering
University of Illinois
Urbana, Illinois 61801

2a. REPORT SECURITY CLASSIFICATION
Unclassified

2b. GROUP

3. REPORT TITLE
1. Flexural Strength of Reinforced Concrete Slabs with Externally Applied In-Plane Forces.
2. Strength of Slabs Subjected to Multiaxial Bending and Compression

4. DESCRIPTIVE NOTES *(Type of report and, inclusive dates)*
Technical report

5. AUTHOR(S) *(First name, middle initial, last name)*
1. Anthony G. Girolami, Mete A. Sozen, and William L. Gamble
2. William L. Gamble, Howard Flug, and Mete A. Sozen

6. REPORT DATE	7a. TOTAL NO. OF PAGES	7b. NO. OF REFS
October 1970	133	11

8a. CONTRACT OR GRANT NO.
DAHC 20-67-C-0136
b. PROJECT NO.
Subcontract 12472 (6300 A-030) US
c. OCD Work Unit 1127D
d.

9a. ORIGINATOR'S REPORT NUMBER(S)
Civil Engineering Studies
Structural Research Series No. 369

9b. OTHER REPORT NO(S) *(Any other numbers that may be assigned this report)*

10. DISTRIBUTION STATEMENT
This document has been approved for public release and sale: its distribution is unlimited.

11. SUPPLEMENTARY NOTES

12. SPONSORING MILITARY ACTIVITY
Department of Defense
Office of the Secretary of the Army
Office of Civil Defense

13. ABSTRACT

This report describes an investigation into the behavior of reinforced concrete floor slabs which are subjected to compression forces in the plane of the slab as well as to transverse bending moments. The first report describes tests of a series of 6-ft sq. slabs representative of typical interior panels of beam-supported slab floors. The slabs were subjected to known in-plane compression forces and then loaded to failure under transverse loads. An approximate analysis is developed which leads to a conservative prediction of the strength of such structures, and which gives a reasonable prediction of the load-deflection relationship and consequently of the energy absorbing capacity of the system.

The second part of the report describes tests on six slabs in which the reinforced concrete section was subjected to a uniform moment and compression field in all directions. The tests confirmed that the response of the slabs under such multiaxial bending and compression could be satisfactorily predicted using the same principles and techniques that are routinely applied to members subjected to uniaxial compression plus bending, as is the case for columns.

14. KEY WORDS	LINK A		LINK B		LINK C	
	ROLE	WT	ROLE	WT	ROLE	WT
Reinforced concrete, Floor slabs, In-plane compression in slabs, Membrane forces, Structural testing, Ductility, Strength						

"Flexural Strength of Reinforced Concrete Slabs with Externally Applied In-Plane Forces," by A. G. Girolami, M. A. Sozen, and W. L. Gamble, and "Strength of Slabs Subjected to Multiaxial Bending and Compression," by W. L. Gamble, H. Flug, and M. A. Sozen, Civil Engineering Studies, Structural Research Series No. 369, Dept. of Civil Eng., Univ. of Illinois, Urbana, Illinois, October 1970. Contract DAHC 20-67-C-0136, Sub. 12472 (6300 A-030) US, OCD Work Unit 1127 D.

Key Words: Reinforced Concrete, Floor slabs, In-plane compressions in slabs, membrane forces, structural testing, ductility, strength.

Abstract: Two test series investigating the effects of in-plane compression forces on the behavior of slab structures are described. One series of tests was on models representative of typical interior panels of beam-support slab floors, and an approximate analysis which leads to conservative estimates of strength and deflections is developed. The second series investigates the response of cross-sections subjected to bending and compression in several directions at the same time. It was found that the methods used for prediction of response to uniaxial compression plus bending were applicable to the more complex case found in slabs.

"Flexural Strength of Reinforced Concrete Slabs with Externally Applied In-Plane Forces," by A. G. Girolami, M. A. Sozen, and W. L. Gamble, and "Strength of Slabs Subjected to Multiaxial Bending and Compression," by W. L. Gamble, H. Flug, and M. A. Sozen, Civil Engineering Studies, Structural Research Series No. 369, Dept. of Civil Eng., Univ. of Illinois, Urbana, Illinois, October 1970. Contract DAHC 20-67-C-0136, Sub. 12472 (6300 A-030) US, OCD Work Unit 1127 D.

Key Words: Reinforced Concrete, Floor slabs, In-plane compressions in slabs, membrane forces, structural testing, ductility, strength.

Abstract: Two test series investigating the effects of in-plane compression forces on the behavior of slab structures are described. One series of tests was on models representative of typical interior panels of beam-support slab floors, and an approximate analysis which leads to conservative estimates of strength and deflections is developed. The second series investigates the response of cross-sections subjected to bending and compression in several directions at the same time. It was found that the methods used for prediction of response to uniaxial compression plus bending were applicable to the more complex case found in slabs.

"Flexural Strength of Reinforced Concrete Slabs with Externally Applied In-Plane Forces," by A. G. Girolami, M. A. Sozen, and W. L. Gamble, and "Strength of Slabs Subjected to Multiaxial Bending and Compression," by W. L. Gamble, H. Flug, and M. A. Sozen, Civil Engineering Studies, Structural Research Series No. 369, Dept. of Civil Eng., Univ. of Illinois, Urbana, Illinois, October 1970. Contract DAHC 20-67-C-0136, Sub. 12472 (6300 A-030) US, OCD Work Unit 1127 D.

Key Words: Reinforced Concrete, Floor slabs, In-plane compressions in slabs, membrane forces, structural testing, ductility, strength.

Abstract: Two test series investigating the effects of in-plane compression forces on the behavior of slab structures are described. One series of tests was on models representative of typical interior panels of beam-support slab floors, and an approximate analysis which leads to conservative estimates of strength and deflections is developed. The second series investigates the response of cross-sections subjected to bending and compression in several directions at the same time. It was found that the methods used for prediction of response to uniaxial compression plus bending were applicable to the more complex case found in slabs.

"Flexural Strength of Reinforced Concrete Slabs with Externally Applied In-Plane Forces," by A. G. Girolami, M. A. Sozen, and W. L. Gamble, and "Strength of Slabs Subjected to Multiaxial Bending and Compression," by W. L. Gamble, H. Flug, and M. A. Sozen, Civil Engineering Studies, Structural Research Series No. 369, Dept. of Civil Eng., Univ. of Illinois, Urbana, Illinois, October 1970. Contract DAHC 20-67-C-0136, Sub. 12472 (6300 A-030) US, OCD Work Unit 1127 D.

Key Words: Reinforced Concrete, Floor slabs, In-plane compressions in slabs, membrane forces, structural testing, ductility, strength.

Abstract: Two test series investigating the effects of in-plane compression forces on the behavior of slab structures are described. One series of tests was on models representative of typical interior panels of beam-support slab floors, and an approximate analysis which leads to conservative estimates of strength and deflections is developed. The second series investigates the response of cross-sections subjected to bending and compression in several directions at the same time. It was found that the methods used for prediction of response to uniaxial compression plus bending were applicable to the more complex case found in slabs.